The development of an IRAF-based scientific photometric package for the UFS-Boyden 1.5-m telescope

Hendrik Jacobus van Heerden

B.Sc. Hons

This dissertation is submitted as required for the fulfillment
for the qualification

Degree of Master of Science

in the

Faculty of Natural and Agricultural Sciences

Department of Physics

University of the Free State

South Africa

Supervisor: **Prof. P.J. Meintjes**

Date of submission: March 10, 2008

Acknowledgements

"A pupil from whom nothing is ever demanded which he cannot do, never does all he can."
John Stuart Mill

Abstract

In this dissertation there will be looked at the development of an (Image Reduction and Analysis Facility) IRAF-based scientific photometric package for the UFS / Boyden 1.5-m telescope. The dissertation consist of a discussion on the history of Boyden Observatory and its instruments, with specific emphasis on the Rockefeller 1.5-m telescope. The discussion will include information on the upgrades and improvements the telescope underwent to compete and do research on an international level.

In the proceeding chapters charged coupled devices (CCDs) will be discussed, as well as how to characterize CCD photometric observation systems, like the 1.5-m telescope. The chapters will include experimental procedures and results obtained during characterization experiments. Chapters on photometry techniques will follow thereafter as well as the development of the Boyden-IRAF photometric data-analysis system. It will include an overview of IRAF, as well as a more in depth discussion of the Boyden-IRAF package. The discussion will specify as to why and how it was developed and how it works. A final chapter will be presented on the testing of the Boyden-IRAF package through the determining of the Boyden atmospheric extinction coefficients using the newly developed package.

With this project, i.e. the development of an IRAF-based photometric program, an attempt is made to fill a void that exists related to the in-house photometric capabilities. A reliable and user-friendly photometric program will definitely also result in Boyden Observatory playing an important role in student training and research programs. Finally a conclusion will be drawn as to the success of the new developments, the IRAF-based photometric package, and what this means for the development of Boyden Observatory and the UFS Astrophysics group i.t.o. research and development.

Key words: - Photometric Pipeline, IRAF, CCD Photometry, Boyden Observatory, Rockefeller Telescope, Atmospheric Extinction Coefficients.

Opsomming

In hierdie verhandeling sal daar verwys word na die ontwikkeling van 'n (Image Reduction and Analysis Facility) IRAF-gebasseerde wetenskaplike fotometriese pakket vir die UV/Boyden 1.5-m teleskoop. Hierdie verhandeling sal bestaan uit 'n bespreking van die geskiedenis van die Boyden Sterrewag en die instrumente wat daar gestasioneer is, veral die Rockefeller 1.5-m teleskoop. Die bespreking sal bestaan uit inligting oor die opgradering en verbeterings wat die teleskoop ondergaan het om dit in staat te stel om te kan kompeteer en navorsing te doen op 'n internasionale vlak.

In die daaropeenvolgende hoofstukke sal "Charged Coupled Devices" (CCDs) bespreek word, en die metode om CCD fotometriese sisteme te karakteriseer, byvoorbeeld die 1.5-m teleskoop. Hierdie hoofstukke sal eksperimentele prosedures en resultate, verkry vanaf karakteriserings eksperimente, bevat. 'n Verdere hoofstuk oor fotometriese tegnieke sal volg, asook 'n hoofstuk oor die ontwikkeling van die Boyden-Iraf fotometriese data-analise sisteem. Dit sal 'n oorsig van IRAF, en 'n meer in-diepte bespreking van die Boyden-IRAF pakket, insluit. Die bespreking sal spesifiseer hoekom en hoe dit ontwikkel is en hoe dit werk. 'n Finale hoofstuk sal handel oor die toetsing van die Boyden-IRAF pakket deur die Boyden atmosferiese uitdowings koëffisiente te bepaal, deur gebruik te maak van hierdie pakket.

Met hierdie projek word 'n leemte gevul met betrekking tot die interne fotometriese navorsing vermoëns. 'n Betroubare en verbruikersvriendelike fotometriese program sal definitief ook daartoe bydra dat Boyden Sterrewag 'n belangrike rol speel in studente opleiding en navorsingsprogramme. Aan die einde sal 'n gevolgtrekking gemaak word wat handel oor die sukses van die nuwe ontwikkelings, die IRAF-gebasseerde fotometriese pakket, en hoe hierdie projek sal bydra tot die ontwikkeling van die Boyden Sterrewag en die UV Astrofisika-groep, in terme van navorsing en ontwikkeling.

Sleutel Terme: - Fotometriese pyplyn, IRAF, CCD Fotometrie, Boyden Sterrewag, Rockefeller Teleskoop, Atmosferiese Uitdowings Koëffisiente.

Contents

List of Figures

List of Tables

Chapter 1

Boyden

1.1 Introduction

In this chapter the history of Boyden Observatory "the first truly international observatory" (Andrews 1998), from its establishment in 1889 to the present will be discussed. There will be looked at locations, personnel, research done and discoveries made. The discussion will also include sections on the instruments used during that time, with specific emphasis on the 60-inch Boyden Rockefeller Reflector Telescope. Some of the reference materials used are web-based, and include websites such as: (Astronomical Society of Southern Africa,`http://www.saao.ac.za/assa/html/his-pl-obs_-_boyden.html`; Moore,`http://star.arm.ac.uk/history/moore/`; DFM Engineering Inc.,`http://www.dfmengineering.com/news_boyden_obsrv.html`; Abrahams,`http://www.europa.com/~telscope/tspoland.doc`). Details about the instrument's specifications, upgrades, new equipment and role as research instrument will be examined. A final section will then be devoted to where Boyden Observatory finds itself today, and where it wants to position itself in the future, specifically in terms of research and education.

1.2 A Concise History

1.2.1 The beginning

The histories of Boyden Observatory near Bloemfontein and the Harvard College Observatory are closely linked. The history of Boyden Observatory starts in 1879 when Uriah A.

Boyden, a mechanical engineer in Boston, United States of America (USA), left $238 000 to Harvard College for extending astronomical research. Only three-quarters of the sky is visible from the Harvard College Observatory, therefore the Director at that time, Prof. Edward C. Pickering, wanted to establish an observatory in the southern hemisphere, allowing access to the Magellanic Clouds. The resources provided by the Boyden Fund made this possible (Jarret 1979).

Harvard decided on South America for their southern site, where conditions were sufficient for astronomical observations. Investigations were concentrated on the west coast of South America where the climate was dry with clear skies, with locations available at high altitudes. From these required specifications, Peru was chosen to establish the Harvard Southern site (Jarret 1979). In 1889 Prof. Solon Bailey (1854-1931) undertook an expedition, encouraged by Pickering, to Peru to find sites with good weather and clean, dry atmospheric conditions. First he decided that the valley of the river Rimac near Lima would provide suitable conditions, but after careful examination it was concluded that the valley did not offer a sufficient free horizon. Furthermore a location should be used that was free from seasonal rain and cloud cover (from November to April), as well as the dense clouds from the coast (from May to November) (Jarret 1979). After careful consideration a hill near Lima was chosen, 8 miles from the small town of Chosica, and were named Mount Harvard accordingly (Jarret 1979, e.g. Calitz 2005).

The first buildings constructed on Mount Harvard were made of wooden frameworks that were covered with canvas and heavy paper. On 7 May 1889 the last of about 80 loads of freight arrived. All the equipment was carried on mules from Chosica on tracks that were especially build for this purpose (Jarret 1979). This included all the equipment - telescopes, meteorological instruments, building materials, furniture, food, and the daily supply of water. Two days later on 9 May 1889, Solon Bailey took the first astronomical photographs from the new Boyden Station (e.g. Calitz 2005).

One year later, the observatory was moved to Arequipa, Peru, (October 1890) because of unstable weather at Mount Harvard. In January 1891 Prof. Edward Pickering came to Arequipa with more equipment, including the 33cm (13 inch) refractor telescope. Observations of Mars, the Moon and the satellites of Saturn and Jupiter were made. In 1893 Bailey took charge of the Arequipa Observatory, and embarked on an observational

study of globular clusters. By 1903 the observatory's equipment included the 61 cm Bruce Astrograph telescope, but by 1908 the possibility of another site was explored because of clouds that occurred constantly from December till March along with an uneven cloud distribution throughout the rest of the year. Communication difficulties also played a role (e.g. Calitz 2005,Jarret 1979).

Important work that was done at Arequipa included those of Henrietta Leavitt (1868-1921) of Harvard. Her research of Cepheid Variable stars with the 25 cm Metcalf telescope among others, became an important foundation to the development of the Period-Luminosity relationship, which is one of the foundations of modern cosmology. Dr. Harlow Shapley's research in the early stages of 1920, related to the limits of our galaxy, was also done with photos taken with the 25 cm Metcalf telescope (e.g. Jarret 1979).

1.2.2   Boyden in South Africa

Sir David Gill recommended South Africa as an alternative site. Unfortunately very few studies were done on the atmospheric stability. After Solon I. Bailey did a thorough examination in South Africa, which included observational testing at sites ranging from Worcester, Kimberley and Hanover during 1908, Bloemfontein was chosen. The relocation of the Observatory was expensive and nothing was done for a long time until Dr. Harlow Shapley (1885-1972) received funding from the International Education Board and Harvard University. During 1923 Dr John S. Paraskevopoulos became the new astronomer in charge of Arequipa. Expeditions were also undertaken in December of 1923 and 1925 at the request of Dr. H. Shapley, to the desert regions of Chile and San José for alternative sites providing acceptable observing conditions (Jarret 1979).

After careful consideration and keeping in mind the observational backlog between December and March, the order to relocate to a hill 24 km outside Bloemfontein, was given by Dr. H. Shapley in 1923. Harvard University and the International Education Board donated approximately $200 000 each, for the relocation of Arequipa to South Africa. Observations at Arequipa, Peru, continued until November 1926, at which time the dismantling of the observatory began. In February 1927 the equipment was transported to Bloemfontein (Jarret 1979). Observations began in September 1927 and in 1933 the new site was officially completed. At that time the instruments in operation were: the 152.4

cm (60-inch) reflector, the 33 cm (13-inch) Boyden refractor and the 25 cm (10-inch) Metcalf photographic refractor, which are all still in operation at Boyden. The 61 cm Bruce Astrograph, the 20 cm Bache refractor, as well as some smaller instruments were installed but are not in operation anymore (e.g. Calitz 2005).

Dr John S. Paraskevopoulos was director from 1927 to 1951. Dr. Eric M. Lindsay went to Harvard College Observatory to study the distribution of stars in the southern sky. After the completion of his PhD in 1934 he came to South Africa for research purposes and became the chief assistant at Boyden Observatory until he accepted the Directorship of Armagh Observatory in Ireland in 1937. Boyden was known as the Harvard University's southern observatory, but in 1954 Harvard announced that it could no longer meet the expenses of the establishment and Boyden was on the verge of closing (Moore and Collins 1977). Dr. Eric M. Lindsay and Prof. Herman Brück of Dunsink observatory suggested an international sponsorship for Boyden, which led to the formation of the Boyden Council in 1955. It consisted of members from Harvard, Dunsink, Belgium, Sweden, Armagh and West Germany (Jarret 1979).

Before Jean Dommanget became the director of the Boyden Observatory in 1963 to 1965, the senior visiting astronomer took charge. These were exiting times since the Russians were very secretive about their launching of Russian probes to the Moon and Boyden was requested to report any sightings to the US Air-Force, especially any signs of retro-rockets slowing down the probe just before impact with the surface of the moon (Andrews 1998). From 1968 to 1989 Dr Alan H. Jarrett was the new director. Astronomers who did research at Boyden included B. Bok, A. G. Velghe, H. Haffner, D. Menzel, Lindsey and P. A. Wayman (e.g. Calitz 2005).

Research activities focused on photographic and photoelectric observations of stars in the Southern Milky Way, the Magellanic Clouds and southern hemisphere variable stars. Boyden is ideally situated for observations of the galactic centre and the Magellanic Clouds and became a major observational centre for this research. This is also utilized presently in collaboration with the PLANET research group (Calitz 2005). A Sky Patrol program functioned between 1950 and 1970 and was based on a related program Harvard used for the Northern Hemisphere (Jarret 1979). Routine surveys of transient phenomena such as variable and flare stars and novae were made. This program was also used to assist with

the tracking of the first satellites. Additional research fields included studies on atomic emissions from nebulae, studies of solar flares with the Coelostat and photographic and spectroscopic studies of comets (e.g. Calitz 2005).

The Boyden council functioned for many years until Sweden withdrew in 1966 because of astronomical obligations somewhere else. It was then that the University of the Free State took up Sweden's position (Jarret 1979). In 1971 West Germany also withdrew from the council and in 1974 Harvard announced their withdrawal from any association with Boyden, to be initiated in 1976. Shortly afterwards Belgium also withdrew and on 30 June 1976 the council dismantled (Jarret 1979). In April 1976 the University of the Free State (UFS) became the sole owner of the observatory (Calitz 2005). The Boyden Observatory was abandoned from international collaboration with Armagh and Dunsink within six years after Lindsay's death in July 1974. Hans Haffner and Donald Menzel who were two major supporters of Boyden Observatory died shortly after Lindsay in 1975 and 1976 respectively (Andrews 1998).

1.2.3 The last 20 years

After the retirement of Professor Jarrett in 1986, the Boyden Observatory was on the brink of being closed by the UFS. Until 1997 the observatory and specifically the 60-inch telescope were used by amateurs and a few dedicated observers primarily for educational purposes. During July 1994 the 60-inch telescope was used, with the help of a group of amateur astronomers from the Bloemfontein and Johannesburg branches of the Astronomical Society of Southern Africa (ASSA), for observations of the Jupiter Shoemaker-Levy 9 impacts. The optical images clearly showed the scars left from the impact with the Jupiter atmosphere. These images were used for television news broadcasts (Calitz 2005).

The Boyden Observatory was inactive between 1989 and 1999, but between 1994 and 1999 a program was initiated to evaluate and upgrade the 60-inch telescope. Contributors included Dr. Peter Martinez, USA astronomers, DFM Engineering and other international institutes, and a new research group at the UFS under leadership of Prof. Pieter J. Meintjes. The requirements of the micro-lens follow-up observations, as well as photometry of faint stars, demanded very accurate pointing and tracking. These requirements resulted in the UFS to approach the DFM Company, requesting the delivery of a custom-made tele-

scope control system. It was followed by the delivery of a Pixelvision CCD camera, on loan from the Lawrence Livermore National Laboratories (LLNL), in collaboration with Dr. K. Cook, principal investigator of the Gamma Ray Burst (GRB) afterglow follow-up program. An internet and LAN (Local Area Network) were also installed at the observatory to give access to fast real-time data transfer between the various institutes (Calitz 2005).

1.2.4   Location and Facilities

Boyden Observatory is located 24 km East North East of Bloemfontein on a koppie (hill) on the banks of the Modder river next to the Mazelspoort holiday resort. The Bloemfontein airport is located only 12 km away, and thus provides a convenient mode of travel to and from Boyden (Jarret 1985).

The current facilities available at Boyden include the main building, which hosts the personnel offices as well as the library, and also a house for the resident astronomer. There is also a science demonstration hall (which was the original ADH Telescope building), a new dual purpose auditorium that can accommodate 100 people indoor and 200 people outdoor on the roof pavilion for open air shows and demonstrations. The telescope buildings include the main telescope buildings, as well as secondary telescope buildings hosting non-affiliated telescopes. There are also a lecture room, a maintenance and storage building, the local amateur astronomy club's clubhouse, and various observation platforms and vantage points.

Table 1.1: A summary of the different locations of the Harvard/Boyden Observatory.

Location	Latitude	Longitude	Elevation
Mount Harvard	11° 56' 35" South	76° 42' 34" West	1980 m
Arequipa	16° 22' 28" South	71° 33' 00" West	2452 m
Boyden	29° 02' 20" South	26° 24' 17" East	1379 m

1.3 Instruments

1.3.1 The UFS-Boyden 60-inch Rockefeller Reflector

The origins of the largest telescope at the observatory are not that straightforward and can even be considered as a curious case in astronomical instrumentation history. This telescope started as a Common 5-foot (152.4 cm) reflector. Andrew Ainslie Common (1841-1903) was an amateur astronomer and telescope maker. In 1886 he began work on his first 5-foot mirror. It consisted of plate glass 61-inches (154.94 cm) in diameter, but was only 4-inches (10.16 cm) thick. It was cast with a central hole, 10-inches (25.4 cm) in diameter, to host the primary optics for a Cassegrain reflector. The 5-foot reflector had an intended focal length of 28-feet 7-inches (871.22 cm) (Ashbrook 1984).

In February of 1889 the new telescope was finally ready for use; unfortunately it produced elliptical star images even after several reconfigurations of the mirror. The poor image quality was attributed to inhomogeneities in the mirror due to streams in the glass caused during the moulding process. Common overcame this problem by ordering a second 60-inch (152.4 cm) Newtonian-configuration mirror from France in 1888. He made little use of his big telescope apart from taking photographs of nebulae, like the Orion, Dumbbell and Pleiades, because it was inconvenient to operate and light and air pollution in London caused severe seeing problems. After his unexpected death in 1903, the 5-foot telescope with its two mirrors was advertised by his executors (Ashbrook 1984).

The telescope and its two mirrors were purchased by Harvard College in 1904, because of intentions by Edward C. Pickering to continue visual photometry of stars (Ashbrook 1984). During the next couple of years the 60-inch (152.4 cm) Common telescope was installed in a small wooden building erected on the Harvard Observatory grounds in Cambridge, Massachusetts. Unfortunately the installation was not without difficulties; Pickering mentioned in his annual reports of 1906, 1907 and 1909 of continued delays and difficulties of the mounting of the telescope. In his 1914 annual report, Pickering announced the abandonment of the project due to poor image definition compared to other Harvard telescopes (Ashbrook 1984).

Dr. Harlow Shapley became the next director of Harvard Observatory in 1921 after the death of Pickering in 1919. Shapley needed a large telescope for his research on the limits

of the observable universe and star clusters (Jarret 1979; Ashbrook 1984). During 1922, Shapley had the mirrors and mounting tested with the assistance of Willard P. Gerrish in the hope of resuming astronomical projects using the telescope. However the Common 60-inch (152.4 cm) telescope was never effective in spite of their efforts (Ashbrook 1984).

One way to describe how the telescope was revived to serve as a successful astronomical instrument is to quote Ashbrook: "How startled Common would have been to hear that his 5-foot giant would be 40 years old before it became a success, and then as three telescopes rather than one" (Ashbrook 1984). The Newtonian-shape Harvard-owned Common-mirror was reconfigured in 1927 and shipped to South-Africa to be mounted in the new Boyden Observatory's Rockefeller telescope, build by the funds provided by the Rockefeller-family. Therefore it was named the Rockefeller 60-inch (152.4 cm) reflector. This telescope was envisioned to become the southern twin of a new 61-inch (154.94 cm) telescope to be stationed at the Harvard College Observatory (HCO). The HCO had a new standard two-pier mounting constructed and installed at Boyden Observatory by the well-known U.S. engineering firm of J.W. Fecker between 1927 and 1933 (Jarret 1979; Andrews 1998; Ashbrook 1984). Thus began an era of successful productivity for this new Boyden 60-inch (152.4 cm) Rockefeller telescope, with the help of one of the Common mirrors.

The Cassegrain-form mirror was first used between 1925 and 1931 at the Perkins Observatory as a loan from the Harvard Observatory. Then in 1933 that mirror was installed at the Harvard Oakridge Station in Massachusetts, to be replaced four years later by a new 61-inch (154.94 cm) mirror. The current location of that Common-mirror is unclear, but is believed to be somewhere in Texas in the USA (Ashbrook 1984).

At that time, until 1951, the Rockefeller Reflector was the largest optical telescope in South-Africa and currently it is the third largest. During the years of the International Council the interest in the Rockefeller and ADH telescopes increased, especially for spectral classification and photometric studies of galactic structure, as well as the search for OB stars, Hα emission objects and planetary nebulae. The two telescopes were used in combination, e.g. the Rockefeller Reflector was used to secure and identify standard stars, and the ADH used to search for Cepheid variables. During the active years of the 1960's, there was a fierce competition for telescope time on the Rockefeller Reflector, resulting in it being constantly occupied (Andrews 1998). During the late 1970's and early 1980's it

was used by the Department of Astronomy at the UFS to do stellar spectroscopy, using a Zeiss spectrograph that was positioned at the Newtonian focus of the Rockefeller Reflector.

In recent years, since its upgrade in 2001 and 2002, it has again been used to do research on a variety of fields. It contributed data to the study of GRBs, variable and cataclysmic variable stars, the search for extra-solar planets using the micro-lens effect, as well as the training of under-graduate and post-graduate students.

Before and after the telescope's arrival in South-Africa, it has experienced a number of improvements and upgrades. The upgrades performed on the telescope during its history in South-Africa, include:

1. Replacing of the majority of the telescope mounting in 1933 as mentioned above. Although it was in a new form (with a weight of 40 tons) the telescope was still hard to use, which was due to a too thin (only 9 cm thick) primary mirror, as well as a non-flat back surface. The normal configuration led to highly astigmatic images. To overcome this Dr. Paraskevopoulos, with the help of Ernest Burton and Michael Bester, devised a new adaptive optics system that could compensate for the mirrors flexure. This was achieved by applying pressure to three supplementary pads behind the mirror. This was the first documented application of adaptive optics, which was highly successful (Jarret 1979; Andrews 1998).

2. A new mirror cell for the Common mirror, with a better support system, designed and built by Heidenreich & Harbeck in Hamburg, Germany, was installed in the early 1960's. Unfortunately this new cell was impractical for the adaptive optics system devised by Dr. Paraskevopoulos (Jarret 1979; Andrews 1998).

3. In 1968, when Prof. Allen H. Jarret became director of the observatory, it was identified that the new mirror cell acquired earlier was designed for the housing of a perfect mirror. It also became clear that the Common mirror by that time was not suitable for modern astrophysical research. The telescope was then upgraded with a new optical system surmounting to R 200 000.00, acquired from Loomis Custom Optics, Tucson Arizona in the USA. The new optics included a new 152.4 cm Cassegrain primary mirror (weighing 4 tons), with the specified diameter/width ratio required for astronomical mirrors of that size. The new optical setup provided the possibilities for both Cassegrain (with a focal length of 2 382 cm) and Newtonian (with a focal length

of 775.6 cm) observational configurations (Jarret 1979; Andrews 1998; Jarret 1985). During the upgrade the opportunity was also taken to renovate the drive mechanisms of the telescope, which was badly worn after 40-years of service. After the completion of the upgrades the telescope was again ready to compete internationally with the best (Jarret 1979).

4. During the 1980's attempts were made to place the telescope under computer control, with the control system and motors replaced with a single micro stepped motor per axis, using commercial motor controls, and for a while the telescope was controlled by an HP85 microcomputer. Unfortunately this system was unreliable, unwieldy, difficult to use and provided no pointing information. At the time there was also a DEC 350 computer available for analysis and storage of data (Calitz 2005; DFM Engineering Inc.; Jarret 1985).

5. As mentioned earlier, a program was initiated in the late 1990's to get the telescope ready for a new era of international research. Dr. Frank Melsheimer and The DFM Engineering Company (DFM stands for Dr. Frank Melsheimer) were contracted for the upgrades to the telescope and its drive mechanisms. During 2001 a team from DFM came to South Africa to perform the required upgrades. DFM was contracted to install their proven Telescope Control System (TCS) as well as providing engineering and technical support to such an extent as to get the telescope ready for competitive research (DFM Engineering Inc.).

Through previous visits, Dr. Melsheimer acquired the specifications needed for the new secondary drives for the Right Ascention and Declination motors as well as for the new focus drive. These were then designed and manufactured by DFM Engineering. To allow repeatable precision focusing of the telescope a new focus position encoder was also added. These new systems were then installed on the telescope. The Right Ascention drive installed easily, but the Declination drive provided some problems. Machining of the Declination counterweight was needed to install and service the drives. These new drives were then controllable from new hand-paddles provided for the telescope, as well as from the new TCS computer (Calitz 2005; DFM Engineering Inc.).

The existing single speed focus motor was replaced with a DC (direct current) servo

motor. This new motor then provided duel speed operation through the new hand paddles as well as a GO TO FOCUS position capability with the TCS computer. The new 2-speed focuser allows for fast focusing as well as for precision focusing. The newly manufactured absolute focus encoder was installed at the secondary mirror to provide focus positions with 12μm resolution. This produces less than 0.1 arc second changes in image diameters per resolution element due to focusing. Successful servicing of the secondary mirror cells' attachment to the focus ram was accomplished as it affected the collimation as well as Declination position repeatability. Pointing measurements afterwards indicated that Declination pointing of better than 10 arc seconds RMS (root-mean-square) could now be achieved (Calitz 2005; DFM Engineering Inc.).

The new TCS system also included an automatic dome control feature, which was achieved by encoding the dome to provide azimuth position information. The existing dome motors were interfaced to the TCS system to control the dome through the new hand-paddles or automatically through the TCS. The dome drive gear reducers were also serviced during that time (Calitz 2005; DFM Engineering Inc.).

The final modifications to the telescope were to the primary mirror cell. The existing radial supports were repaired, and the mirror cells' design was enhanced by replacing three of the 36 counterweighted mirror lever supports by three adjusting screws to allow for tip/tilt and centering of the mirror, which allows collimation of the optics. After the new upgrade was completed, the telescope was thoroughly tested, balanced in 4 axes, pointing measurements made (resulting in accuracies of 25 arc seconds RMS), and the Boyden personnel trained in its use and maintenance before it was declared ready for use in 2002 (Calitz 2005; DFM Engineering Inc.).

The telescope also had a number of different attachments throughout its history. This was because of the ease with which a changeover could be made between different attachments, depending on research requirements at that time. Attachments included and currently in operation are:

1. Initially the telescope was used with visual fittings for visual photometric studies of stars. Later photographic plates were added (Jarret 1985).

2. During the upgrades of the new optics during the late 1960's photoelectric photometers was acquired for the telescope for new UBVRI photometric research activities, like variable star observations. An image tube camera could then be mounted at the Cassegrain focus (Jarret 1985). A spectrograph was also available for spectroscopic studies.

3. A Jena Universal Grating Spectrograph, from the Zeiss company, which was in operation by the late 1970's, was also used for studies of stellar spectra. The spectrograph had gratings for dispersions from 70 Å/mm - 280 Å/mm. The Schmidt camera on the spectrograph had a focal length of 110 mm and an aperture of 125 mm. The spectrograph is currently stored at the Department of Physics at the UFS (Jarret 1979; Andrews 1998; Jarret 1985).

4. By 1985 accessories included a Celestron 8 (20 cm, f/10) which was piggy-back mounted, making it possible to take standard 35 mm field photographs, as well as an intensifier video monitoring system that could be attached either on the 20 cm finder telescope or at the Cassegrain focus (Jarret 1985). The Celestron 8 was later removed to be used independently, and the 20 cm finder was replaced with a 15 cm finder. Also mounted on the telescope is a 41 cm Eloptro Cassegrain telescope which was installed by Laser M to be used in Laser measurements of the earth-moon distance. There is also a SBig ST-7 CCD camera.

5. During the upgrades of 2001, a ST-6 autoguider CCD camera was installed at the Cassegrain focus of the telescope. Unfortunately this autoguider never really worked very effectively, and is currently not in use. Fortunately the telescope pointing and tracking is of such a precise and accurate nature that the lack of an autoguider proved to be non-critical.

6. During the upgrade, a photometric filter-wheel was also installed containing Kron-Cousins filters for UBV and Johnson-Kron-Cousins filters for RI. It also contains a Clear-filter, and a pinhole and has a closed position to protect the CCD camera during inactivity. At this stage, efforts are being made to replace the current filter-wheel controller system from a computer ISA card and encoder box, to a custom made encoder box that is to be mounted on the filterwheel assembly. This encoder will then connect to the control system through a serial port to be controlled by custom software.

7. A Pixelvision CCD camera, on loan from the Lawrence Livermore National Laboratories (LLNL) was installed during 2002 onto the new autoguider and filterwheel assembly at the Cassegrain focus. Unfortunately, only a few years after installation, one of the control cards for this camera experienced an irreparable technical fault, causing the camera to produce poor quality data. Although it was a high quality camera, this error resulted in the replacement of the camera.

8. Since a CCD camera was still required for photometric research, especially for the Planet search program, an Apogee AP-10 CCD camera was acquired on loan from the Lawrence Livermore National Laboratories (LLNL), to replace the defective Pixelvision camera system. Unfortunately the mechanical shutter on the camera proved problematic, leading to poor data acquisition. This compelled the research program to acquire a new CCD camera.

9. In 2006 an Apogee U55 back-illuminated CCD camera was bought for the telescope. Results to date show good quality data. Regular servicing of the optics (re-alluminization), good seeing conditions and correct observational procedures would produce good research quality data. This CCD system and its characteristics, specifically for application in photometric research will be discussed further in Chapter 2 and Chapter 3.

The UFS-Boyden 60-inch Rockefeller Reflector went through different stages of form, use and effectiveness in its history. With the current drive from the new group of astronomers and astrophysicists that want to use it for research purposes, it is being revived into service, like an old warhorse to again become a dependable competitor in the international scene of Astronomy and Astrophysics, until such a time arrives that it is finally retired in a museum to stand in all its glory after acquiring decades of data and interesting stories. The current scenario considering the 1.5 m Rockefeller telescope is summarized in Table 1.2.

Table 1.2: A summary of the technical information for the Rockefeller Reflector

Primary type and diameter	Cassegrain	152.4 cm
Focal length	Cassegrain Newtonian f-ratio Plate Scale	2382 cm 775.6 cm f/15.63 8.66 arcsec/mm
Mass	Structure Primary mirror	40 tons 4 tons
Driving mechanisms Tracking	DFM TCS system Precise RA and Dec	Hand paddle Computer controlled Automatic dome control
Accessories	External mountings Cassegrain focus	Finder telescopes Other photographic telescopes ST-6 Autoguider CCD Filter wheel with Kron-Cousins UBV filters, Johnson-Kron-Cousins RI filters, C-filter and Pinhole and Closed positions Apogee U55 Back-illuminated CCD camera
Accessories	Note	With ease of changeover between fittings it is possible to mount other types of measuring devices.

1.3.2   Other facilities, instruments and equipment

Although the Rockefeller Reflector is the largest, and currently the main focus in terms of astrophysical research at the observatory, it is not the only instrument to be hosted at the observatory. Following is a history and description of all other facilities, instruments and equipment stationed at Boyden during its lifetime.

The 61 cm Bruce Astrograph

This telescope was built and completed by the firm Alvan-Clark and Sons in 1894. Preliminary testing and trails were completed at Cambridge, before it was moved to Arequipa and mounted in 1895 by Prof. Bailey. With its wide field, the telescope was used for the production of photographic star-atlases to very faint magnitudes. At the turn of the

century (1904) this telescope was the most powerful instrument of its type in the world. It was stationed at Arequipa until the closing of the station in 1927. During the transfer of the equipment to South Africa, the opportunity was used to acquire a new mounting. Thus the telescope was first sent to Pittsburg, Pennsylvania (USA) for the construction of a new Fecker mounting. This was needed because the original mounting, which was of a open fork type, tended to flex. The new mounting consisted of a more rigid two pier arrangement. This telescope remained in operation until 1950 when it was replaced by the 91 cm Baker-Schmidt. The dismantled telescope was returned to Harvard University for safe-keeping (Jarret 1985).

The 91 cm ADH Baker-Schmidt Telescope

The 91 cm Baker-Schmidt telescope was called the ADH, because it was a co-operative venture between the Armagh, Dunsink and Harvard Observatories. The scheme for this telescope was initiated by Dr's Lindsay and Shapley between 1946 and 1947. It was a modification of the famous Schmidt telescope principle, and was designed by Prof. James Baker of Harvard University, thus the Baker-Schmidt type telescope. It was installed on the Fecker mounting of the Bruce telescope and was completed and in operation by 1950. By 1951 it hosted the world's largest spectroscopic prism of 84 cm in diameter, which led to it being the largest wide-angled instrument with an objective prism in the southern hemisphere at that time. The telescope had a flat field of nearly 5 degrees. It was used extensively for research of the Large and Small Magellanic Clouds. It operated for over a quarter of a century, before it was dismantled in the late 1970's, with the optics along with the great 84 cm objective prism being transferred to Dublin, Ireland for safe-keeping (Jarret 1985; Andrews 1998; Moore).

The 41 cm Nishimura Cassegrain Reflector

The 41 cm Nishimura telescope with its focal length of 800 cm was installed at Boyden by Harvard between 1963 and 1965. It was installed for the purpose of doing multi-colour narrow-band photometry of solar system planets. By 1966 it was used for photoelectric monitoring for multi-wavelength studies of UV Ceti-type flare stars (Andrews 1998). In later years, around the 1980's, it could be operated manually or by HP85 microcomputer. The telescope was also fitted with a manual UBVRI photometer, which could be CO_2 cooled (Jarret 1985). The telescope is still at Boyden, but is inactive and mounted on the 41 cm Newtonian mounting.

The 41 cm Newtonian Reflector

This 41 cm Newtonian telescope with its focal length of 220 cm had a semi-automated light weight photometer, with the possibility of a variety of standard filter permutations (Jarret 1985). The telescope was mounted on a Fecker mounting. The telescope itself was, along with the Nishimura mounting, sold to a private collector. The Nishimura telescope was then mounted on the remaining Newtonian mounting.

The 41 cm Watcher Robotic Reflector

The 41 cm Watcher Robotic Reflector was installed and mounted by the University College Dublin (UCD), Ireland during 2006 and was in operation by 27 March 2006. It is to be used for GRB afterglow follow-up programs. It was originally mounted using a Millennium robotic mounting, but this mounting caused some problems and the telescope was thus remounted on a Paramount robotic mount. It is a Classical-Cassegrain with Ritchey Crétien Optics, a thermally stable carbon fiber tube, and an Apogee AP6E CCD camera at the Cassegrain focus for photometric observations. The system also has a set of Johnson UBVRI filters. The telescope and dome are both controlled through a system of computers that determine observational programs according to alerts from the Gamma-ray burst Coordinate Network (GCN) and the local weather conditions acquired from an on-site weather station (Hanlon et al. 2006ba).

The 33 cm Boyden Refractor

The 33 cm Alvan-Clark refractor with its 482 cm focal length and 42.4 arcsec/mm plate scale is still used extensively even after a century of extensive use. It was the first instrument obtained from the capital of the Boyden fund, and after its completion by the famous telescope making firm Alvan-Clark and Sons, it was moved to Willows, California to be used in the total solar eclipse expedition of 1 January 1889. It was thereafter set up on Mount Wilson by Edward S. King and R. Black. On 11 May 1889, at Mt. Wilson near Los Angeles, the first photographs were obtained through this telescope. The telescope arrived in Arequipa in 1891, along with Prof. Pickering, to be used for studies of bright spectroscopic binaries as well as variable stars in globular clusters. Its unusual design, which was an ingenious scheme proposed by Prof. Pickering in association with the Alvan-Clark firm, proved to be extremely useful. It consisted of a reversable configuration where, with the objective lens in one configuration, it could be used visually, and then by

reversing one of the components it becomes corrected for photographic work. It was then also one of the instruments that came to South Africa during the 1927 transfer (Jarret 1985). This telescope was used along with the 25 cm Metcalf Triplet in the final touches of the Henry Draper (HD) catalogue, the so-called HD extension (HDE). This involved the spectroscopic survey of stars of up to 8.5 magnitude over the entire sky. This as well as other work done at Boyden Observatory, during its early years, made Boyden Observatory world famous specifically as the centre for photographic spectroscopy in the southern hemisphere (Andrews 1998). The telescope is now permanently set up for visual observations, with a manual variable tracking control system on the right ascension axis. A 20 cm Clark Refractor, as well as three smaller finder telescopes are also mounted on the telescope. It is unclear when the 20 cm Clark was mounted on the 33 cm Refractor, but it might have been since the very beginning. It has been used in parallel with the 33 cm Refractor for a number of research studies, as it also had photographic capabilities. The spectroscopic prisms for both of these telescopes are still at Boyden. These telescopes are used by staff for educational purposes during public outreach programs of the Boyden Science Centre.

The 25 cm Metcalf Triplet

The 25 cm Metcalf telescope with its 124 cm focal length, plate scale of 167 arcsec/mm and field of 7.5°, has a triplet objective for quality definition over its large field of view. The objective was ground and figured by Reverend J.H. Metcalf. Rev. Metcalf became associated with Prof. Pickering in Taunton, Massachusetts (USA), where Rev. Metcalf lived at a later stage of his life. There was also a 2.5° angle objective prism available for the telescope. Also piggy-back mounted on the telescope were two patrol cameras. They were the 7.6 cm Ross-Fecker Patrol Camera, with a 53 cm focal length, 390 arcsec/mm plate scale and a 17.3° field, and the 3.8 cm Cooke Patrol Camera, with a 33 cm focal length, 600 arcsec/mm plate scale, and a 26.7° field. All three of the instruments used 16 cm x 16 cm photographic plates (Jarret 1985). The Metcalf telescope is still used occasionally for wide star field demonstrations as well as historical presentations during public outreach programs of the Boyden Science Centre.

The 20 cm Bache photographic refractor

The 20 cm Bache telescope's objective-lens was originally a Voigtlander portrait lens. The lens was then refigured by Alvan-Clark and Sons to a 20 cm aperture f/6 with a 114.6 cm focal length, giving it a plate scale of 2 cm equivalent to 1° (Abrahams). This telescope

was in constant use since 1886. Initially it operated for several years at Harvard College observatory, after which it was moved to Mount Harvard, Peru in 1889 where it was stationed for one and a half years. Thereafter it was moved to Arequipa. Prof. Pickering used spectra obtained with the telescope for his monumental work on the classification of stellar spectra (Jarret 1985). The telescope was sent to Torun, Poland, in 1954 as a long term loan to the Observatory of Nicolaus Copernicus University. Also sent along with the telescope were two 6° objective prisms (Abrahams).

The 20 cm Coelostat

The 20 cm Coelostat solar telescope, which was installed at Boyden between 1968 and 1972, is configured to feed light from the coelostat into a 15 cm horizontal refractor telescope into a "Dark-Room". It was used during the 1970's by Prof. A.J. Jarret for studies of solar limb prominences. There are still facilities for narrow band H_α investigations of solar features (Jarret 1985), as well as a CCD camera hook-up to a desktop computer station. The Coelostat is used during public outreach programs of the Boyden Science Centre. It is also used for Sun-spot measurements and transit phenomena by members of the local Astronomical Society of Southern Africa.

Other

There were also some smaller instruments stationed at Boyden throughout its lifetime. These included the 2.5 cm Cooke Telescope. This small aperture telescope was used for photographic surveys of the sky. There was also the Boyden Meridian Telescope, which was used to determine longitude, and from there accurate sidereal times and universal times, for observations of phenomena like transits and occultations. There are still some smaller instruments stationed at the observatory, along with other instruments from local researchers and interested parties. These include a number of smaller mobile instruments, amongst others a pair of 20 cm Schmidt-Cassegrain telescopes, used at the science centre for public outreach and educational purposes.

Table 1.3: Summary and Technical information of Boyden Instruments

Name (Years active)	Type	Pri. Dia.	Focal length	F-ratio	Plate scale	Field
Bruce Astrograph (1893 - 1950)	Reflector	61 cm	341.6 cm	f/5.6	60 arc-sec/mm	
Baker-Schmidt / ADH (1950 - 1970's)	Reflector	91 cm	303.2 cm	f/3.75		5°
Nishimura Cassegrain (1965 - 1989)	Reflector	41 cm	800 cm	f/19.5		
Newtonian (? - 1989)	Reflector	41 cm	220 cm	f/5.4		
Watcher Robotic (2006 - Present)	Reflector	41 cm	570 cm	f/14.25		14.5 x 14.5 arcmin^2
Alvan-Clark (1889 - Present)	Refractor	33 cm	482 cm	f/14.6	42.4 arc-sec/mm	
Metcalf Triplet (1915 - Present)	Refractor	25 cm	124 cm	f/5	167 arc-sec/mm	7.5°
Ross-Fecker Patrol (1928 - 1952)	Camera	7.6 cm	53 cm	f/7	390 arc-sec/mm	17.3°
Cooke Patrol (? - 1989)	Camera	3.8 cm	33 cm	f/8.7	600 arc-sec/mm	26.7°
Bache Photographic (1885 - 1954)	Refractor	20 cm	114.6 cm	f/6	179 arc-sec/mm	
Coelostat (1970 - Present)	Solar	20 cm				

Computing Facilities

In 1985 a HP125 computer was used for stand-alone data analysis and graphics. A modem link was also available between the observatory and the University of the Free State (UFS) Computing Centre main-frame Univac 1106 computer (Jarret 1985). Current (2007) computing facilities include a dedicated data acquisition computer, and dedicated data analysis desktop servers. There are also a Fast-Ethernet LAN at the observatory and a microwave network connection to the UFS Network Server for data transfer between the observatory and the Department of Physics, as well as local and international collaborators.

Measuring equipment

A Joyce Loebl Micro-densitometer (Mark III C), an Askania Iris diaphragm photometer and a Pye two-dimensional measuring microscope (Jarret 1985) is not in use any more and is in storage.

Photographic equipment

Darkroom facilities and equipment were available, including hypersensitization facilities as well as a tube sensitometer (Jarret 1985). The darkroom facilities at the 152.4 cm Rockefeller telescope were still used occasionally in the recent past.

Aluminizing Facilities

An on-site aluminizing facility with a vacuum tank capable of aluminizing mirrors up to 152.4 cm in diameter, was acquired by Prof. Jarret in 1979 specifically for the Rockefeller Reflector, thus adding a final technical requirement for an observatory (Jarret 1985; Andrews 1998). This facility was never used for aluminizing of the Rockefeller Reflector optics, and was dismantled during Boyden's inactive period because of technical and financial difficulties.

1.4   Today and Tomorrow

Currently Boyden Observatory serves a two-fold function, i.e. a research facility associated with the Physics Department of the UFS, as well as an educational centre. In this sense it hosts two different but equally important groups, namely the Department of Physics Astrophysics Group and the Boyden Science Centre. These two groups play a fundamental role in the development and improvement of the Boyden Observatory.

The Boyden Science Centre

The Boyden Science Centre was started with the aim of both improving the Boyden Observatory and the effectiveness of the public outreach programs of the UFS in terms of Science and Technology. It reaches over 6 000 school learners, as well as university students and other broader public groups per year. The developments to the Observatory's infrastructure for the Science Centre because of received sponsorships include a new auditorium. It

has seating for 100 people inside, with quality sound and media presentation equipment, and seating for 200 people on the roof for open air presentations. A new Educational Walk around the Boyden Observatory, introduces visitors to the Observatory, its history as well as its fauna and flora. A new "story telling area" was completed recently at the observing platform, as an extension of the Charl van der Merwe Educational Walk. Future plans for the Science Centre include a small planetarium, the completion of the Educational Walk, as well as other development projects. Establishing a museum at the Observatory is envisioned to preserve its rich and wonderfull history. The completed Science Centre is aimed to reach in the region of 10 000 people per annum, without interfering with the day-to-day research activities of the Observatory. Hopefully some of the young visitors to the Observatory could be motivated to become the scientists, specifically astronomers and astrophysicists of the future.

The Astrophysics Group

The Astrophysics Group of the Department of Physics of the UFS is currently active in the Planet Search program, as well as other post-graduate research projects, concentrating specifically on galactic and extra-galactic accretion driven systems. The group also participates in multi-wavelength studies of astronomical objects, with specific emphasis on the more exotic systems. The group is constantly growing since the re-establishment and re-opening of the Boyden Observatory. The group is currently upgrading the research infrastructure of the observatory, specifically the Rockefeller Reflector, as well as developing new high computing facilities for theoretical modelling. The research emphasis is leaning towards multi-wavelength studies. With this project, i.e. the development of an IRAF-based photometric program, an attempt is made to fill a void that exists related to the in-house photometric capabilities. A reliable and user-friendly photometric program will definitely also result in Boyden Observatory playing an important role in student training and research programs.

Chapter 2

The Charge-Coupled Device (CCD)

2.1 Introduction

In this chapter the history, function and characteristics of Charge-Coupled Devices (CCDs) will be discussed. How they work, how they are used in astronomy, and how they are characterized and tested will also be examined. This discussion will be based to a large extent on web based technical discussions and guides from Apogee Instruments Inc (`http://www.ccd.com/`).

2.1.1 History of CCDs

Before the advent of digital electronics, astronomers used imaging tubes and photographic plates. Although plates and film offered excellent resolution and a choice of detector size, they were highly non-linear. Furthermore they had a very low quantum efficiency (the efficiency of a detector in recording radiation) (Ridpath 1997). In 1969 W. Boyle and G. Smith invented the Charge-Coupled Device (CCD) at AT&T Bell Labs, which was introduced to the world with a pair of papers in 1970 in the Bell System Technical Journal. It was initially developed to serve as a serial memory device. They initially called the design 'Charge "Bubble" Devices'. It was to be an electronic analogue to the magnetic bubble memory used at that time. The design was developed so that the semiconductor had the ability to transfer the developed charge along the surface of the semiconductor. It was soon clear however that the device could not only be charged via a direct input register, but could also receive charge via the photoelectric effect, therefore allowing the creation of digital images.

In 1970 Bell researchers acquired images using simple linear devices, the first CCD. By 1974 companies, like Fairchild Electronics, had commercial devices available, such as a 500 element linear CCD and a 100 x 100 pixel 2-Dimensional CCD. These early CCD devices were unfortunately still very inefficient with quantum efficiencies of the same order as photographic plates at that time. But by 1979 with the installation of a much more efficient (up to 50 times more than photographic plates) RCA 320 x 512 LN_2 cooled CCD system on the 1-meter telescope at the Kitt Peak National Observatory, the CCD as an astronomical research instrument was launched (Janesick and Elliot 1992).

2.1.2 CCDs in Astronomy

For photometry a photometer is used, which is a device used to measure the brightness of stars and other objects. For accurate photometric studies, electronic devices, like CCDs, are preferred above photographic, because their characteristics are better. That is, their small size and weight, low power consumption, ultra low noise, linearity, dynamic range, photometric accuracy, broad spectral response, quantum efficiency or sensitivity to light, geometric and temperature stability, reliability and durability. CCDs also have no reciprocity failure unlike photographic emulsion, i.e. the increasing inefficiency of the photographic emulsion with increasing exposure time. Current CCDs have a high quantum efficiency (QE) across much of the visible spectrum, are highly linear, responsive and come in a wide range of specifications. They also offer the advantage of almost immediate availability for display and data analysis after exposure. Because the data are in digital format, the data images could also be enhanced using different image processing techniques (Ridpath 1997; Howell 2006; Janesick and Elliot 1992).

2.2 Structure – How they work

The CCD consists of a semiconductor (mostly silicon-based (Si)) chip, containing an array or grid of light sensitive diodes or cathodes. The structure of the CCD is thus made up of these diodes/cathodes arranged as individual pixels in rows and columns. These pixels become charged when they are irradiated with light. The charged pixels then utilizes the absorbed photon energy to release an electron, thus creating an electron-hole (e^- - h^+)

pair within the semiconductor, via the photoelectric effect (e.g. Ridpath 1997; Beiser 2003; Janesick and Elliot 1992 for a discussion). The physics behind the photoelectric principle utilized in digital imaging CCDs is the creation of an electric current in a light sensitive material when it is irradiated with photons. One of the properties of semiconductors is their specific energy gap or band gap between the valence and conduction energy bands, with Si having a band gap of $E_g = 1.14$ eV. Incoming photons interact with the Si atoms and can excite valence electrons from the valence band into the conduction band, thus creating a electron-hole pair. The number of electron-hole pairs that are created depends on the energy of the incoming photon. The energy of the photon for a given frequency is

$$E(\text{eV}) = h\nu. \tag{2.1}$$

Here E is the photon energy, h the Planck constant, and ν the frequency of the incident photons. The kinetic energy of the ejected electrons resulting from the irradiation is given by Einstein's equation

$$KE_{max} = h\nu - \phi. \tag{2.2}$$

Here ϕ represents the work function of the material/semiconductor. The work function of a material is the minimum energy needed to produce a photoelectron or an electron-hole pair. This critical energy can be defined by a critical photon frequency ν_0 as (e.g. Beiser 2003; Janesick and Elliot 1992)

$$\phi(\text{eV}) = h\nu_0. \tag{2.3}$$

These work functions can be defined in semiconductors as the energy gap E_g. The greater the energy gap, the higher the required photon frequency to produce a photoelectron or electron-hole pair in the semiconductor material. The definition for the work function can then be used to redefine the maximum photoelectron energy as (e.g. Beiser 2003; Janesick and Elliot 1992)

$$KE_{max}(\text{eV}) = h(\nu - \nu_0). \tag{2.4}$$

The number of photoelectrons n_e created versus the number of incident photons n_p will depend upon the efficiency of the semiconductor to utilize this maximum photoelectron energy. The photoelectrons or electron-hole pairs created are then free to diffuse and move in the crystal lattice structure of the Si-semiconductor, with Si having a diamond (tetrahedral) crystal structure. The lifetime of these charge carriers, when created in high-quality Si are of the order of 100 μs or more, after which the electron-hole pair will recombine.

Photons with energies from 1.1 - 5 eV will create single electron-hole pairs in Si, whereas photons with energies greater than 5 eV will generate multiple pairs. The greater the photon energy, the more electron-hole pairs are created, with single soft x-ray photons (100 eV - 10 keV) being capable of producing hundreds to thousands of photoelectrons. The usefulness of this photoelectric capability of semiconductors is dependant on the energy range where the semiconductor material is non-transparent to the incoming photons, with Si having a energy range of 1.1 eV to 10 keV, or a spectral range from the near infrared (NIR), through the visible to soft x-ray energies. At the NIR cut-off the photons do not have enough energy to lift the valence electron into the conduction band, and at the soft x-ray cut-off the probability of interaction with the incident photons with the Si atoms is small. Because of this property, the type of semiconductor material used for the CCD will be dependant on the research requirements (e.g. Ridpath 1997; Beiser 2003; Janesick and Elliot 1992).

Because the digital image or "photo" is made up of the corresponding charge associated with each individual pixel, the photoelectrons must be held within the pixel where they were produced. Each pixel represents a potential well containing the total electric charge generated up until read-out. This is achieved by applying metal electrodes called gates to the semiconductor, which are arranged as arrays in each individual pixel. Along with a thin separation layer consisting of an electric insulator, a parallel plate capacitor-like structure is then created. The charge is thus stored in the depletion region of the metal insulator semiconductor (MIS) capacitor, which turns each pixel into an electrostatic potential well. This process of turning the pixels into electrostatic potential wells, is because of the short lifetime of the electron-hole pairs in the semiconductor. The created photoelectrons have to be "captured" for measurement before recombination can occur. This means that the longer the CCD is exposed to incident photons, the more photoelectrons will be captured inside the potential wells. From the above discussions it could therefore be seen that the amount of charge/electrons created in the pixels depends on the photon flux as well as the exposure time (Ridpath 1997; Janesick and Elliot 1992).

The total charge (number of electrons) that a pixel can hold is called the well depth. The well depth of a CCD depends on its structure, but can vary from 85 000 electrons to over 450 000 electrons. After exposure, the charge of each pixel must be measured. The pixels are read out, column by column, to provide an analogue signal by moving the

charge of each row to the readout section or register at the edge of the CCD by "clocking" the pixel gates. The register is then read out to an output amplifier where it is counted and converted by an analogue to digital converter (ADC) from an analogue signal to a digital signal for display and storage purposes. The CCD pixels are then reset for the next exposure sequence (Ridpath 1997; Janesick and Elliot 1992). See Figure 2.1 for a graphical representation of the readout process.
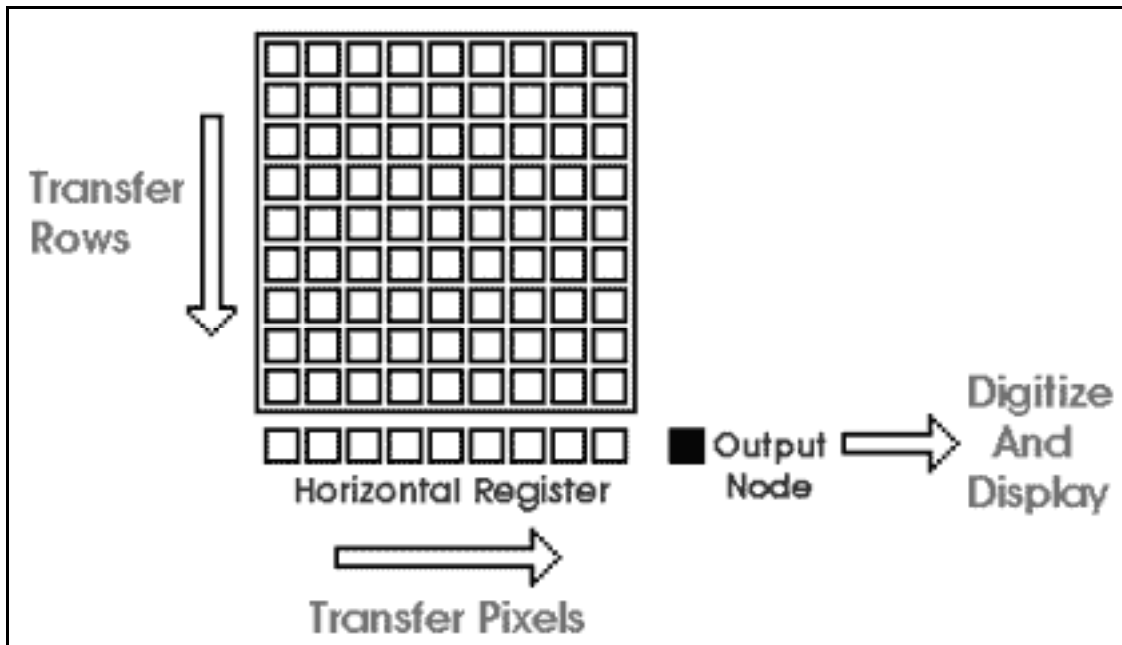
Figure 2.1: CCD readout mechanism. (Apogee Instruments Inc. b)

The measured signal, consisting of the counted analogue to digital units (ADU), is represented on the computer screen as a gray scale, with minimum charge equal to black and maximum equal to white. These photos or images can be used to do astronomical and astrophysical research and analysis (Ridpath 1997; Janesick and Elliot 1992).

Architecture

There are a variety of different architectures implemented for CCD image detector construction. The most common are full-frame, frame-transfer and interline. These architectures' main distinguishing characteristic relates to how the shutter is approached (e.g. Howell 2006 for a general discussion).

26

1. Full-frame: In this device the whole image area is active, and no electronic shutter is present. A mechanical shutter is needed for these kind of devices, to eliminate image smear during read out or clocking.

2. Frame-transfer: In this device half of the CCD image area is covered by an opaque mask (usually aluminium). The image is then quickly transferred to the opaque or storage area from the image area, with acceptable smear of a few percent. Thus no mechanical shutter is needed. The stored image is read out while a new image is exposed on the active area. Unfortunately these CCDs are expensive.

3. Interline: In this device every other column of the image area is covered by opaque masks, thus serving as storage. With this kind of architecture, however, 50% of the image area is lost. But with only single column readout from image to storage, microsecond exposures are achievable and smear is essentially eliminated. The design, unfortunately, creates a fill problem; This is because the image area is covered by opaque strips, the "fill factor" drops by half, along with the QE. The "fill factor" is the ratio of the light sensitivity area to the total size of the pixel. The fill problem has been addressed in modern designs, by adding microlenses to the surface of the CCD, to direct the light to the active regions. This technique can bring the "fill factor" up to 90%, thereby improving the efficiency of the CCD.

Front-Illuminated (FI) vs Back-Illuminated (BI)

Front: Because of their physical thickness (200-300 microns), FI CCDs have a small spectral range that includes the near IR (7 000 - 11 000 Å), visible (4 000 Å - 7 000 Å), and some of the x-ray spectrum (1 Å - 100 Å). FI CCDs are also more sensitive in the red than the blue wavelengths. This is because the absorption depth of blue photons in Si is 2000 Å , while the insulation gates of the electrodes are 5000 Å thick. Therefore many blue photons are absorbed before they can penetrate the gates. FI CCDs were used throughout the 1980's (Janesick and Elliot 1992).

Back: BI CCDs have a wide spectral range, which include the near IR (7 000 - 11 000 Å), the visible (4 000 Å - 7 000 Å), the UV (1 000 Å - 4 000 Å), the extreme UV (100 Å - 1 000 Å) and the soft x-ray (1 Å - 100 Å). BI CCDs are produced by thinning the CCD from 300 microns down to 10 microns. The CCD is mounted upside-down allowing the backside to be exposed to light, specifically blue photons, allowing the photons to reach the

electrode without being absorbed by the gate. This greatly increases the QE of the CCD in the blue and ultraviolet, without much sacrifice to the QE in the red. Most modern CCDs are BI (Janesick and Elliot 1992).

2.3 CCD Characteristics

Quantum Efficiency

The response of a detector to illumination of different wavelengths of electromagnetic radiation, determines its quantum efficiency (QE), with an ideal detector having a quantum efficiency of 1. As mentioned above, back illuminated CCDs have a better QE than front illuminated CCDs. Back illuminated CCD systems can have efficiencies from 0.6 - 0.8 or more, therefore they can record very faint objects during short exposures. They can also detect very small variations in the light received from the measured object.

A detector's QE measures the photon loss, which includes: Reflection loss at the surface of the detector, loss by the absorption in the gate electrodes, loss in the gate insulator, loss of carriers via recombination in the semiconductor substrate, and the lack of sufficient photon-absorption in the material on which the CCD is built, for wavelengths in the near-infrared and X-ray. Figure 2.2 illustrates the QE curves for different CCDs (Ridpath 1997; Janesick and Elliot 1992).

Other factors, for instance compensating for blooming effects (to be discussed next), also influences the QE of a detector. CCDs with anti-blooming have about half the QE of CCDs without anti-blooming. A systems' QE is sometimes expressed as a percentage. (Ridpath 1997).
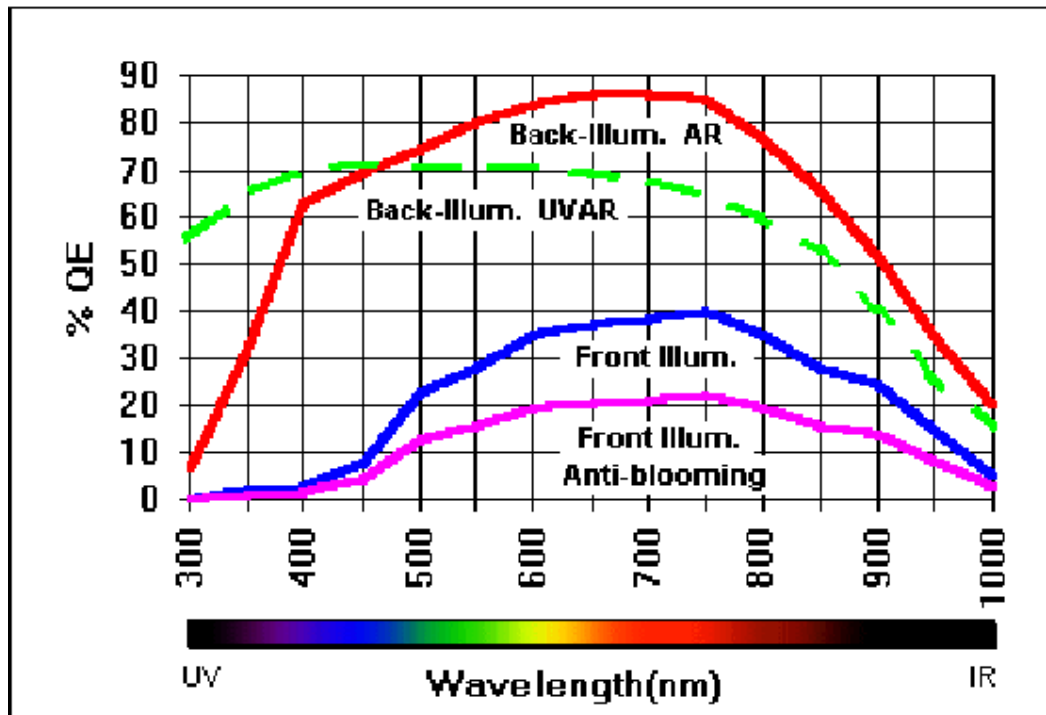
Figure 2.2: Typical QE curves for FI and BI CCDs (Apogee Instruments Inc. b)

Blooming and Anti-Blooming

Blooming is a defect that can occur in CCD images when observing bright objects. It appears as long bars on the sides of the bright source on the image, and is caused when charge spills over into adjacent pixels from the saturated pixels. This blooming effect can become a serious problem when the saturation bars bleeds into the program object, causing data corruption with no way to recover the lost data (Ridpath 1997; Janesick and Elliot 1992). See Figure 2.3.

Currently there are CCDs available with optional anti-blooming gates. These gates are designed to bleed off pixel saturation overflow. Unfortunately these anti-blooming gates reduce the sensitivity of the detector, with the gate structure occupying 30% of the pixel area. This results in a 70% fill factor, reduced sensitivity and reduced well depth. The gate structure also leaves a large gap between pixels reducing the effective resolution of the detector (Janesick and Elliot 1992).

Figure 2.3: Example of ccd blooming of bright source.

The drawbacks associated with anti-blooming CCDs have to be weighed against the research requirements. Blooming can, however, also be overcome through techniques like image stacking. That is; instead of taking long exposures with the risk of blooming, short exposures could be used where the brightest objects have not yet begun to bloom. To get the same signal to noise (S/N) ratio as the long exposures the technique of image stacking is used. This eliminates the necessity for an anti-blooming CCD.

Digitization

To be recognized by the computer, the CCD charge should be in a binary form. The process by which this is accomplished, is called digitization, which is also referred to as analog to digital convertion. Binary refers to the base 2 number system, thus for a 12 bit camera the output will be 2 raised to the 12th power or 4 096 levels. Most modern CCD cameras uses 16 bit digitization, which gives a value of 65 536 levels, with modern image processing software having the capability of scaling the raw data into the gray scale levels

available on the computer system used. Image scaling algorithms used for this processing includes: histogram equalization, gaussian, linear and minmax. For systems requiring high dynamic range detectors, 14-16 bit digitization is preferable and systems requiring higher readout speeds, 8-12 bit digitization could be used with the acceptable loss of dynamic range. The speed of system throughput depends on the digital resolution, with an increase in resolution leading to a slower system throughput. The appropriate digitization required for the specific system are determined by factors like the well depth, readout-noise and system gain.

Charge Transfer Efficiency

CCD image acquisition occurs through the transfer of pixel rows to an output register, followed by a charge transfer to an output node, where it is digitized and then transferred to the computer for display. There will however be a less than perfect transfer efficiency, with a small loss in electrons during charge transfer. This loss is quantified by the Charge Transfer Efficiency (CTE) of the CCD, and is defined as: The measure of the ability of a detector to transfer charge from one pixel to the next. CTE is therefore a CCD detector level specification and is detector dependant, with an improper camera system design causing a less than optimum charge transfer efficiency. A CCD, for instance, with a CTE of 0.99997 and a well depth of 85 000 electrons, has a loss of 2.5 electrons out of the 85 000 electrons that is not transferred to the computer display. The 2.5 electrons is lost through electron-hole recombination, or dribbles out as a deferred charge in trailing pixels (Janesick and Elliot 1992).

Pixel Binning

On-chip pixel binning is possible because of the mechanisms by which charge transfer on a CCD is performed. Binning is the process by which a super pixel representing the charge within an area of a group of individual pixels, is created. That is, most CCDs have an ability to clock multiple pixel charges in both directions, therefore creating a single larger charge or super pixel: Pixel binning of 1x1 means that the individual pixel is used as is. Pixel binning of 2x2 is achieved by combining the area of 4 adjacent pixels into one larger pixel, with 3x3 binning using 9 pixels and so forth. This is illustrated in Figure 2.4.
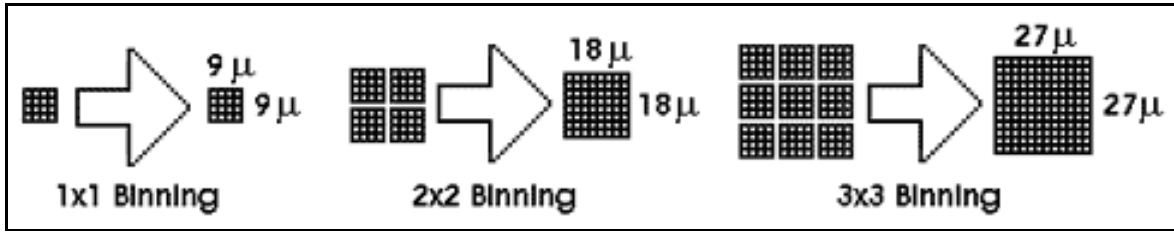
Figure 2.4: Illustration of binning effect. (Apogee Instruments Inc. b)

Binning is used to increase the CCDs light sensitivity, with 2x2 binning increasing the light sensitivity 4 times. Unfortunately pixel binning decreases the CCD resolution by the reciprocal of the sensitivity. Pixel binning is a good mechanism used for focussing. Because binning effectively increases the pixel size, it not only increases the sensitivity, but also increases the speed of image acquisition, therefore improving focussing at lower out-of-focus light levels. Pixel binning also increases the flexibility of research programs, where the research and observational programs require different optimum pixel sizes, depending on telescope focal length and optics. Binning also influences the CCD well depth. With the output nodes generally having a greater charge capacity than the pixels, pixel binning offers a greater charge collection from the super pixels than is possible from individual unbinned pixels.

Readout-Noise

The major contributions to readout-noise are the CCD detector and the total system. It can be specified through the readout-noise of the CCD and the system electronics. The first source is the injection of unwanted random signals by the detector and electronics because of the process through which the CCD relies on an amplifier to measure the electrons within the pixels. The CCD readout-noise can thus be defined as: The mean error contributed to a pixel value by the CCD amplifier is the CCD readout-noise. The unwanted random signals from the CCD readout-noise can also be digitized by the ADC, adding to the overall system noise. The second source is through variability of the digitization process of the ADC. Therefore, there will be an uncertainty in the data referred to as noise, which is specified in electrons (Howell 2006; Janesick and Elliot 1992; Gilliland 1992).

To determine the CCD readout-noise component of the total system noise, the nature of the readout-noise component need to be examined. The CCD readout-noise should be

uniform over the whole surface of the CCD, because it is generated in the amplifier when the pixels are read out. It can be assumed that the pixels of a CCD are the same, because of the precise nature of current CCD manufacturing processes, thus the values read-out to the amplifier would be approximately the same, with the standard deviation about the mean of the measured pixel values then defined as the CCD readout-noise.

To determine the CCD readout-noise, bias frames can be used, which are zero-second exposures. These zero-second exposures would only contain noise inherent on the CCD. Sometimes there is a gradient present in the average pixel data of the bias frame. This gradient is because of system electronic noise rather than pure amplifier noise, with the gradient then not being part of the CCD readout-noise. This gradient, if constant, could be removed by taking the difference between two bias frames, therefore subtracting out the gradient value. The difference frame left contains just the relevant noise. The readout-noise can be calculated using the following statistical method. Through error calculations, the standard deviation will be $\sqrt{2}$ times the readout-noise (Janesick and Elliot 1992; Howell 2006; Gilliland 1992), i.e.

$$\text{Readnoise(ADU)} = \frac{\sigma_{(B_1 - B_2)}}{\sqrt{2}}. \tag{2.5}$$

To convert the readout-noise in ADU to readout-noise in electrons, the readout-noise could be multiplied with the system gain, i.e.

$$\text{Readnoise(e}^-) = \left(\frac{\sigma_{(B_1 - B_2)}}{\sqrt{2}}\right) \times \text{Gain(e}^-/\text{ADU}). \tag{2.6}$$

Dynamic Range

The dynamic range of a CCD system can be represented as a log ratio of the well depth and the system noise, and is expressed in decibels.

$$\text{Dynamic Range(dB)} = 20 \log\left(\frac{\text{Well Depth}}{\text{Read Noise}}\right). \tag{2.7}$$

The higher the dynamic range, the better, with a system with a dynamic range of 90dB performing better than a system with a dynamic range of 70dB. The ratio is also used to determine the number of digitization levels that might be appropriate for a given detector. (Howell 2006).

System Gain

Because the CCD uses an ADC to convert the signal received from the CCD amplifier, the conversion factor has to be specified. Therefore the system gain is defind as: The number of electrons per data unit produced by the ADC is the system gain (e$^-$/ADU). Therefore the amount of electrons of charge that are represented by each count or ADU is expressed as the system gain, with a system gain of 2.5 electrons/ADU denoting that each count or gray level represents 2.5 electrons. Therefore, the pixel value for a CCD with a total well depth of 85 000 electrons, could be represented as 85 000/2.5 = 34 000 counts.

To minimize the noise contribution from electronics and to increase resolution, it is better to use a lower gain; as long as the total well depth of the detector could be represented. This means that unnecessary high gains result in higher digitization noise, while too low gains minimize noise at the expense of well depth. When CCDs are designed, their system gains are balanced between digitization counts, digitization noise and total well depth (Howell 2006; Gilliland 1992).

To determine the system gain, images with a high average signal value is used, i.e. flat frames, and biaslevel images to remove noise (Howell 2006). The system gain could be represented by

$$s = N/g. \tag{2.8}$$

Here s is the average measured signal value, N the average number of electrons detected, and g the system gain. But the standard deviation in the signal must also be considered. The standard deviation of the signal used in determining the system gain has a contribution from both the readout-noise r and the random arrival rate of the photon flux. The second component has to be considered, because photon flux has a Poisson statistical distribution, meaning that the arrival rate of photons is a Poisson statistical process. Thus for a single exposure having N photons detected, n exposures scaled to the same time-frame will then have a standard deviation of $\sqrt{N}$ photon counts about their mean value (Howell 2006). The standard deviation of the signal σ_s is then given by the quadrature sum of the variation

in N and the variation due to r as

$$
\begin{aligned}
\sigma_s^2 &= \left(\frac{\sigma_N}{g}\right)^2 + r^2 \\
&= \left(\frac{\sqrt{N}}{g}\right)^2 + r^2 \\
&= \frac{sg}{g^2} + r^2 \\
&= \frac{s}{g} + r^2.
\end{aligned}
\tag{2.9}
$$

Solving for the system gain then gives

$$
g = \frac{s}{\sigma_s^2 - r^2}.
\tag{2.10}
$$

The average signal s used in determining the system gain is calculated using measured signal values from two different flat frames; thus:

$$
\bar{s} = \frac{\bar{s}_1 + \bar{s}_2}{2}.
\tag{2.11}
$$

The data signal s consists of two components, the flat field component and the biaslevel component. The signal must therefore be corrected for the biaslevel noise in the images, with

$$
s = s(Flat) - s(Bias).
\tag{2.12}
$$

The values for $s(Flat)$ and $s(Bias)$ are then measured from the mean values of the flat and bias frames. Thus $s(Flat) = \bar{F}$ and $s(Bias) = \bar{B}$. Therefore the average signal is defined as

$$
\begin{aligned}
\bar{s} &= \frac{\left(\bar{F}_1 - \bar{B}_1\right) + \left(\bar{F}_2 - \bar{B}_2\right)}{2} \\
&= \frac{\left(\bar{F}_1 + \bar{F}_2\right) - \left(\bar{B}_1 + \bar{B}_2\right)}{2}.
\end{aligned}
\tag{2.13}
$$

To remove the gradient present in the standard deviation of the data due to the system's electronic noise, it is better to subtract two signal frames to produce a difference image containing only data from the CCD (Howell 2006). For the standard deviation of the signal σ_s and the definition of the readout-noise r, the following relations can be written using

35

statistical methods:

$$\sigma_s = \frac{\sigma_{(F_1 - F_2)}}{\sqrt{2}} \tag{2.14}$$

$$r = \frac{\sigma_{(B_1 - B_2)}}{\sqrt{2}}. \tag{2.15}$$

Putting the above equation's and Equation 2.13 into Equation 2.10 and rewritting, gives the following equation, known as the Janesick method that can be used in determining the system gain (Howell 2006):

$$\text{Gain}(\text{e}^-/\text{ADU}) = \frac{\left(\bar{F}_1 + \bar{F}_2\right) - \left(\bar{B}_1 + \bar{B}_2\right)}{\left(\sigma_{(F_1 - F_2)} - \sigma_{(B_1 - B_2)}\right)}. \tag{2.16}$$

Dark-Count

One of the most important specifications after quantum efficiency, noise figure and resolution (number of bits) is the "dark-count" or "dark-current" of the CCD. CCDs, like most semiconductors, have the property of accumulating thermal electrons in the pixels over time. Through temperature fluctuations or thermal excitation, free-electrons can be excited or boosted into the conduction band, resulting in an accumulation of thermal electrons in the pixel. This property of the detector, to produce thermally excited electrons, is called dark-count. Dark-count varies according to an empirical relation, which could be derived using statistical mechanics (Howell 2006; Janesick and Elliot 1992; Gilliland 1992).

Because electrons within a solid behave like a Fermi gas below a specific temperature, there exists a Fermi level for a specific temperature, with the Fermi level defined as the energy level below which the electrons occupy all the available states for a temperature of absolute zero. With the Fermi energy related to the Fermi temperature as (Huang 2001,p121)

$$\epsilon_F = kT_F. \tag{2.17}$$

Because the occupation number $n(\epsilon)$ is a function of the single particle energy state ϵ, at a finite temperature, the occupation number will have a qualitative shape, depending on the temperature (Huang 2001,p121). See Figure 2.5

36
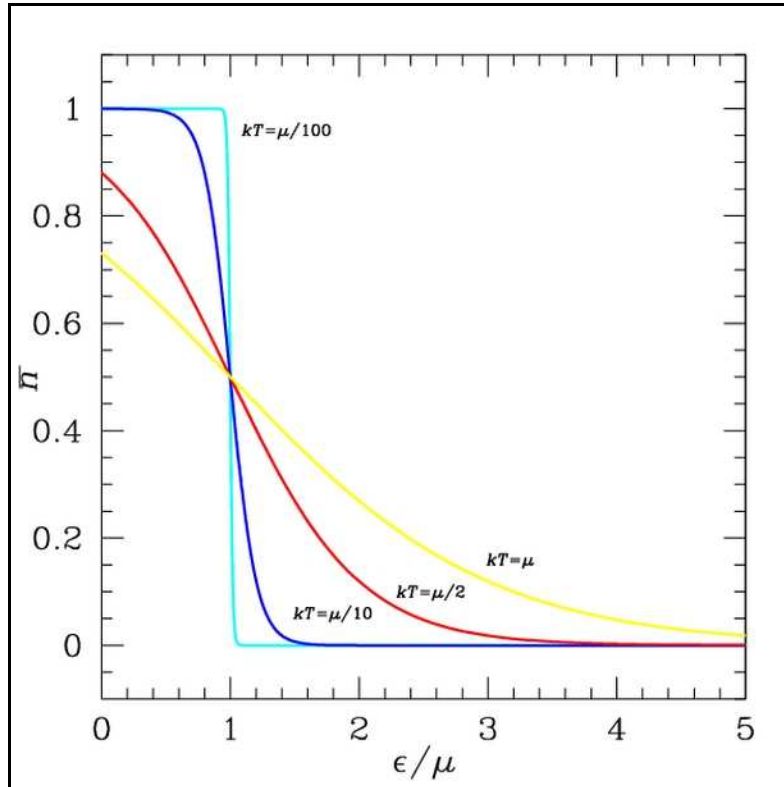
Figure 2.5: Occupation number of a Fermi gas near absolute zero (http://content.answers.
com/main/content/wp/en/thumb/7/7c/300pxFD_e_mu.jpg).

Figure 2.5 then describes different situations for specific temperatures. For T $\approx$ 0 the
graph will have a step structure, with the vertical line representing the Fermi level. With
an increase of temperature, there will be an increase in the electron energy, resulting in
some particles being excited to above the Fermi level. A "natural semiconductor" can be
defined as a semiconductor where the valence band is completely filled and the conduction
band completely empty, with the energy gap containing the Fermi level. From Figure 2.5
it can be seen that with an increase in the temperature of the semiconductor, thermal exci-
tation will cause some electrons to be excited across the Fermi level, creating electron-hole
pairs within the semiconductor, with the electrons accumulating in the conduction band
and holes forming in the valence band. These electron-hole pairs then behave like free
charge carriers (Huang 2001,p124).

The energy of an excited electron near the bottom of the conduction band is defined

by

$$\epsilon_c = \epsilon_0 + \Delta + \frac{\mathbf{p}^2}{2m_c}. \tag{2.18}$$

With $\mathbf{p}$ an effective momentum vector, Δ the energy gap E_g and m_c the effective particle mass. The energy for an empty state (hole) just below the top of the valence band can then similary be defined by

$$\epsilon_v = \epsilon_0 - \frac{\mathbf{p}^2}{2m_v}. \tag{2.19}$$

Using the Fermi-Dirac density functions, the density of the particles and holes could then be defined, e.i.

$$n_{part} = 2 \int \frac{d^3p}{h^3} \frac{1}{e^{\beta(\epsilon_c - \mu)} + 1} \tag{2.20}$$

$$n_{hole} = 2 \int \frac{d^3p}{h^3} \frac{1}{e^{\beta(\mu - \epsilon_v)} + 1}. \tag{2.21}$$

Whith $g_s = 2$ representing the number of spin states related to the electrons. With $\beta = \frac{1}{kT}$ and $\frac{1}{kT} \gg 1$ it can be assumed that $\beta(\epsilon_c - \mu) \gg 1$ and $\beta(\mu - \epsilon_v) \gg 1$, and solving the equations for the defined energies, the following relations are obtained, i.e.

$$n_{part} = 2e^{-\beta(\epsilon_0 + \Delta - \mu)} \left(\frac{m_c kT}{2\pi\hbar^2} \right)^{3/2} \tag{2.22}$$

$$n_{hole} = 2e^{-\beta(\mu - \epsilon_0)} \left(\frac{m_v kT}{2\pi\hbar^2} \right)^{3/2}. \tag{2.23}$$

Electrical neutrality requires that $n_{part} = n_{hole}$, with the chemical potential being presented by (Huang 2001,p127)

$$\mu = \epsilon_0 + \frac{\Delta}{2} + \frac{3}{4}kT \ln \frac{m_c}{m_v}. \tag{2.24}$$

For T = 0, the Fermi energy is $\epsilon_0 + \frac{\Delta}{2}$, located in the middle of the energy gap, for the approximation of $\beta\Delta \gg 1$. This leads to the particle and hole densities given by

$$n_{part} = n_{hole} = 2e^{-\beta\Delta/2} \left(\frac{\sqrt{m_c m_v}kT}{2\pi\hbar^2} \right)^{3/2}. \tag{2.25}$$

For free electrons in a semiconductor the mass goes as $m_c = m_v = m_e$, and using the definitions for β and Δ, the equation can be rewritten as

$$n_{electron} = 2e^{-E_g/2kT} \left(\frac{m_e k}{2\pi \hbar^2} \right)^{3/2} T^{3/2}. \tag{2.26}$$

This equation can then be adopted for application to dark-count, by defining $DC = n_{electron}$ and $A = 2 \left(\frac{m_e k}{2\pi \hbar^2} \right)^{3/2}$, resulting in the following form:

$$DC = AT^{3/2} e^{\left(\frac{-E_g}{2kT} \right)}, \tag{2.27}$$

with DC the dark-count in ADU/pixel/second, A a constant (ADU/p/s/Kelvin$^{3/2}$), T the detector temperature in Kelvin, E_g the bandgap for the semiconductor in eV, and the Boltzmann constant $k = 8.6175 \times 10^{-5}$ eV/Kelvin. The constant A and the bandgap E_g could be determined using empirical CCD characterization methods (Howell 2006). See Figure 2.6 for a general qualitative dark-count model for normal opperating temperatures for a CCD camera.

From Figure 2.6 it can be seen that the dark-count will be lower with a low detector temperature, and higher with a high detector temperature. At ambient temperature, the dark-count could possibly exceed astrophysically interesting signals, and for this reason CCDs are cooled down to minimize the dark-count during operation. Dark count can be expressed either as electrons per unit of time at a given temperature or as a current per detector area at a given temperature. The CCDs dark noise cannot be subtracted like the dark-count, with the dark noise being approximately the square root of the dark-count. Dark noise can easily degrade low light images, if the CCD is not cooled properly. Most detectors have a so-called doubling temperature, where the dark noise doubles for a given temperature range (Howell 2006; Janesick and Elliot 1992; Gilliland 1992).

Corrections in the finished image can be made for dark contributions through dark subtraction, but the process error increases with increasing dark-count. Because every system has a given degree of temperature instability and dark noise, it is important to minimize the amount of dark-count in the imaging system. This could be achieved through different methods of cooling. The most extreme is liquid nitrogen (LN$_2$) cooling, but these sys-
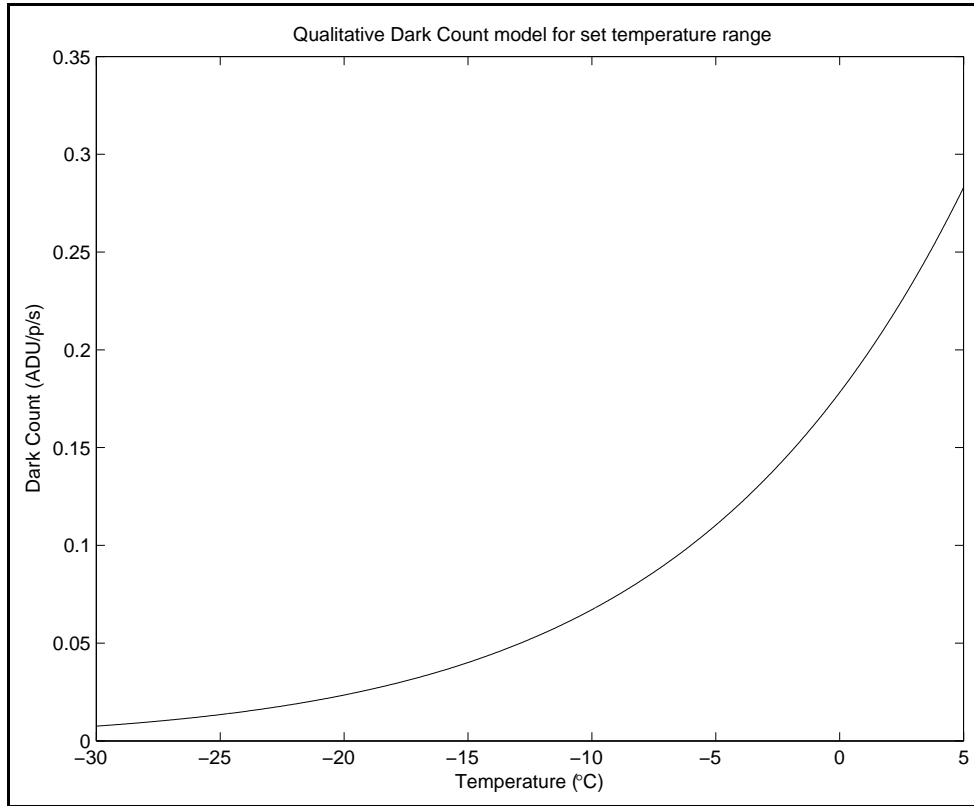
Figure 2.6: Qualitative Dark Count Model.

tems are very expensive. Others include vacuum systems, with hard vacuum combined with thermoelectric cooling (TEC) used on some systems, but unfortunately these systems require periodic pumping to restore the vacuum, and could also become expensive. Currently the most cost effective system, providing low maintenance without compromising performance, is the sealed soft vacuum chamber with Argon back-fill. The process involves the creation of a vacuum chamber to remove inherent gasses, with Argon back-fill used to remove all trace elements from the chamber, after which it is sealed to form a soft vacuum chamber. Argon is used in this process not only because it is a neutral gas, but also because of its heavy atomic mass, which during the back-fill procedure displaces the inherent trace elements. The Apogee Alta series of detectors use this kind of cooling system. Although eliminating dark-count is important, a stage will be reached when other factors like shot noise or S/N supercede dark-count considerations (Janesick and Elliot 1992).

System Throughput

The system speed is specified by the frame rate, data rate, transfer rate or system throughput and is measured in pixels/second or frames/second. The total system throughput has to take into consideration as to how long it takes to display the data image from the time the shutter closes, with the CCD exposure time not considered. Thus, factors like data transfer rate to the system memory, digitization speed of the ADC, and CCD clocking and readout speed have to be considered. The shorter the system throughput time, the greater the efficiency at which the system can be used, with tasks, like focussing, becoming much easier. The production of dark-count must also be considered, as dark-count continually builds during delay and readout, with the top-to-bottom dark-count gradient increasing with longer charge transfer times from the CCD. The total system throughput must take the digitization, data transfer, memory storage and image display into account, and can be defined as (Apogee Instruments Inc. b)

$$\text{Total System Throughput(p/s)} = 1 \ / \ \left(\frac{\text{Total Time}}{\text{Number of Pixels}} \right). \tag{2.28}$$

Here the Total Time is defined as follows:

$$
\begin{aligned}
\text{Total Time} \quad = \quad & \text{Charge Transfer and Digitization} \\
+ \quad & \text{Transfer to the Computer Memory} \\
+ \quad & \text{Image Display Time.}
\end{aligned}
\tag{2.29}
$$

A standard system would therefore have an approximately constant total system throughput, that is independent of the CCD exposure time (Apogee Instruments Inc. b).

Telescope Optics and Pixel Size

Three important factors have to be considered when defining, describing and characterizing a possible CCD-Telescope system. Sampling, Pixel Sensitivity and Field of View have to be examined before designing a CCD-Telescope system that can produce beautiful images, as well as scientifically useful data (Apogee Instruments Inc. b).

1. Sampling: The amount of pixels used to produce image detail is called sampling.

With CCD pixels having a square structure, image structure will have a stair-step appearance. Therefore the more pixels used, and the higher the amount of levels used for the gray shades during image display, the smoother the edges of the image structures will be. Two types of errors can occur when sampling, namely undersampling and oversampling (Apogee Instruments Inc. b). Undersampling occurs when the pixels of the detector are too big to resolve the detail in the image. This means that objects, for instance stars, could appear blocky or square. This can occur when the seeing conditions are better than the sampling size for a given detector (Ridpath 1997; Apogee Instruments Inc. b). Oversampling occurs when there are more pixels than required to sample the finest details for an object or image, or the star image consists of too many pixels (Ridpath 1997).

The relationship between the telescope focal length, the physical size of the pixels (given in μm) and the object/star size (given in arcseconds) determine the number of pixels that make up an object/star image. Of the three parameters, a measure of control is possible over the telescope focal length (through the use of focal reducers), and the pixel size (through the use of pixel binning), but little control is possible over the star size. That is because the star size will vary, with the seeing conditions of the observing site having the biggest influence. Seeing can be defined as the movement or distortion of images because of atmospheric cells in the earth's atmosphere that act like lenses. These cells are caused/produced by turbulence between seperate layers of air, influencing or disturbing the path of the light waves. See Figure 2.7 for a schematic diagram of how seeing influences light waves.

The scale of the seeing cells determines the quality of the images, with the cells increasing in size with an increase in altitude. This is simply because the atmosphere is less dense at higher altitudes, and are therefore more steady/stable. The seeing limits the resolution of even the best observing sites to about 0.5 arcseconds. This seeing problem was one of the reasons why the Hubble Space Telescope was commisioned. The Antoniadi scale is commonly used to define the seeing conditions (Ridpath 1997; Seeds 2001). To determine sky coverage per pixel for a given pixel size and telescope focal length the following formula could be used:

$$\text{Sampling (arcseconds)} = \left(\frac{206.265}{\text{focal length(mm)}}\right) \times (\text{pixel size}(\mu\text{m})). \qquad (2.30)$$
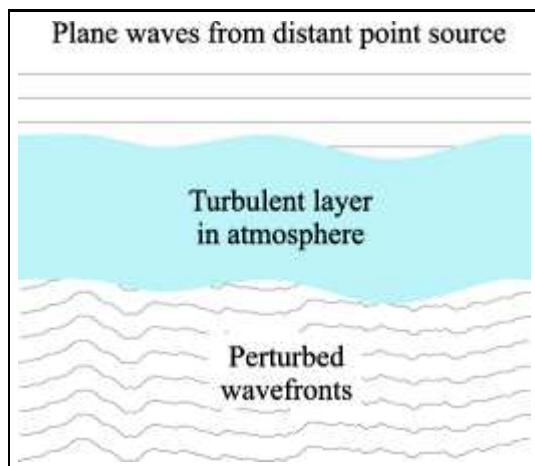
Figure 2.7: Illustration of how optical light from a distant source can be distorted by a seeing cell or turbulant layer in the atmosphere. Image is not to scale (Tubbs 2003).

2. Pixel Sensitivity: Pixel sensitivity depends on the pixel size, i.e. with an increase in pixel size, the camera will have an increased sensitivity for a given focal length and a decrease in pixel size resulting in a decrease in sensitivity. Sampling has an influence on the pixel sensitivity, where oversampling (small pixels) will reduce the CCD sensitivity, but will improve the resolution, and undersampling (large pixels) will improve the sensitivity, but reduce the resolution. A good balance will have to be found between CCD pixel size, telescope focal length and seeing conditions to optimize both the sensitivity and the resolution of the detector.

3. Field of View: From the telescope focal length and the determined sky coverage per pixel, the field of view for a detector could be determined. It is the full angular extent of the sky being viewed (Ridpath 1997). Some important factors in terms of the telescope characteristics, need to be understood to determine the final system parameters. The plate scale or image scale p of a telescope is the factor by which the linear measure l on the detector is converted to an angular measure w on the sky, and is equal to the inverse of the focal length of the telescope (Ridpath 1997).

$$\text{Image Scale } p \text{ (radians/focal length units)} = \left(\frac{1}{f}\right). \qquad (2.31)$$

The focal length f is the distance between the lens/mirror and the focal point of the telescope. The focal ratio is the ratio between the aperture size D of the telescope and the focal length f, and is expressed as the telescope's f/number (Ridpath 1997),

43

i.e.

$$\text{f} - \text{ratio} = \left(\frac{f(\text{mm})}{D(\text{mm})}\right). \tag{2.32}$$

The f-ratio could also be used to determine the image scale of a telescope, for instance: for a given telescope aperture size, a smaller f-ratio would have a smaller image scale and therefore a brighter image. The image scale could thus be defined as (Ridpath 1997)

$$\text{Image Scale } p \text{ (''/mm)} = \left(\frac{w(\text{arcseconds})}{l(\text{mm})}\right). \tag{2.33}$$

Here l, w and f relates as

$$\tan w = \left(\frac{l(\text{mm})}{f(\text{mm})}\right). \tag{2.34}$$

The above relation could also be expressed in terms of the angle subtended by each pixel θ, the pixel size s and the focal length f of the system, i.e.

$$\theta = \left(\frac{s(\text{mm})}{f(\text{mm})}\right). \tag{2.35}$$

The plate scale p of the system and the linear measure l of the detector are then used to determine the field of view (FOV), with the FOV defined as

$$(FOV) = (p \times l_c)(\text{arcminutes}) \; by \; (p \times l_r)(\text{arcminutes}), \tag{2.36}$$

for a square detector. The linear measure l of a detector could be determined by simply multiplying the pixel size s by the amount of pixels per column for l_c and the amount of pixels per row for l_r.

Camera Test Methods

Certain parameters and characteristics are important indicators of the quality of the CCD camera system. To measure these parameters, specific tests have to be performed on the CCD camera system. The CCD characteristics and camera test experiments can be performed using a controlled environment, for instance a laboratory, with the CCD tested directly. To get a true reflection of the CCD-camera system, it is recommended that the CCD characteristics and camera test experiments be conducted on the CCD-Telescope system at the observing site, as some of the results can depend on the specific CCD-Telescope system setup, and the observing environment. Tests include system noise, system linear-

ity, bias level, dark-count, temperature stability and signal variance or gain. Other tests include system throughput or data readout time (Howell 2006).

System noise can be determined using the biaslevel of a set of standard bias frames, and will give a value i.t.o. ADU. The noise i.t.o. electrons could be determined by using the gain factor of the CCD. A simple method to test the noise of a CCD is to measure the data value from a region of interest, preferably the center, of the bias frames, and then calculating the standard deviation between the measured data values. The standard deviation value is the system noise. The mean value of the measured bias frames is the bias level for the CCD during the experiment and is mostly for informational purposes only. When the test is performed, caution has to be taken that the test environment is as dark as possible, with the camera well sealed, as the camera shutter could leak light, influencing the data.

System linearity is the measure of how well the CCD responds to light over the well depth, and can be defined as the degree to which the detector output signal is proportional to the incoming photon flux received by the detector. A measure of non-linearity is when there is a deviation in the response from a straight line. A simple method to measure linearity is by taking flat frame (dome or sky) exposures of a stable light source at ever increasing exposure-times, until the CCD saturates. Flat frames will be discussed in more detail in Chapter 4. The test has to be kept as short as possible, with the camera cooled to a maximum to minimize dark-count influences. The exposure times should be increased using even increments, with the minimum increment time large enough to eliminate shutter uncertainty. The measured values from the flat frames could then be plotted as Counts (ADU) vs Time, and should be reasonably straight throughout the detectors well depth. The linearity could also be expressed i.t.o. Electrons vs Time by multiplying the counts by the system gain.

Dark count is dependant both on the CCD temperature and the CCD characteristics, with most CCDs having a doubling temperature of 5-6 °C. A simple method to determine the dark-count of a CCD is to take a set of 60-second dark frames at the CCD operating temperature, as well as a set of bias frames, and then measuring the mean pixel values from the dark and bias frames from a common region of interest. The dark-count is then the difference between the mean dark and mean bias levels, which is divided by the exposure

time to give a value i.t.o. ADU/pixel/second. The dark-count can also be multiplied by the system gain to give a value i.t.o. electrons/pixel/second. Therefore:

$$\text{Dark Count}(\text{e}^-/\text{p/s}) = \left(\frac{(\text{Dark} - \text{Bias})(\text{ADU})}{60(s)} \right) \times \text{System Gain } (\text{e}^-/\text{ADU}). \quad (2.37)$$

When the test is performed, caution has to be taken that the test environment is as dark as possible, with the camera well sealed, as the camera shutter could leak light, influencing the data.

Temperature stability is a measure of how stable the CCD and the CCD control system are under temperature changes, system changes and control changes. One of the measured values often quoted is the delta value, which is the maximum temperature delta that could be achieved from ambient room temperature. The other value is the zero-scale. The zero scale is the numbers used by the software that interprets the data from the temperature control subsystem of the CCD. To measure true temperature stability for a system, direct monitoring of the temperature sensor telemetry is required, which is difficult to measure without electronic expertise, and is done mostly by the CCD manufacturers.

Signal variance is one of the methods used to determine system gain. The system gain (electrons / ADU) could then be measured by following the same principle method used during the linearity test. A set of bias frames, and a set of flat frames (dome or sky) are taken at increasing exposure times or increasing light levels until flat frame saturation. The mean count values, as well as the standard deviation values from the bias and flat frames are then used in determining the system gain, where the net signal value is plotted against the variance, with the slope representing the system gain.

The system throughput or data readout time could be determined by measuring the total time it takes to obtain data from the CCD. This could be achieved by timing the different components of a complete exposure sequence. The sequence is the time it takes the computer to issue the start of the exposure sequence, the time to query the camera status, the exposure time and the time to download the data frame. The system throughput is usually measured using a set of bias frames at different binning and bit values, and a set of data frames (usually a set of dark frames) at different binning and bit values. Thus for a system with 12 bit and 16 bit digitization, and 1x1 and 2x2 binning capabilities, a total

of 8 measurements will be made, which will give 4 different frame rates. This is because the system throughput is independent of exposure time, with the exposure types averaging out i.t.o. frame rate.

Chapter 3 will include an experimental discussion on the CCD test procedure used and the results obtained for the Boyden 1.5m CCD-Telescope system, with the above mentioned test methods used as a basis for the experiments.

Chapter 3

Characterizing the Boyden CCD System

3.1   Introduction

For the development of this project, the CCD-Photometric system, for which it was developed, needs to be defined, described and characterized. This was done because the procedures of the photometry package depend on the parameters of the CCD-photometry system used during data acquisition. The photometric research equipment were characterized through a set of experiments. The experiments included: Defining and describing the telescope optics and CCD-camera, determining the system throughput, and testing the CCD linearity, dark count, readout-noise and system gain.

3.2   Instrumentation

The instrumentation used during the experiments to characterize the Boyden CCD System include: The 1.5m Rockefeller Telescope, the CCD camera system, and the control and data analysis computers.

3.2.1   Telescope

The 1.5-m Telescope is a cassagrain reflector telescope. It has Loomis optics consisting of a 152.4 cm primary mirror mounted on a fully adjustable Heidenreich & Harbeck mirror cell, with additional modifications by DFM for increased collimation capabilities. The

secondary mirror is mounted on a moveable focus ram for focusing of the telescope optics. The telescope is mounted on a Fecker mounting in a cross-axis English form. The telescope movement is controlled by electric drive motors on the polar and declination axes, that is controlled by a DFM-TCS system. The tracking of the telescope is also of a very precise nature, with small variations at large angles i.t.o. the zenith, or because of wind turbulence. The variations are only noticeable at very long exposure times. The camera mounting contains a ST-6 CCD autoguider system for accurate tracking during long exposures. The dome is also controlled from the DFM-TCS system, with the only manual component being the opening of the dome shutters, and the telescope primary mirror shutter. The rest of the telescope control system is electronically controllable from the control room computers. See Chapter 1, Section 1.3.1 on page 7 for a full discussion on the 1.5m Rockefeller Telescope.

3.2.2 CCD Camera

The CCD camera system consists of an Alta U55 BI CCD from Apogee Instruments Inc. that is mounted at the Cassegrain focus of the telescope.
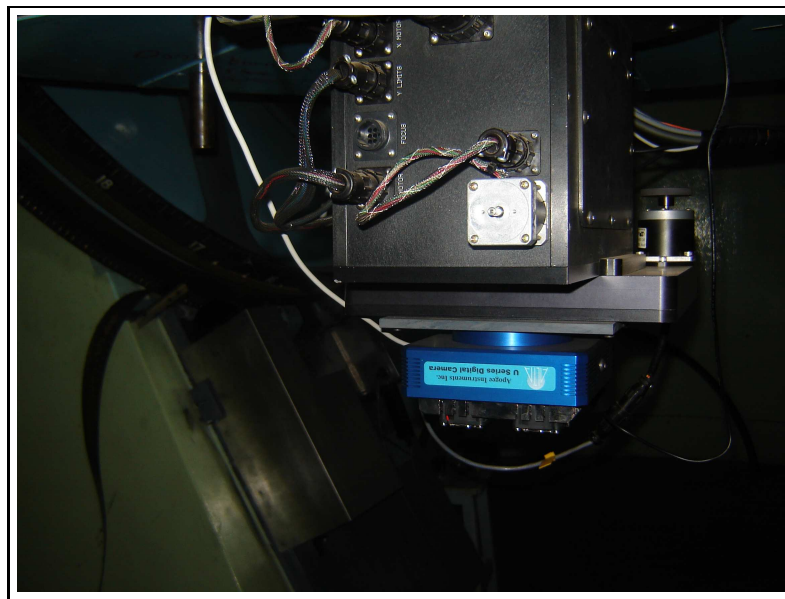
Figure 3.1: The CCD-camera mounted on the 1.5m Rockefeller telescope

The CCD is a full-frame 770 x 1152 pixel detector with a very high dynamic range, and comes in midband and broadband variants. Because of exceptional sensitivity and low noise it is a ideal detector for spectroscopy and photometry. Below are tables containing the

full set of technical specifications for the CCD camera as specified by the manufacturers, Apogee Instruments Inc.

Table 3.1: U55 BI CCD Specifications (Apogee Instruments Inc. a http://www.ccd.com/)

CCD	E2V CCD55-20 Back-illuminated
Array Size (pixels)	770 x 1152
Pixel Size	22.5 x 22.5 microns
Imaging area	17.3 x 25.9 mm (448 mm^2)
Imaging diagonal	18.83 mm
Linear Full Well (type)	450 000 e$^-$
Dynamic Range	93 dB
Digital resolution	2 MHz 12 bit and 700 kHz 16 bit
System noise	2 counts at 2 MHz and 10 e$^-$ at 700 kHz
Pixel binning	1 x 1 to 10 horizontal x 1024 vertical on-chip
Imaging sequencing	1 - 65535 image sequences under software control
Temperature stability	$\pm0.1°$C
Dark current (type)	<0.7 e$^-$/pixel/second (-30°C)
Operating environment	Temperature: -22°C to 27°C. Relative humidity: 10% to 90% non-condensing
Cooling	Thermoelectric cooling with forced air. Maximum cooling to 50°C below ambient temperature. Programmable fan speed for zero vibration.
Frame sizes	Full frame, subframe, fast focus mode (multiple subframes per second)
Redout	Precision time delayed integration readout; Subarray readout modes.
Camera memory	32 Mbyte

Power	40 W maximum power with shutter open and cooling maximum. Power supplied by AC/DC "brick" supply. Alternate 12 V input for user's source.
Shutter and windows	Melles Griot 43 mm. External triggering and strobe controls. Fused silica windows.
I/O ports and PC Interface	General purpose programmable I/Oportt with USB 2.0 PC interface. Two serial port outputs for control of peripheral devices: Noplug-in cards or external controllers
Maximum cable length	Total 30 m with 5 m between hubs.
Diagnostics	Extensive self test capability.
Servicing and upgrading	Field upgradable firmware.

The camera used on the 1.5 m telescope is of the midband variant. This camera was chosen, because of the greater sensitivity in the red passbands that was required for specific research programs, like the planet search project. The camera is connected through an USB 2.0 connection to the control room computers. See Figure 3.2 for the QE response curve for the CCD camera, as provided by the manufacturers.
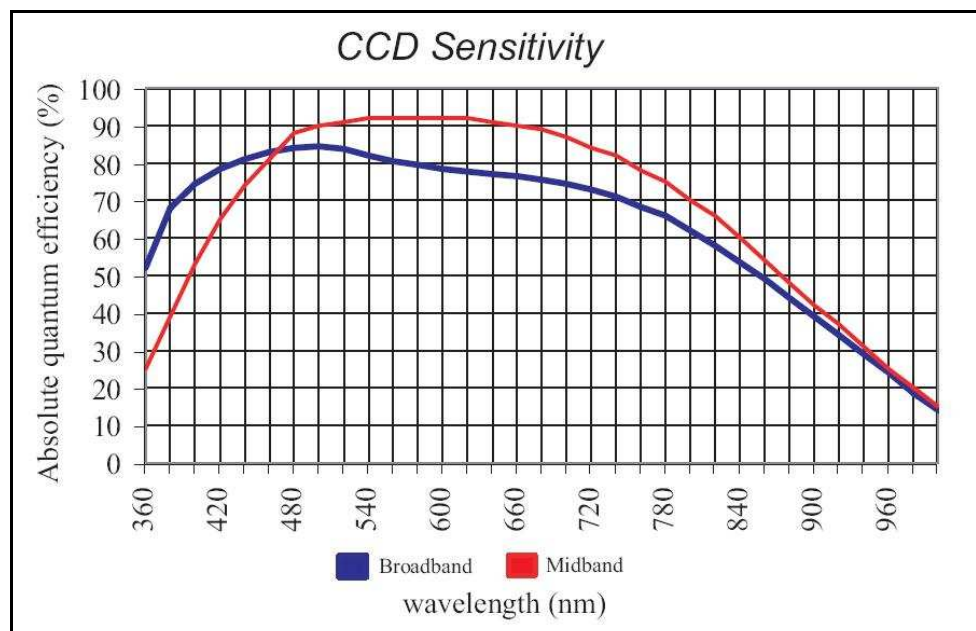
Figure 3.2: Quantum Efficiency curves for the U55 BI CCD camera. (Apogee Instruments Inc. a)

3.2.3 Other

The camera mounting also includes a filter wheel. The filter wheel used on the 1.5-m telescope contains filters supplied by M. Bessel with Kron-Cousins UBV transmission curves and Johnson-Kron-Cousins RI transmission curves. It also contains a Clear position (without any filter), a pinhole and a closed position that are used during photometric studies.
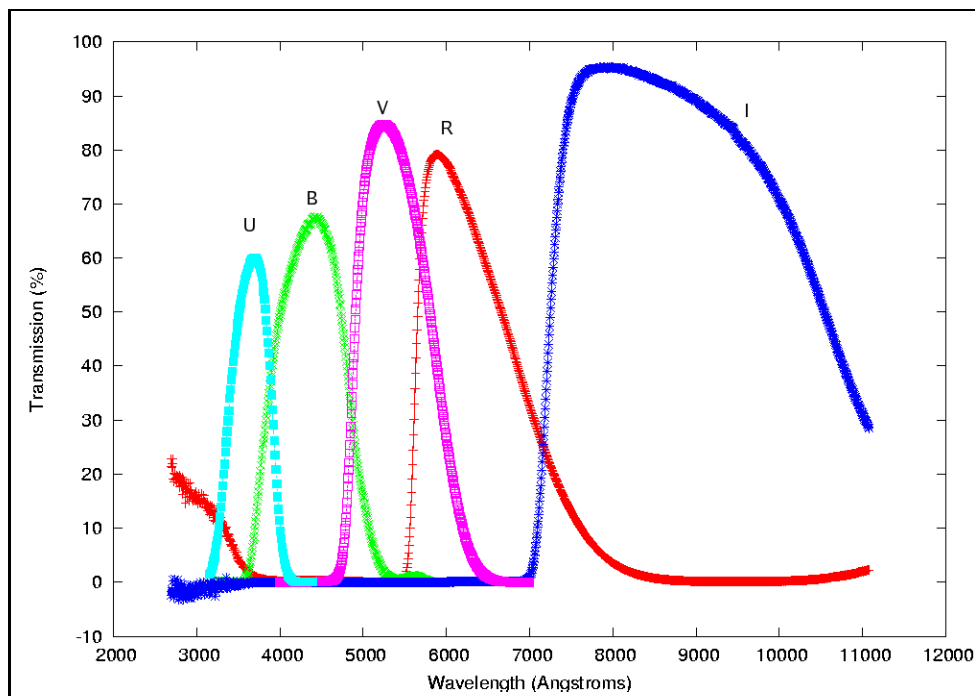
Figure 3.3: The transmission curves for the photometric filters used on the 1.5-m Telescope. (Filter data from Kitt Peak Observatory)

The filterwheel, camera and telescope are controlled through the control room computers. The control room of the telescope houses a number of different computers. Each has its own purpose, and is therefore named for identification. The computers are:

1. AURIGA: This computer runs PC-DOS and controls the TCS system and telescope control software from DFM, i.e. it controls the rotation of the dome, the drives of the telescope, and the tracking.

2. BOOTES: This computer runs the software that controls the camera, the filter wheel and autoguider. This is a Windows-based system. The CCD camera control software used is a locally in-house developed application called SPICA. (Calitz 2005) The custom software that controls the filter wheel is called ACE and was provided by the filterwheel manufacturers.

3. MENSA: This is a Linux-based system and contains the IRAF package used for data analysis. It is also used for other general applications and work.

3.3 CCD Test Procedure

The CCD Tests that were conducted consisted of calculations done to define and describe the telescope optics and CCD-camera system, tests performed to determine the system throughput, and experiments done to determine the CCD linearity, dark count, readout-noise and system gain.

3.3.1 Telescope and Camera

The first step in defining, describing and characterizing the CCD-telescope system was the determining of the sampling factor, the f-ratio, the plate scale and the FOV for the system. The known and supplied data for the telescope and CCD detector were used to determine these values. The values were then calculated using Equations 2.30, 2.32, 2.33, 2.34, 2.35 and 2.36. (See Chapter 2, Section 2.3 on page 41 for a full detailed discussion on the procedures involved. See CCD Test Results and Discussion on page 55 for results obtained and the discussion of those results).

3.3.2 CCD Readout-time and Throughput

In testing the efficiency and effectiveness of the CCD-telescope system, the system throughput needs to be determined. This includes the data transfer speed to and from the CCD, the storage and display times, and the frame rate. These values are required to determine the minimum periodicity for an astronomical system that could be detected with the CCD-telescope system, excluding exposure-time considerations. This means for a frame rate of 0.5 frames/second (fps) only periodicity's above (exposure-time + 2(s)) could be detected, with one exposure readout every (exposure-time + 2(s)).

To determine the system throughput, the times required for the different components to complete their specified tasks need to be measured. This was accomplished by using a frame rate measuring tool. These tools are designed to work on the same principle as discussed in Section 2.3 on page 41 in Chapter 2. The one used in this experiment was provided by Apogee Instruments Inc. and is called Alta Performance Test Tool (Version

1.2). When initialized, the camera that is to be tested can be searched for. A set of parameters are set, like the digitization, binning factor, exposure time, number of images and sequencing. The tool is then initialized, with the results displayed in a status window. The results can be saved to a text-file for further reference, with the parameters reset for another test.

For this experiment the exposure times were kept constant, with tests run for 12 bit and 16 bit digitization at 1x1 and 2x2 binning factors for dark frames and standard frames. This resulted in 8 distinct measurements. (See CCD Test Results and Discussion on page 55 for results obtained and the discussion of those results.)

3.3.3   CCD Linearity

To test the system linearity as well as the CCD saturation turnoff a set of experiments were run, nl. Test1 and Test2. Both experiments were based on the same procedure as discussed in Section 2.3 on page 44 in Chapter 2. The procedure involved the taking of flat-frames. Test1 was run on the 13th of August 2007, and Test2 on the 14th of August 2007. The skyflat frames were taken using a C-filter during twilight, with exposure times from 0.1 seconds until saturation, with the exposure time increased in steps of 0.1 seconds. See Appendix A on page 136 for the relevant observation logs. The flat frames were analyzed using the IRAF task **imstatistics** with the measured values written to text files for further data-analysis and reference. (See CCD Test Results and Discussion on page 55 for results obtained and the discussion of those results.)

3.3.4   CCD Dark Count

To determine the Dark Count for the system, the method discussed in Section 2.3 on page 44 in Chapter 2 was used. The experiments involved the taking of dark and bias frames. The data was acquired on the 26th and 28th of June, and on the 14th, 18th and 19th of August 2007. The data were sorted into 4 sets. The dark frames of set1 had exposure times of 720 seconds, with the dark frames of set 2-4 having exposure times of 60 seconds. See Appendix A on page 136 for the relevant observation logs. IRAF was used to correct the dark frames for bias, using the newly developed IRAF Boyden package. The

bias subtracted dark frames were analyzed using the IRAF task **imstatistics** with the measured values written to text files for further data-analysis and reference. The exposure times and CCD-temperatures were added as additional information for data analysis to the relevant text files. Because the CCD-temperature values in the headers are defined as the cooling temperature below ambient temperature the CCD-temperature values were normalized using the relevant temperature and weather data from the oservation logs. This was achieved by adding the ambient temperature value for the time of observation to the CCD-temperature values. Equation 2.37 were used to determine the system's dark count. (See CCD Test Results and Discussion on page 55 for results obtained and the discussion of those results.)

3.3.5   CCD Readout-Noise and System Gain

To determine the system readout-noise and gain, the method discussed in Section 2.3 on page 44 in Chapter 2 was used. The experiments involved the taking of skyflat and bias frames. The data were acquired on the 13th and 15th of August 2007. The skyflat frames were taken using a C-filter during twilight at high signal levels. See Appendix A on page 136 for the relevant observation logs. The data were sorted into two sets. The IRAF task **findgain** was used to determine the system's Readout-noise and Gain. **findgain** uses the Janesick method to determine the different values. The measured values were saved to text files for data analysis and reference. (See CCD Test Results and Discussion on page 55 for results obtained and the discussion of those results.)

3.4   CCD Test Results and Discussion

The data obtained during the experiments that were conducted, included calculations to define and describe the telescope optics and CCD-camera system and experimental data from tests performed to determine the system throughput, as well as experimental data from experiments performed to determine the CCD linearity, dark count, readout-noise and system gain. The data were analyzed and discussed, and thereafter used to characterize the Boyden CCD System.

3.4.1 Telescope and Camera

From the methods described and equations defined in Section 2.3 on page 41 in Chapter 2, and using the data tabulated in Table 1.2 on page 14 and Table 3.1 on page 50 the following results were obtained.

Using equation 2.30, with the focal length $f = 23\ 820$ mm, and the pixel size $s = 22.5$ μm, the sampling for the CCD-telescope system was calculated to be 0.70 arcseconds/pixel.

Using equation 2.32, with the focal length $f = 23\ 820$ mm and the primary diameter $D = 1\ 524$ mm, the f-ratio for the telescope was determined to be f/15.63. A f-ratio of this size would be termed "slow", and would also mean that the FOV would be very small, because of a small image scale.

Using equations 2.33 and 2.34, with the focal length $f = 23\ 820$ mm and the linear measure of the CCD $l_{1,2} = 17.3$ mm; 25.9 mm, the angular measure of the CCD was determined to be $w_1 = 4.1613$ x 10^{-2} and $w_2 = 6.2299$ x 10^{-2}. These values were used to calculated the plate scale p as

$$ p\ ("/\text{mm}) = \left(\frac{w_1(")}{l_1(\text{mm})} \right) = \left(\frac{w_2(")}{l_2(\text{mm})} \right) = 8.66("/\text{mm}). $$

The angular measure per pixels was also calculated by using equations 2.34 and 2.35 to be $w \approx 0.20$ arcseconds/pixel. Comparing this value with the sampling it can be seen that the limiting factor for the CCD-telescope system is the sampling value and not the pixel size.

Using equation 2.36 with the linear measure of the CCD $l_{1,2} = 17.3$ mm; 25.9 mm, and the calculated plate scale $p = 8.66("/\text{mm})$, the FOV for the CCD-telescope system could be calculated:

$$ (FOV) = (2'29.82") \ by \ (3'44.29"). \tag{3.1} $$

This small FOV corresponds with the F-ratio calculated for the telescope.

3.4.2 CCD Readout-time and Throughput

The results obtained from the Alta Performance Test Tool were tabulated with the data for the 16 bit digitization and the 12 bit digitization test runs tabulated in two separate tables. The average frame rates were calculated for dark frames and standard frames.

Table 3.2: Performance Test results for 16 bit digitization

Image type	Standard	Dark	Standard	Dark
Binning	1x1	1x1	2x2	2x2
Pixels/Image	887040	887040	221760	221760
Avg. total time per image (including 20ms exposure)	2.097 s	2.095 s	0.940 s	0.940 s
Avg. time to issue start exposure sequence	0.006 s	0.004 s	0.006 s	0.006 s
Avg. time to query status	0.078 s	0.124 s	0.124 s	0.139 s
Avg. time to download	2.013 s	1.967 s	0.811 s	0.796 s
Download rate (MPixels/s)	0.441	0.451	0.275	0.280
Frame Rate (based on avg. total time)	0.477 fps	0.477 fps	1.063 fps	1.063 fps

Table 3.3: Performance Test results for 12 bit digitization

Image type	Standard	Dark	Standard	Dark
Binning	1x1	1x1	2x2	2x2
Pixels/Image	887040	887040	221760	221760
Avg. total time per image (including 20ms exposure)	1.765 s	1.761 s	0.568 s	0.568 s
Avg. time to issue start exposure sequence	0.006 s	0.004 s	0.006 s	0.006 s
Avg. time to query status	0.154 s	0.154 s	0.154 s	0.154 s
Avg. time to download	1.606 s	1.603 s	0.409 s	0.408 s
Download rate (MPixels/s)	0.552	0.553	0.543	0.543
Frame Rate (based on avg. total time)	0.566 fps	0.568 fps	1.759 fps	1.760 fps

It can therefore be seen from the results that the fastest photometric setup would be a CCD that is 2x2 binned, with 12 bit digitization. The standard CCD setup for the 1.5m is

2x2 binned at 16 bit digitization. This setup means that for bright sources with exposure times of 1-2 seconds would mean a frame rate in the order of 0.35 fps, with the minimum periodicity that could be observed being larger than 3-seconds. The system speed could be enhanced through hardware upgrades, for instance, faster I/O ports and higher data-rate transfer cables.

With exposure time having a greater influence on the frame rate that could be achieved than the system throughput, observing sources that require exposure times that are in the order of minutes do not require an exceptional system throughput. The system throughput are dependent on the type of research, with slow photometry research having a smaller dependence on system throughput than fast photometry research.

3.4.3   CCD Linearity

The measured linearity data were plotted as Counts (ADU) vs Exposure time (s) on two separate graphs, Linearity Test1 and Linearity Test2. See Figure 3.4 and Figure 3.5. These graphs were analyzed and discussed with the graphs showing that the CCD-system has a linear response over 95% of its range, with saturation turnoff in the region of 62 000 ADU. This means that during observations of bright sources the signal level has to be kept below 62 000 to avoid unnecessary blooming effects, and uncertainty in data measurements. The variation in the signal from a pure linear in the linear region of the linearity plot is because skyflats were used to perform the tests. The twilight sky has a non constant illumination which results in non-linear response curves during CCD linearity tests, for this reason it is more adviseble that linearity tests be performed using more constant illumination sources like dome-flats.
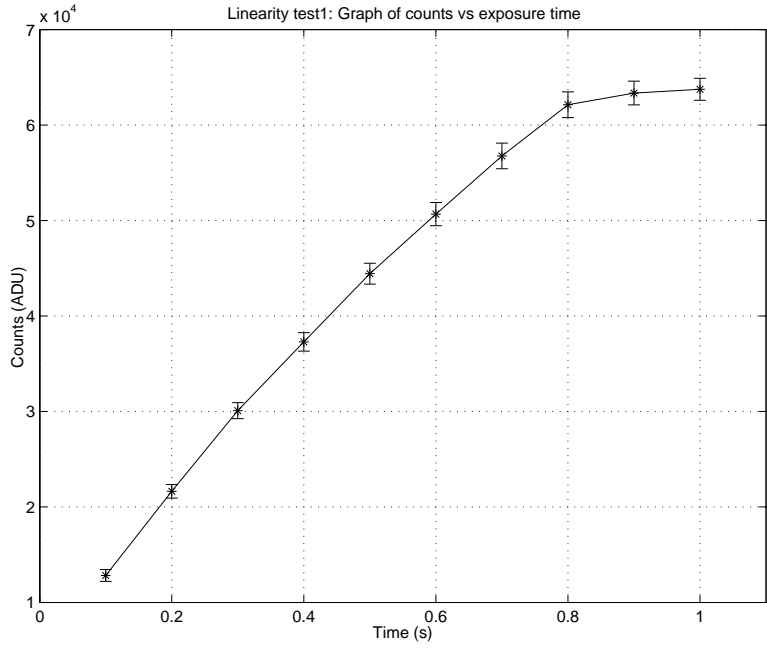
Figure 3.4: Linearity Test1: Counts (ADU) vs Exposure time (s)
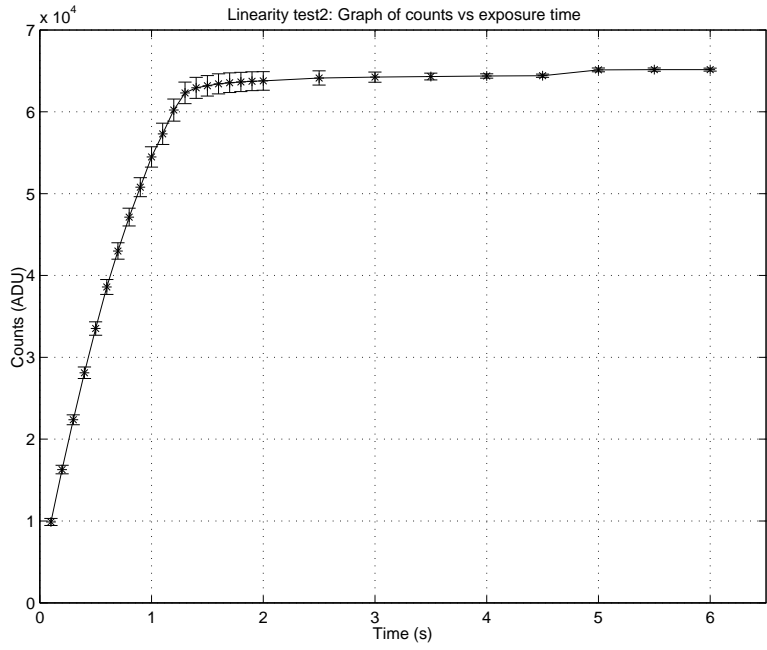
Figure 3.5: Linearity Test2: Counts (ADU) vs Exposure time (s)

59

3.4.4 CCD Dark Count

The calculated CCD dark-count was plotted in a histogram to determine data distribution and mean dark-count. See Figure 3.6. A graph was also plotted of dark-count vs CCD-temperature to determine the variation of dark-count with temperature, e.g. see Figure 3.7. From the data a mean dark-count of 0.50±0.23 ADU/p/s was determined at a mean CCD temperature of -28.95±1.56 °C, over a larger temperature variation, i.e. non-optimal operating conditions. At optimal operating conditions, with the temperature at maximum cooling, the mean dark-count was determined as 0.37±0.12 ADU/p/s at a mean temperature of -29.95±0.2 °C. The graph of dark-count vs temperature also showed the dependence of dark-count on temperature, i.e. with an increase in temperature there's an increase in dark-count. The graph then also has the same shape as the general dark-count model (See Figure 2.6) as defined in Section 2.3 on page 36 in Chapter 2.
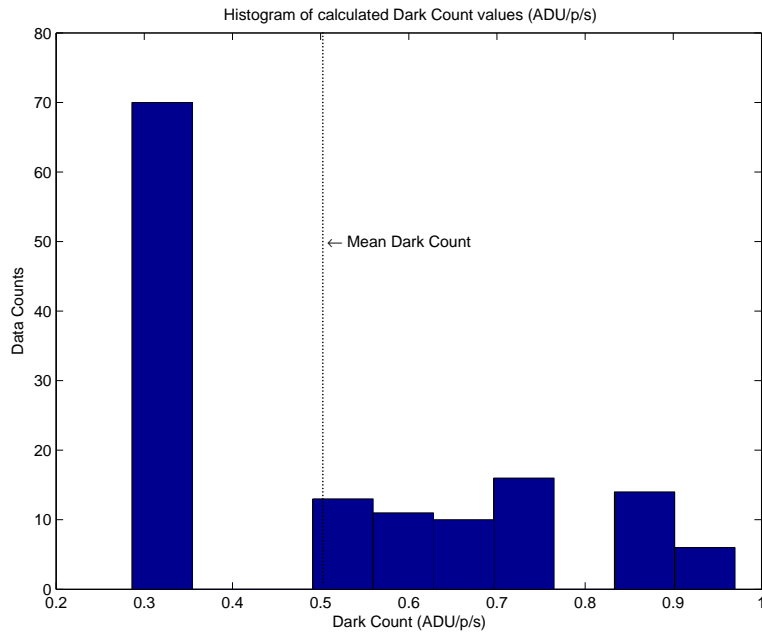
Figure 3.6: Histogram of calculated Dark Count values for the data sets.
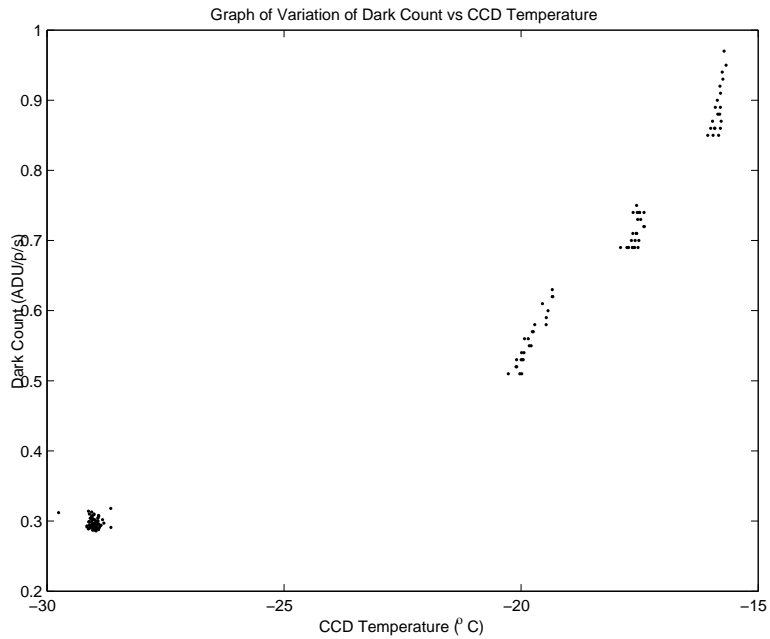
Figure 3.7: Graph showing variation of Dark Count vs Temp

3.4.5 CCD Readout-Noise and System Gain

The calculated CCD Readout-Noise and System Gain were plotted in histograms to determine data distribution and mean values. See Figure 3.8 and Figure 3.9. A graph was also plotted of readout-noise vs gain to determine the variation of readout-noise with gain. See Figure 3.10. From the data a mean system gain of 3.54 ± 0.56 e$^-$/ADU and a mean readout-noise of 11.7 ± 1.88 e$^-$ were determined. From the graph of readout-noise vs gain the linear dependence of readout-noise to gain was shown where the readout-noise increases with an increase in system gain.
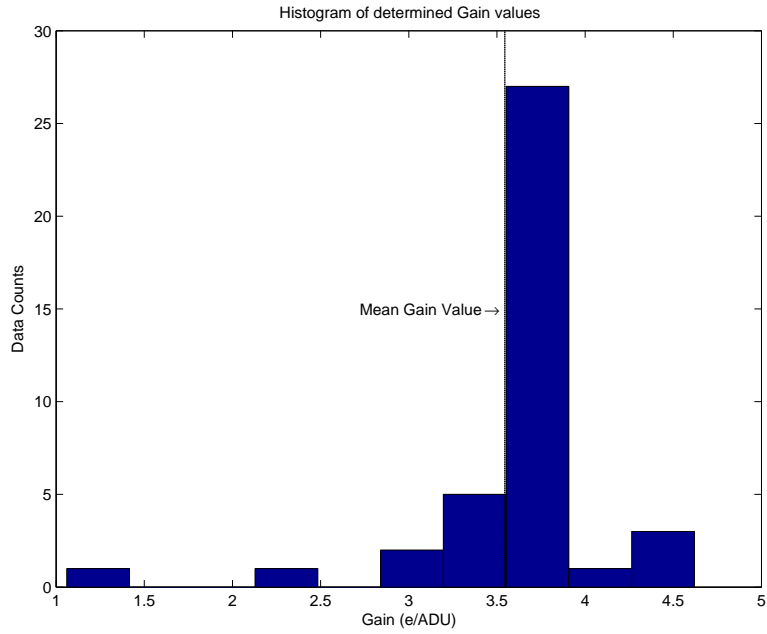
Figure 3.8: Histogram of determined System Gain (e/ADU)
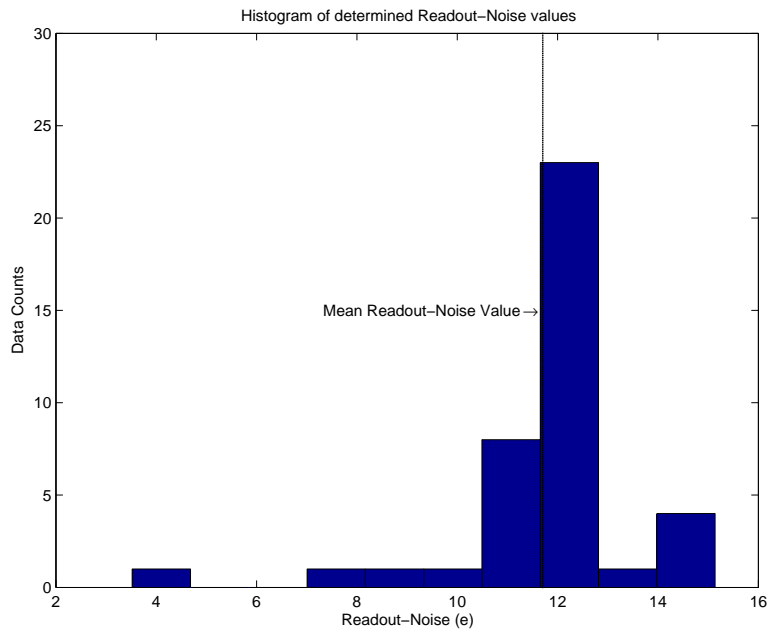
Figure 3.9: Histogram of determined Readout-Noise (e)
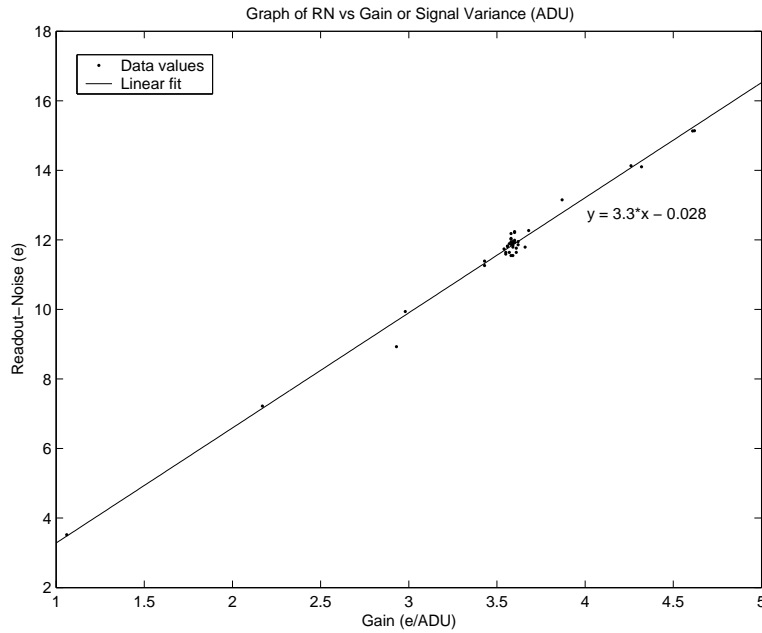
Figure 3.10: Graph of Readout-Noise vs Gain or Signal Variance (ADU)

3.5 Comparison with manufacturer values

The CCD test results obtained were compared to that of the manufacturer. The measured dark count of 0.37 ± 0.12 ADU/p/s could be converted using the determined gain value of 3.54 ± 0.56 e$^-$/ADU to a dark count value of 1.31 ± 0.07 e$^-$/p/s. Compared to the manufacturer value of 0.7 e$^-$/p/s it could be seen that the variance between the measured dark count and the manufacturer value is:

$$\mathrm{Var} = \sqrt{(1.31 \text{ e}^-/\mathrm{p/s} - 0.7 \text{ e}^-/\mathrm{p/s})^2}$$
$$= 0.61 \text{ e}^-/\mathrm{p/s}.$$

Even though the variance is large, the dark count is still relatively small. When comparing the measured system readout-noise of 11.7 ± 1.88 e$^-$ to the manufacturer value of 10 e$^-$ it could be seen that the variance between the measured readout-noise and the manufacturer

value is:

$$\mathrm{Var} = \sqrt{(11.7 \ \mathrm{e}^- - 10 \ \mathrm{e}^-)^2}$$
$$= 1.7 \ \mathrm{e}^-$$

Comparatively the readout noise is still small, when comparing the dynamic range achievable with the measured readout noise. Using Equation 2.7 with a full well depth of 230 000 e^-, calculated from the gain value of 3.54 e^-/ADU using the 16 bit digitization of 65 535 ADU, the dynamic range was calculated as ±86 dB, which gives a variance from the manufacturer value of:

$$\mathrm{Var} = \sqrt{(93 \ \mathrm{dB} - 86 \ \mathrm{dB})^2}$$
$$= 7 \ \mathrm{dB}$$

The dynamic range is still high, which means that the CCD is capable of delivering a very high performance, and does indeed deliver research quality performance levels, when considering the test values measured. The other factor that determines the quality of research, like photometry, is the atmospheric extinction. The proceeding chapters will discuss how the atmospheric extinction coefficients for an observing site could be determined i.t.o. photometric methods, with photometric techniques being discussed in Chapter 4, and the determining of the atmospheric extinction coefficients for Boyden Observatory being discussed in Chapter 6.

Chapter 4

Photometry

4.1 Introduction

In this chapter a discussion on photometry will be presented. The discussion will focus on the theoretical aspects related to photometry and its applications, with special emphasis on photometric procedures used to measure stellar magnitudes, and the different factors that influence those measurements.

4.2 What is photometry

4.2.1 Intensity, flux and luminosity

Photometry is the science that involves the measurement of visual radiation i.t.o. values such as luminous intensity and luminous flux (e.g. Ridpath 1997; Palmer and Davenhall 1999; Rybicki and Lightman 1979 for a general discussion). Intensity, flux and luminosity are all just different descriptions of the radiation energy emitted by a luminous object. The radiation intensity of a radiating body at a specific frequency could be determined from the amount of energy that it emits over an area at that specific frequency. This could be described as follows: For radiation passing through a surface, with a surface element dA, some of the radiation will leave dA within a beam of solid angle $d\Omega$. See Figure 4.1 for a geometrical representation.
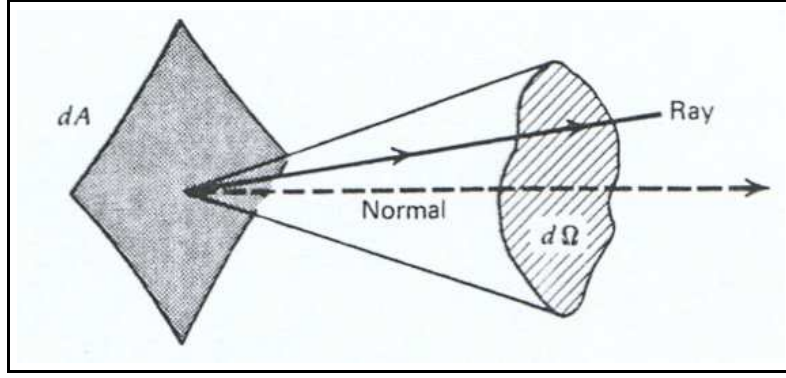
Figure 4.1: Geometry for radiation intensity (Rybicki and Lightman 1979).

The specific intensity I_ν of the radiation at the frequency ν in the direction of the solid angle can then be defined by the amount of energy dE entering the solid angle within a frequency range $[\nu, \nu + d\nu]$ in a time dt as

$$I_\nu = \frac{dE}{dA d\nu d\Omega dt} \ (\text{erg cm}^{-2}\text{Hz}^{-1}\text{ster}^{-1}\text{s}^{-1}). \tag{4.1}$$

Here I_ν depends on the frequency, direction and location in space of the radiating source. The total intensity I can be obtained by integrating over all the frequencies, i.e.

$$I = \int I_\nu d\nu \ (\text{erg cm}^{-2}\text{ster}^{-1}\text{s}^{-1}). \tag{4.2}$$

Of greater interest to observational photometry is the differential energy flux F_ν. This is the amount of energy passing through a surface per unit area per unit frequency interval between $[\nu, \nu + d\nu]$ per unit time, and can be defined as

$$F_\nu = \frac{dE}{dA d\nu dt} \ (\text{erg cm}^{-2}\text{Hz}^{-1}\text{s}^{-1}). \tag{4.3}$$

This can also be expressed in terms of intensity as follows: For the radiation leaving a surface at an angle θ, see Figure 4.2, the net flux can be defined by integrating over all solid angles which is

$$F_\nu = \int I_\nu \cos\theta d\Omega \ (\text{erg cm}^{-2}\text{Hz}^{-1}\text{s}^{-1}). \tag{4.4}$$
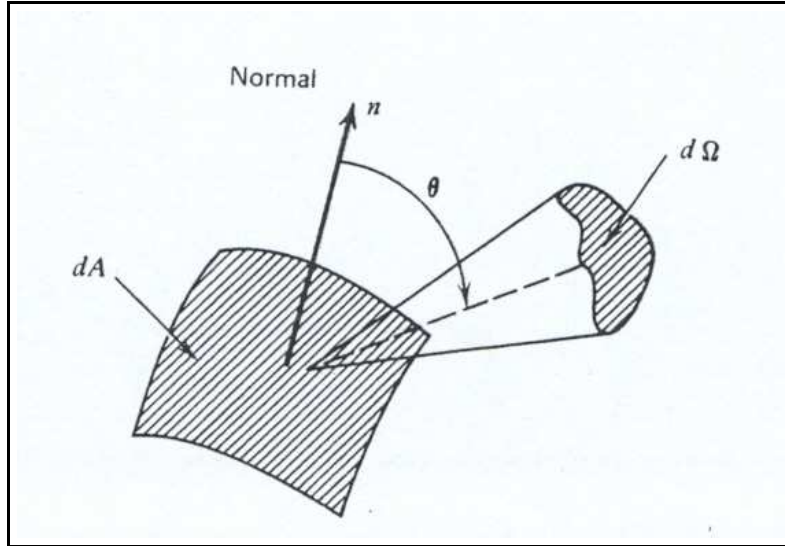
Figure 4.2: Geometry for oblique radiation intensity - flux (Rybicki and Lightman 1979).

The differential flux F_ν is also sometimes called the flux density in units of Jansky (Jy) with 1 Jy = 10^{-26} W m^{-2} Hz^{-1} = 10^{-23} erg cm^{-2} Hz^{-1} s^{-1}. The total flux is the net flux integrated over the all the frequencies

$$F = \int F_\nu d\nu \ (\text{erg cm}^{-2}\text{s}^{-1}). \tag{4.5}$$

For a star as the radiation source, the total flux emitted into a solid angle $d\Omega$ from that star will determine its luminosity, which is

$$
\begin{aligned}
dL &= r^2 F d\Omega \\
   &= 4\pi r^2 F \frac{d\Omega}{4\pi}.
\end{aligned}
\tag{4.6}
$$

Here F is the total flux observed at a distance r from the star. For the star radiating isotropically over a spherical surface, the above equation becomes

$$L = 4\pi r^2 F. \tag{4.7}$$

This is illustrated in Figure 4.3.
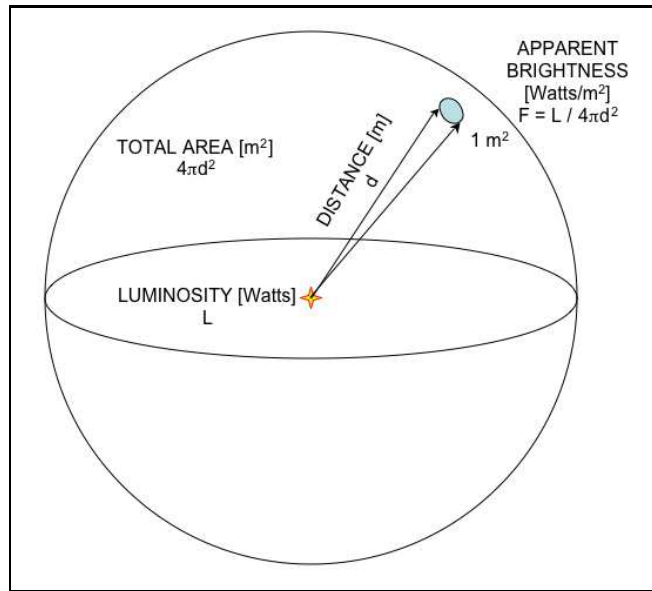
Figure 4.3: The flux-luminosity relation for an isotropically radiating source (http://www. astro.physik.uni-goettingen.de/ hessman/ImageJ/Book/An Introduction to Astronomical Image Processing with ImageJ/Cosmic Distance ScaleIII /index.html).

As can be seen the flux-luminosity relation behaves as an inverse square law where the total flux decreases by the inverse square of the radius from the total luminosity. See Figure 4.4.
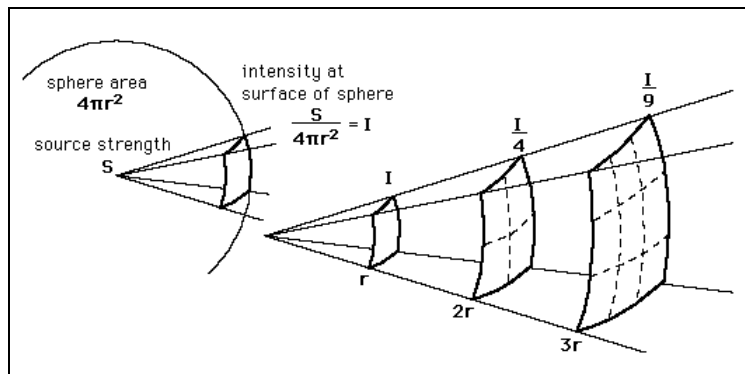
Figure 4.4: The inverse square law i.t.o. intensity or flux (http://imagine.gsfc.nasa.gov /docs/science/try_l2/inverse_square.gif).

The law also applies to radiation intensity, because the flux is just the intensity integrated over all solid angles for a specific angle θ. The luminosity of a star can also be related in terms of temperature, because stars can in general be considered as sources of

blackbody radiation, with the differential flux from a spherical blackbody defined by the Planck distribution function

$$F_\nu(T)d_\nu = \frac{2\pi h\nu^3}{c^2}\frac{d\nu}{e^{h\nu/kT}-1} \; (\text{erg cm}^{-2}\text{Hz}^{-1}\text{s}^{-1}), \qquad (4.8)$$

with h the Planck constant, c the speed of light, k the Boltzmann constant and ν the frequency. It can be seen that the flux is therefore only dependant on the temperature of the radiating source. The total flux in terms of the temperature can be determined by integrating over all the frequencies, with the value of the integral used to define the Stefan-Boltzmann law

$$
\begin{aligned}
F &= \int F_\nu d\nu \; (\text{erg cm}^{-2}\text{s}^{-1}) \\
&= \sigma T^4.
\end{aligned}
\qquad (4.9)
$$

Here σ is the Stefan-Boltzmann constant. The luminosity of a radiating source in terms of temperature can therefore be defined as

$$L = 4\pi r^2 \sigma T^4. \qquad (4.10)$$

The luminosity or blackbody spectrum of a star can be used to describe the temperature characteristics of the star. For a star of known luminosity L and radius R, an effective temperature can be defined using Equation 4.10, i.e.

$$T_{eff} = \left(\frac{L}{4\pi R^2 \sigma}\right)^4. \qquad (4.11)$$

Another temperature that can be used to characterize the star, is the colour temperature T_c. By fitting a blackbody curve, see Figure 4.5, to the measured flux values from the star at different frequencies, the colour temperature for an unique frequency range can be determined. T_{eff} and T_c are usually different for normal blackbody stars. The colour temperature value for a star can be used to define a colour index using the magnitude scale, or the colour index can be used to determine the colour temperature. Colour indices are discussed in Section 4.2.5 on page 84.
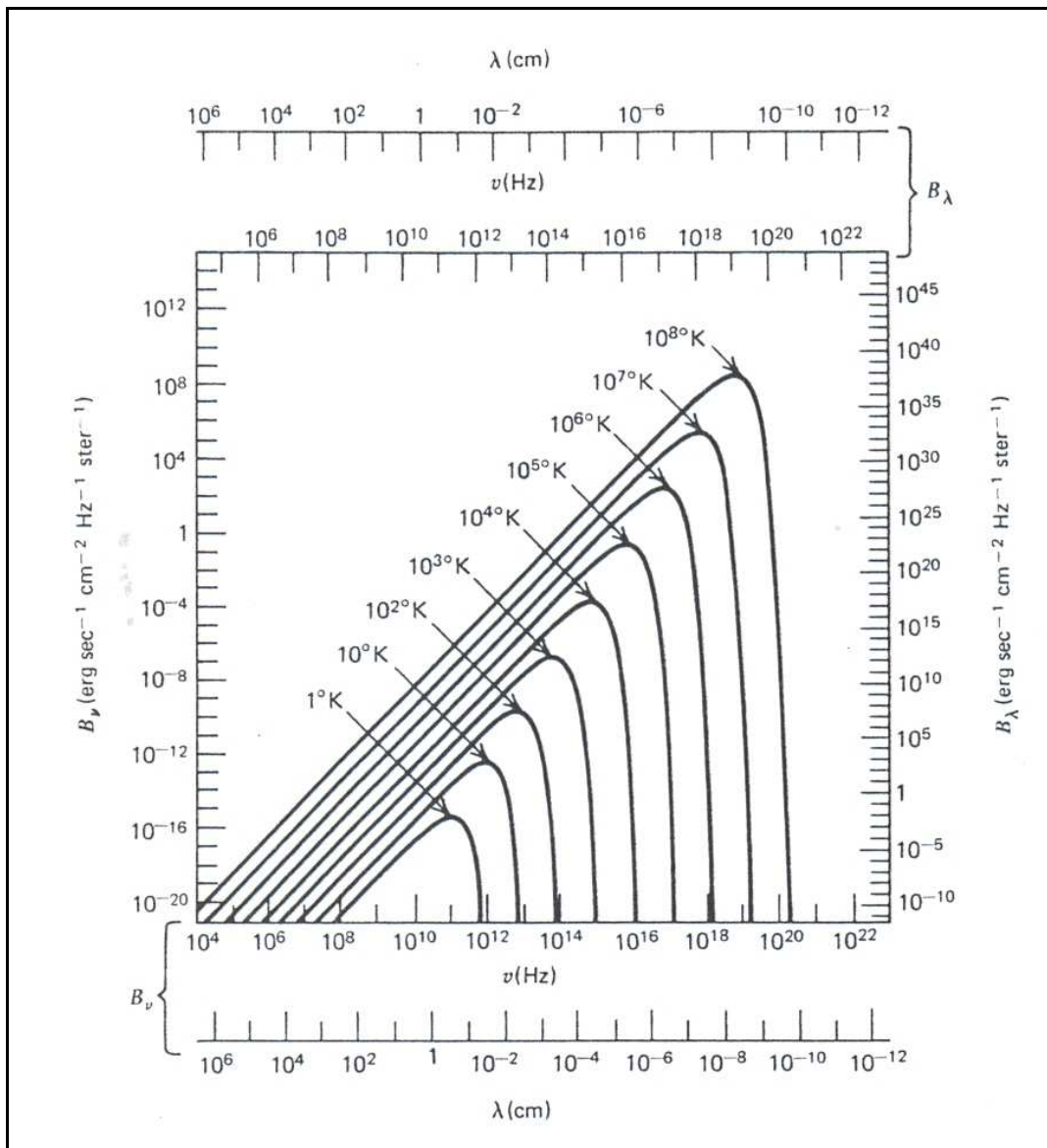
Figure 4.5: Spectrum of blackbody radiation at various temperatures (Rybicki and Lightman 1979).

4.2.2 Magnitude Scale

Photometry is based on the astronomical magnitude scale. The basis for the astronomical magnitude scale originates from the earliest estimates of stellar brightnesses made with the naked eye. In 120 BC, ancient Greek astronomers, such as Hipparchus, defined first magnitude stars as the brightest star first to appear after sunset, with the scale continuing in steps of decreasing brightness down to sixth magnitude for stars only visible in total

darkness. This first crude magnitude scale has since been extended to a strictly defined standard Pogson Scale. This brightness ratio between two brightness classes that differs by one magnitude was formulated mathematically by N.R. Pogson in 1856 as follows: For two brightness classes n and $n+1$, there will be a brightnesses ratio of $\sqrt[5]{100} \simeq 2.512$. Accordingly a difference in 5 magnitudes will correspond to a difference in intensity of $2.5^5 \approx 100$ between the different classes. The first magnitude estimates depended on the naked human eye, which roughly corresponds to the modern visual or V-magnitude. Modern magnitude comparisons are done through the use of photometric devices like photo-multiplier tubes (PMT) and CCDs to compare program objects (stars) to photometric standards or standard stars (e.g. Ridpath 1997; Palmer and Davenhall 1999).

Two different definitions for magnitude are defined, namely apparent magnitude and absolute magnitude (e.g. Ridpath 1997; Palmer and Davenhall 1999 for general discussions). The apparent magnitude m of a celestial object is the brightness as seen from the Earth, or the brightness of a celestial object as measured by the observer. The apparent magnitude could be defined i.t.o. stellar flux as follows; For a defined arbitrary standard reference flux F_0, the apparent magnitude m of a source with an observed flux F is

$$m = -2.5 \log \frac{F_0}{F}. \tag{4.12}$$

It could also be extended to define how relative magnitudes of two different stars with observed flux values of F_1 and F_2 relate, i.e.

$$m_1 - m_2 = -2.5 \log \frac{F_1}{F_2}. \tag{4.13}$$

The absolute magnitude M of a star is the actual intrinsic brightness of the star, or the brightness that a star would have if it is at a distance of 10 parsecs in perfectly clear space without interstellar absorption. Since this magnitude is evaluated at a fixed distance for all astronomical objects, i.e. $d = 10 \, pc$, a distance independent measure of their brightnesses can be made. This is a measure of the true intrinsic brightness of the star. This could also be defined i.t.o. flux as follows: The flux at a distance of 10 parsecs relates to the flux at an observed distance of r parsecs as

$$\frac{F(r)}{F(10)} = \left(\frac{10}{r} \right)^2. \tag{4.14}$$

This could be used along with Equation 4.13 to determine the relationship between apparent and absolute magnitudes as

$$m - M = -2.5 \log \frac{F(r)}{F(10)} = -2.5 \log \left(\frac{10}{r} \right)^2 \tag{4.15}$$

or

$$m - M = 5 \log \frac{r}{10}. \tag{4.16}$$

This equation can be cast in the following form

$$m - M = 5 \log r - 5. \tag{4.17}$$

From these expressions, in particular Equation 4.14, it can be seen that the stellar brightness reduces as a function of distance as shown in Section 4.2.1.

4.2.3 Radiative Transfer

Space is not a pure vacuum and is filled with gas and dust in the interstellar medium (ISM), and the radiation intensity that is emitted from radiative sources is not a constant radiation intensity, but a varying radiation intensity due to radiative transfer processes. This is due to the addition or subtraction of energy because of emission or absorption when the radiation beam passes through matter, leading to a non-constant specific intensity (e.g. Rybicki and Lightman 1979 for a general discussion).

Emission

The energy emitted per unit volume per unit solid angle per unit time define the spontaneous emission coefficient j and can be expressed as

$$j = \frac{dE}{dV \, d\Omega dt} \, (\text{erg cm}^{-3}\text{ster}^{-1}\text{s}^{-1}). \tag{4.18}$$

For spontaneous emission at a specific frequency j_ν is defined as

$$j_\nu = \frac{dE}{dV \, d\Omega d\nu dt} \, (\text{erg cm}^{-3}\text{ster}^{-1}\text{Hz}^{-1}\text{s}^{-1}). \tag{4.19}$$

The emission coefficient is in general direction dependant, but for an isotropic emitter the radiated power P_ν per unit volume per unit frequency in terms of the emission coefficient is

$$j = \frac{1}{4\pi} P_\nu \ (\text{erg cm}^{-3}\text{Hz}^{-1}\text{s}^{-1}). \tag{4.20}$$

The emissivity ϵ_ν, i.e. the energy emitted spontaneously per unit mass per unit frequency per unit time, is sometimes used to define the spontaneous emission. For isotropic emission, where the fraction of energy radiated into $d\Omega$ is accounted for, the emissivity is then

$$e_\nu = \frac{dE}{\rho dV \, d\nu dt \frac{d\Omega}{4\pi}} \ (\text{erg gm}^{-1}\text{Hz}^{-1}\text{s}^{-1}). \tag{4.21}$$

Here ρ is the mass density of the emitting medium. Comparing equations 4.19 and 4.21 the relation between spontaneous emission and emissivity for isotropic emission is

$$j_\nu = \frac{\epsilon_\nu \rho}{4\pi} \ (\text{erg cm}^{-3}\text{ster}^{-1}\text{Hz}^{-1}\text{s}^{-1}). \tag{4.22}$$

Defining the volume traversed by a radiating beam in terms of a beam cross sectional area dA transversing a distance ds, i.e. $dV = dAds$, the intensity added to a beam by spontaneous emission can be determined through

$$dI_\nu = j_\nu ds. \tag{4.23}$$

It can therefore be seen that the radiation intensity is no longer constant, unlike the case for radiation intensity in free space where

$$I_\nu = constant \tag{4.24}$$

or

$$\frac{dI_\nu}{ds} = 0. \tag{4.25}$$

Absorption

From the previous theory the loss of intensity due to absorption can be quantified by

$$dI_\nu = -\alpha_\nu I_\nu ds. \tag{4.26}$$

Here $\alpha_\nu(\text{cm}^{-1})$ defines the absorption coefficient. This phenomenological law can be explained in terms of a microscopic model in which randomly distributed particles in a medium of density n (cm^-3) each present an effective absorbing area, or cross section of magnitude σ_ν (cm^2). See Figure 4.6 and Figure 4.7.
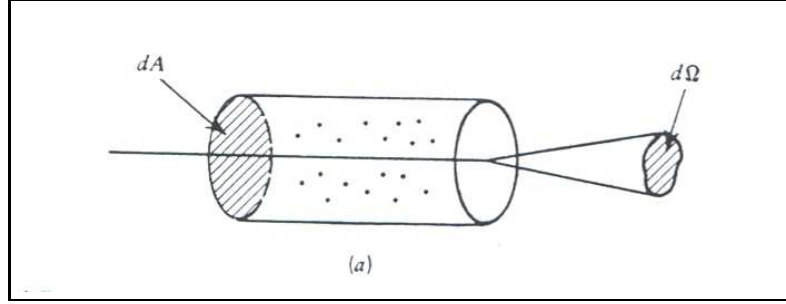
Figure 4.6: Radiation passing through an absorbing medium (Rybicki and Lightman 1979).
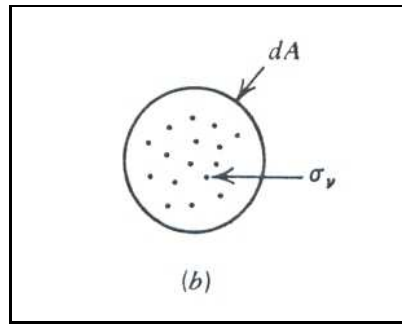
Figure 4.7: Cross sectional view of medium (Rybicki and Lightman 1979).

The effect of these particles on radiation passing through an area dA along a distance ds within a solid angle $d\Omega$ can be considered by the number of particles in the element $ndAds$ and the total absorbing area presented by those particles $n\sigma_\nu dAds$. The energy absorbed out of the radiation beam is then

$$- dI_\nu dAdtd\Omega d\nu = I_\nu(n\sigma_\nu dAds)d\Omega dtd\nu. \tag{4.27}$$

This equation can be rewritten as

$$dI_\nu = -n\sigma_\nu I_\nu ds. \tag{4.28}$$

It can be seen that this equation is the phenomenological law defined by Equation 4.26.

Comparing these equations, the absorption coefficient can be defined as

$$\alpha_\nu = n\sigma_\nu. \tag{4.29}$$

The absorption coefficient is sometimes written as

$$\alpha_\nu = \rho\kappa_\nu. \tag{4.30}$$

Here ρ is the mass density and κ_ν ($\mathrm{cm^2 g^{-1}}$) the mass absorption coefficient or the opacity coefficient. This microscopic model for the absorption is only valid if:

1. The linear scale of the particle cross section $\sigma_v^{1/2}$ is small in comparison to the mean particle distance d. This can be expressed in terms of the absorption coefficient as $\alpha_\nu d \ll 1$.

2. The particles have to be independent and randomly distributed.

These conditions are fortunately always true for the ISM.

Radiative Transfer Equation

The effects of emission and absorption can be combined into a single equation that can be used to determine the variation of the specific intensity. The radiative transfer equation can be defined by combining the contributions for emission and absorption, i.e.

$$\frac{dI_\nu}{ds} = -\alpha_\nu I_\nu + j_\nu. \tag{4.31}$$

This transfer equation can be used to solve the intensity in an emitting and absorbing medium, by incorporating most of the microscopic aspects of radiation into a single equation, and relating them into two coefficients α_ν and j_ν. Two effects of radiative transfer that influences photometric studies are interstellar extinction and atmospheric extinction. Correction for interstellar extinction is discussed below, while correcting for atmospheric extinction due to the atmosphere of the earth will be discussed in Section 4.3.3 on page 92.

4.2.4 Interstellar Extinction

Interstellar absorption or extinction is the effect of dust and gas in the interstellar medium (ISM) on starlight, see Figure 4.8, with the gas and dust concentrated towards the plane of the Milky Way galaxy (e.g. Palmer and Davenhall 1999 for a general discussion). Interstellar dust scatters stellar radiation, while interstellar gas tends to absorb and then re-radiate stellar radiation at different wavelengths.
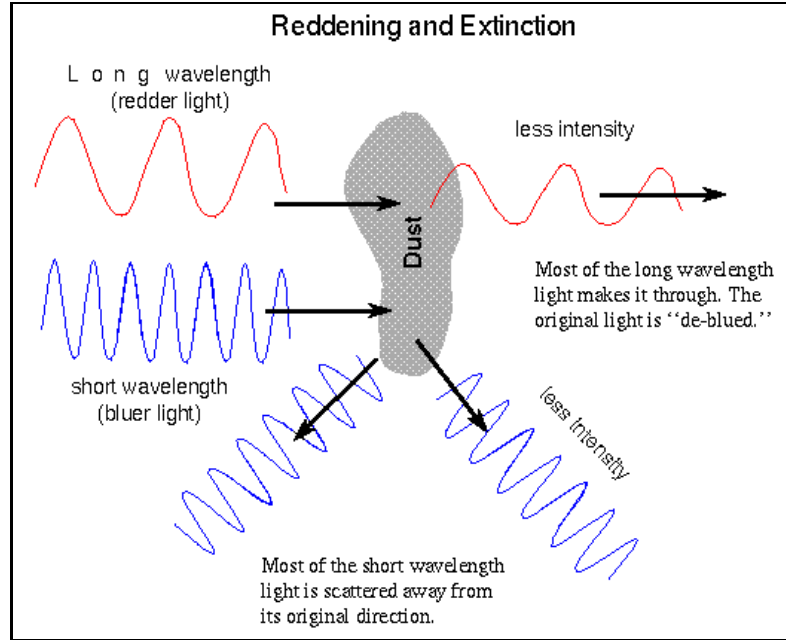
Figure 4.8: The effect of dust and gas on radiation (http://chandra.harvard.edu/edu /formal/stellar_ev/story/dustefct.gif).

This extinction effect is unfortunately non-uniform across the observable spectrum. The observed magnitude m_{obs} of a star will consist of its intrinsic magnitude m_{int} and an added extinction factor $A(\lambda, position)$ called the total absorption, i.e.

$$m_{obs} = m_{int}(\lambda) + A(\lambda, position). \tag{4.32}$$

The total absorption factor is dependant on both the wavelength, and the position, because the position of the star determines the amount of ISM that the observed light transverses. The extinction corrections can thus be written as

$$A(\lambda, position) = \zeta(\lambda) A_1(position). \tag{4.33}$$

Here $\zeta(\lambda)$ is a product of an absorption coefficient $\kappa_a(\lambda)$, which is a function of wavelength, and is only dependant on the amount of ISM along the line of sight. Thus a wavelength function could be defined

$$\zeta(\lambda) = \frac{\kappa_a(\lambda)}{\kappa_a(\lambda = 5500\text{Å})}. \tag{4.34}$$

This Interstellar Absorption Law is normalized at 5500Å, and is also called the reddening curve, because of the manner in which shorter wavelengths are affected more than longer wavelengths. With $A_1(position)$ now only a function of the location of the observed star. Equation 4.32 then becomes

$$m_{obs} = m_{int}(\lambda) + \zeta(\lambda)A_1(position). \tag{4.35}$$

When the reddening curve is plotted against $1/\lambda$ across the UBVRI bands, an approximately linear factor is seen. See Figure 4.9.
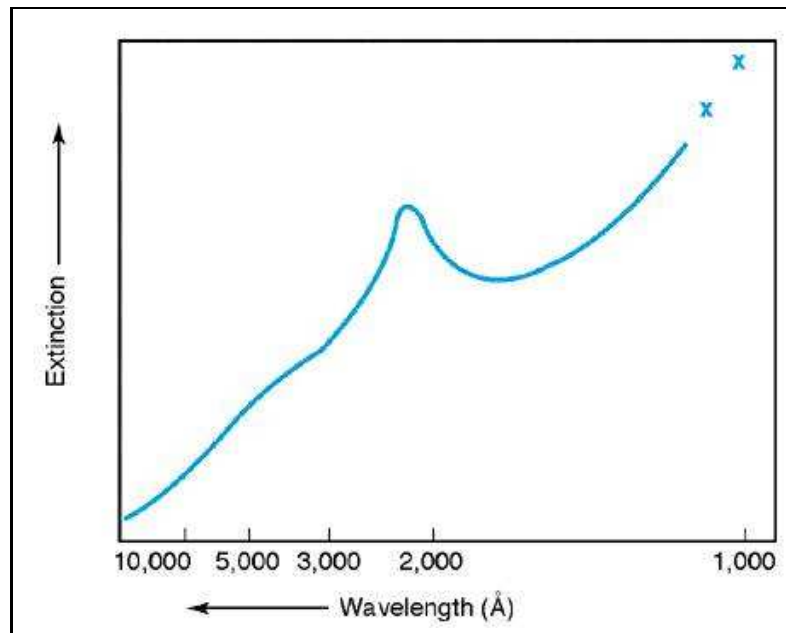
Figure 4.9: Extinction or reddening curve (http://www.astro.livjm.ac.uk/courses/phys134 /pic/magcol/extinction.jpg).

The peak at 2200 Å is thought to be because of the presence of carbon in the ISM. Observed magnitudes could therefore be corrected for interstellar extinction relatively easily. As mentioned above interstellar extinction increases towards the blue end of the electromagnetic (EM) spectrum, with stars appearing redder, thus the term interstellar reddening is also used (Ridpath 1997). A visual example of this extinction effect is the reddening of

77

stars observed near dust clouds or star forming regions. This reddening effect can also be seen on a larger scale with the reddening of stars towards the center of the Milky Way, because of the concentration of the interstellar gas and dust towards the plane of the Milky Way. Because of the location of the earth in the Milky Way it means that any observations done towards the center of the galaxy will require higher sensitivities in the red end of the spectrum than the blue. This effect was one of the reasons for the acquisition of a red-sensitive CCD for the planet research program for the 1.5m telescope, as the search programs are concentrated towards the center of the Milky Way.

4.2.5 Photometric Systems, Colour Indices and Standard Stars

Photometric systems must be defined to facilitate the transformation of measured photometric data into a common standard, to increase the validity of photometric research. A number of different filters are used during photometric studies, depending on the objects studied, with broad-band filters ($\geq$ 300 Å) used for faint objects, and intermediate (100 Å to 300 Å) and norrow band (a few tens of Å wide) filters used for brighter objects. These filters are configured into different photometric systems, e.g. Johnson, Johnson-Morgan, Cousins, Kron-Cousins, Strömgren and JHKLM System (e.g. Ridpath 1997; Palmer and Davenhall 1999 for general discussions).

Johnson

The Johnson system is one of the most widely used photometric systems, and is considered the "photometric standard". The system was originally developed for photometry with photomultiplier tubes (PMT), with little sensitivity in the red and strong response in the blue.

Johnson-Morgan

The Johnson-Morgan UBVRI photometric system was started in the 1950's with only the UBV bands, to be used with PMTs. The RI bands were added later, with the increased sensitivity in the red that CCDs offered. The system is calibrated to a zero-point where

an A0-spectral type star will have U = B = V.

Cousins

This photometric system is an addition to the Johnson-Morgan UBV system, with the RI bands calculated using southern hemisphere data. The UBV bands for the Cousins and Johnson-Morgan systems are identical, while the Cousins RI bands are shifted towards the blue, with wavelength peaks of 6700 Å and 8100 Å respectively. The RI bands are thus denoted as R_C and I_C, where "C" stands for "Cape". One disadvantage of the UBV bands is because of the short-wavelength cut-off of the U filter which is to a large extent determined by the atmosphere of the Earth and not by the detector or filter. This leads to variability in the observed magnitudes with observing location and weather conditions. Figure 4.10 can be seen as representative of standard and modified Johnson systems.
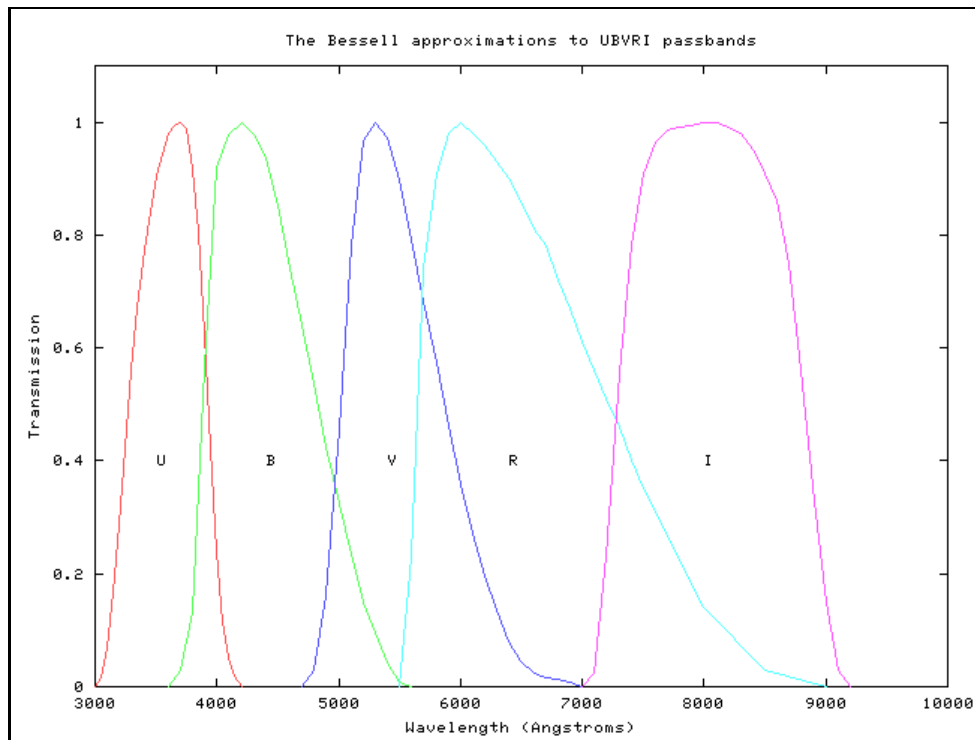
Figure 4.10: Bessell UBVRI filters for Johnson system (http://spiff.rit.edu/classes/phys440 /lectures/filters/bessell.png).

Kron-Cousins

The Kron-Cousins UBVRI photometric system was developed to take advantage of the responsiveness of CCDs in the red and near infrared spectral regions. To prevent infrared leakage the UBV and R filters are carefully masked. The 1.5-m Rockefeller telescope uses this filter system, with modified Johnson-Kron-Cousins RI filters. See Figure 3.3 on page 52 for the response curves for these filters. See Figure 4.11 for the standard Kron-Cousins filters.
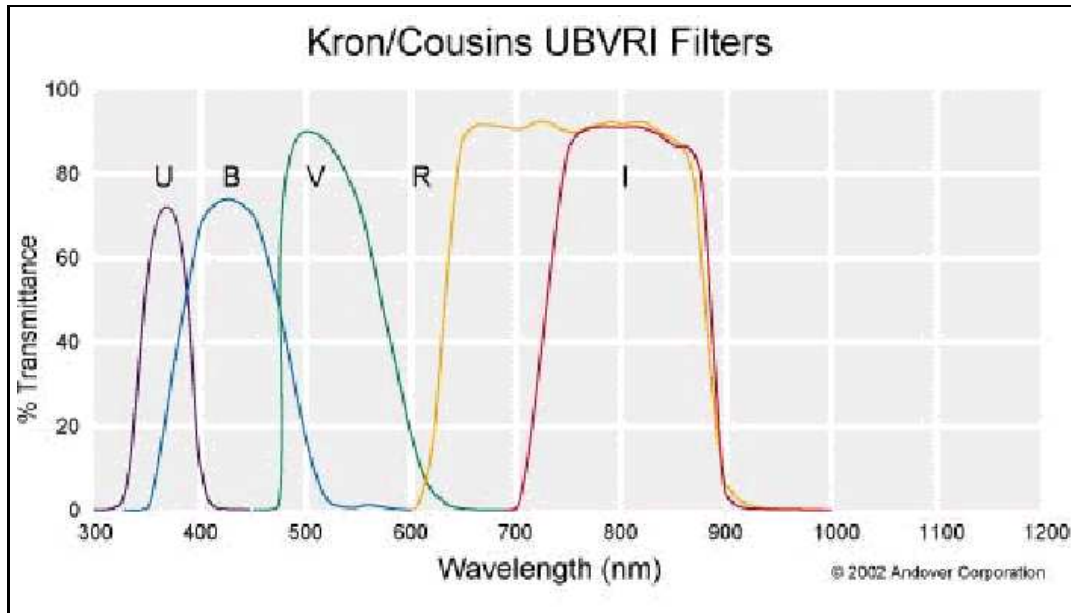
Figure 4.11: The standard Kron-Cousins UBVRI Filter system (http://www.lotoriel.com /site/images/andover_02.gif).

Strömgren

The Strömgren intermediate-band *uvby* system is also a widely used photometric system, and correlates well with the Johnson-Morgan V-magnitudes. It is also often supplemented by two interference filters to measure the strength of the Hβ line. See Figure 4.12 for the response curves for the Strömgren filter system.
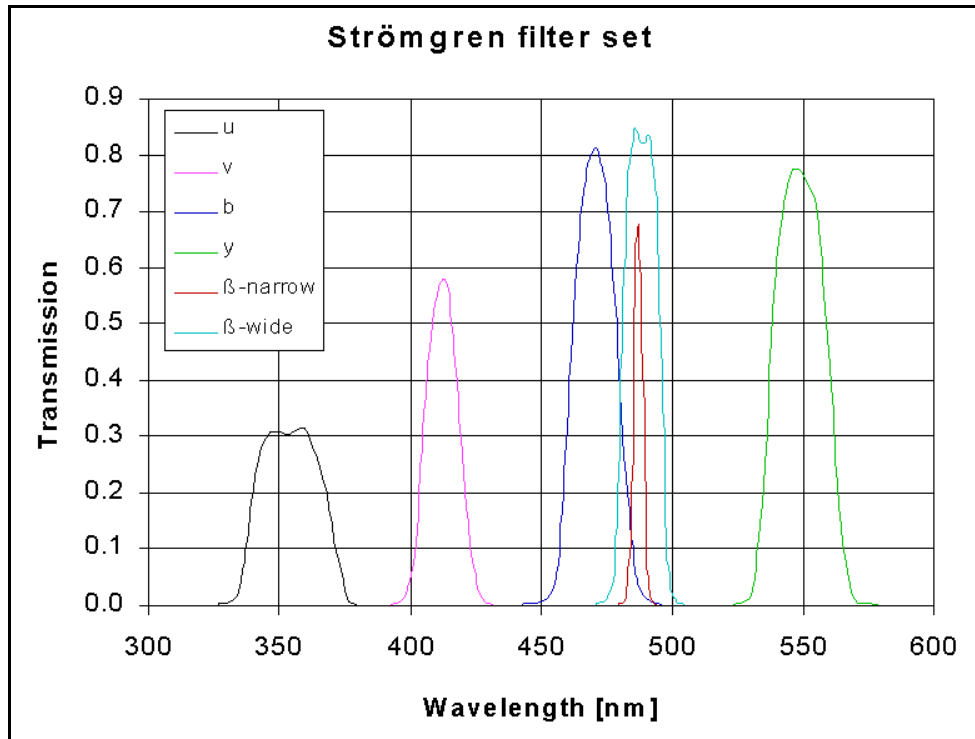
Figure 4.12: The Strömgren response curves (http://www.konkoly.hu/staff/racz
/stromgrens.gif).

JHKLM System

This photometric system is an extension to longer wavelengths of the UBV system. The names are derived from the transparency windows of the atmosphere of the earth at infrared wavelengths, and are matched accordingly. See Figure 4.13 for the transparency windows of the atmosphere of the earth for EM radiation, and Figure 4.14 for the transparency windows for the JHKLM system.
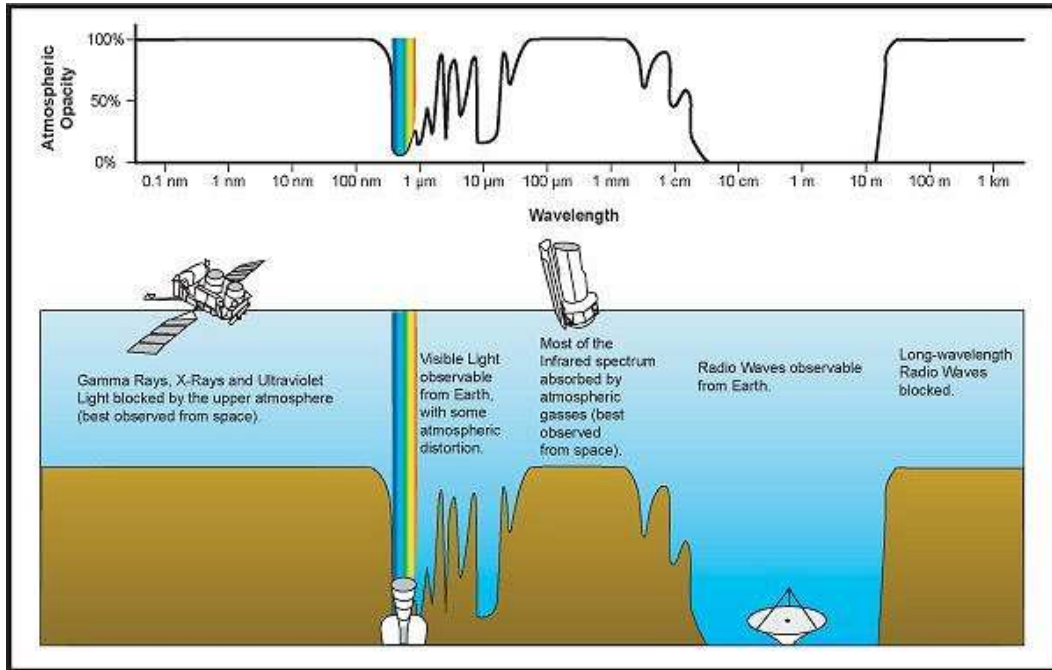
Figure 4.13: The opacity of the Earth's atmosphere to EM radiation (http://content. answers.com/main/content/wp/en/thumb/a/a8/600pxAtmospheric_ electromagnetic_transmittance_or_opacity.jpg).
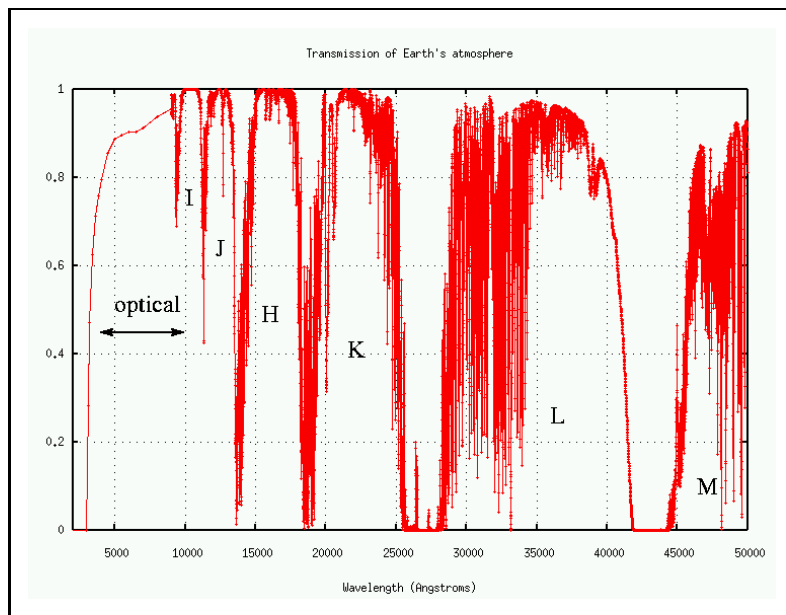
Figure 4.14: The transparency windows at infrared wavelengths for the JHKLM system (http://spiff.rit.edu/classes/phys440/lectures/filters/bessell.png).

The L-band was later replaced by a L'-band that had a better match to the specific atmospheric window. The JHKLM system is also calibrated to a zero point for an A0 spectral type star, like the Johnson-Morgan system, where J = H = K = L = M = U = B = V. The standard star used is Vega (α Lyrae).

Table 4.1: Wavelength definitions for different photometric systems (Palmer and Davenhall 1999)

System	Band	Effective Wavelength (Å)	Bandwidth (FWHM)(Å)
Visual	m_v	~5500	-
Photographic	m_{pg}	~4250	-
Johnson-Morgan	U	3650	680
	B	4400	980
	V	5500	890
	R	7000	2200
	I	9000	2400
Kron-Cousins	U	3600	700
	B	4400	1000
	V	5500	900
	R	6500	1000
	I	8000	1500
Strömgren	u	3500	340
	v	4100	200
	b	4670	160
	y	5470	240
	$H\beta_w$	4860	150
	$H\beta_n$	4860	30
		μm	μm
JHKLM	J	1.25	0.38
	H	1.65	0.48
	K	2.2	0.70
	L	3.5	1.20
	L'	3.8	0.6
	M	4.8	1.0

Colour Indices

Photometric systems containing multiple colour bands, or filters are called multi-colour systems. The measured magnitudes from the different filters of the photometric systems can be compared to obtain colour indices for the objects being studied. The colour index of an object is the difference between magnitude in any two filter bands, e.g U-B, B-V, V-R, and etc. The colour indices of stellar objects are used to describe their properties, with B-V related to the temperature and spectral class, and U-B a function of both the luminosity and temperature.
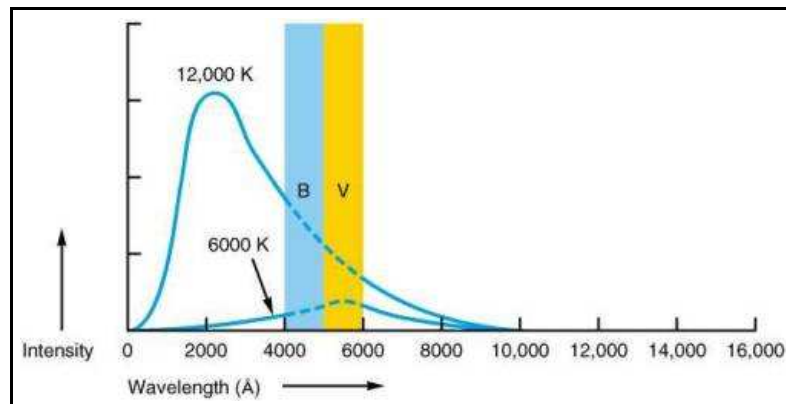
Figure   4.15:   Continuous   spectra   of   two   different   stars
(http://www.astro.livjm.ac.uk/courses /phys134/pic/magcol/colindx.jpg).

Figure 4.15 depicts the continuous spectra of two different stars and the ranges of B and V magnitude measurements. It can therefore be seen that the two stars can be defined by their B-V colour index, with the hot star having a negative B-V value, and the cool star having a positive B-V value. The results of multicolour photometry are usually condensed to a single magnitude value (usually the V-magnitude) and a set of colour indices (e.g. Rybicki and Lightman 1979).

Standard Stars

After a standard photometric system is set up it will be defined by the detector and the passbands used. Unfortunately, not all photometric systems are alike, no matter how precisely the system are reproduced i.t.o. the defined standard. There will thus be a difference between the instrumental system used and the photometric standard system. To

calibrate observational data it is therefore necessary to convert instrumental magnitudes to standard magnitudes. This is achieved by using the system defined standard stars, with every photometric system having its own intercompared set of standards. Standard stars are stars used to calibrate observations of program stars being studied, specifically during photometry. Photometric standards are stars of accurately known magnitudes and colours, which are used to compare against the program stars. Standard stars must also be limited to a brightness range. Accordingly standard stars must be bright enough to be observable with small telescopes, while faint enough not to saturate the photometric instrumentation of larger telescopes (Ridpath 1997; Palmer and Davenhall 1999).

When choosing standard stars for calibration purposes, a number of criteria have to be looked at, namely the specific photometric system used, the location of the observing site, the position and magnitude range of the program stars, and the colour measurements required. There are a number of catalogues of photometric standard stars that could be used to define and calibrate photometric systems, with many of the catalogues available in electronic format. The catalogues used for the Boyden photometric system include the Johnson, E-region, F-region and Landolt catalogues. The E-region standards are centered around declination (Dec) $-45°$, with a magnitude range of $2 < V < 11.5$ and a colour range of $-0.2 < (B - V) < 1.6$. The F-region standards are evenly spaced in RA, at Dec $-75°$. For his catalogue, Landolt used the E-region and Johnson catalogues as reference to observe more than 250 stars with $V > 11$, with the stars centered around the equator. These catalogues should however not be used blindly, as there may be limitations and special criteria i.t.o. applicability and use that have to be taken into account. Most catalogues are accompanied by support documentation containing instructions towards the proper use of these catalogues (Ridpath 1997; Palmer and Davenhall 1999).

The procedure to use in selecting standards for observational purposes can thus be summarized as follows (Palmer and Davenhall 1999):

1. Choose the required catalogues.

2. Decide on the number of standards required (usually between 15 and 20), depending on the aim of the observational program.

3. Select a range of zenith distances (and hence airmasses) similar to, but slightly larger than those of the program objects. With the standards distributed every 30 arcmin-

utes, up to an airmass of 2.0 on both sides of the zenith.

4. Select a range of celestial coordinates similar to those of the program objects.

5. Select a range of colours and magnitudes that are similar or larger than the range of those of the program objects.

It is not desirable to mix standards from different catalogues, as different colour measurements may be present, but it can be done if the observational program requires it. The above selection criteria are just a special case of the usual requirement that calibrators should occupy a similar volume of parameter space as the objects they are calibrating (Palmer and Davenhall 1999).

4.3 Photometric techniques

There are two basic photometric techniques used, namely Differential or Absolute Photometry (e.g. Palmer and Davenhall 1999; DaCosta 1992; Howell 1992 for general discussions). These techniques differ regarding the process involved to obtain the magnitudes for the program stars. The basic principle, however, remains the same, with the desired object being observed, the instrumental magnitudes being measured, and the measured instrumental magnitudes being calibrated to the desired system through photometric analysis procedures.

Differential photometry offers the most accurate photometric measurements obtainable. The technique consists of the measurement of the program star as well as a number of "check" stars on the same image field. The check stars must be non-variable with well known properties, and if possible, a real previously calibrated "standard star". The secondary stars are then used to measure the instrumental magnitude and magnitude variation of the program object. This technique has the advantage that only reduction-processes and no calibration-processes are required.

Absolute photometry is a bit more difficult to perform. The technique consists of the measurement of the program star and a set of standard stars, all on different image fields. The known properties of the system, standard stars, and the observational conditions are

used to apply reduction procedures as well as to calibrate the measured instrumental magnitudes to a standard system.

Before the stellar magnitudes could be measured, or the values analyzed, other instrumental and atmospheric contributions to the signal of the measured object need to be removed. These contributions towards the signal are the system noise parameters of the CCD system, the discrepancies between the instrumental and target photometric systems used and the effects from the atmosphere of the earth. These contributions have to be removed from the data. This is done through data reduction and calibration techniques. Thus, there is a certain procedure that has to be followed when doing photometry, namely:

1. The photometry technique to be used is identified.

2. All necessary objects to be observed are identified.

3. Images (data frames) of the fields containing the program stars are taken using the required filters.

4. In addition bias, dark and flat-field frames are taken for data reduction.

5. The bias, dark and flat field reductions are applied to the data frames.

6. The reduced data frames are used to obtain instrumental magnitudes.

7. The measured values are used to calibrate (if required), and analyze the data.

.

4.3.1 Photometric Image Reduction

Utilizing CCDs for photometry involve digital image processing. This is possible because of the nature of the signal obtained from the CCD system. The signal is represented as an image containing pixels arranged in columns and rows, with each pixel having a specific value, much like a matrix. This allows for addition, subtraction, multiplication and division of the images with each other or with a specified value. Digital image processing thus allows for manipulation of the image through reduction processes (subtraction of noise), enhancement (image stacking) and analysis (measuring data values). This property allows for the removal of instrumental effects, due to the CCD system, from the data. There are three basic reduction frames that are used to remove the inherent system effects, namely

bias, dark and flat frames.

Bias

During the amplification process of the signal in the CCD, an electronic offset is added. The "bias" is noise that is added to the actual data, to insure that the ADC always receives a positive value. Unfortunately, this noise also has a slight variation across the CCD chip, that changes with time. Part of the intrinsic noise of the bias is the readout-noise that is induced during signal amplification. See Section 2.3 on page 32 for a complete discussion. To remove this bias, bias-frames are used: if the whole CCD area is used to obtain data. Sometimes bias strips are used, which is just a pair of narrow strips on the side of the chip where the bias and noise values are stored. A bias frame is an image frame taken with an effective exposure time of 0 seconds. This bias frame only contains the inherent system bias as well as the small scale structure in the noise. The number of bias frames required for reduction processes will be depending upon the noise structures present, with about 25 bias frames per observation night being a good average. These bias frames can be added together to form a "master" bias which can in turn be subtracted from all the data (dark, flat and program) frames to remove the bias (e.g. Calitz 2005; Massay 1997; Gilliland 1992).

Dark

All CCDs have some level of dark current. This dark current is the accumulation of thermal noise due to the excitation of thermal electrons. This dark current acts as an additive quantity to the electron count of the pixels, of a few electrons/pixel/second. This dark current can be kept to a minimum through the use of cooling mechanisms, to such an extend that it could be deemed negligible. See Section 2.3 on page 36 for a complete discussion. To remove this dark count, as well as other constant noise patterns present, dark frames are used. A dark frame is an image frame taken with an integration time larger or equal to the longest exposure time used during the observation, and at the same operating temperature as the data frames, with the shutter CLOSED. For increased effectiveness it is recommended that very long integration times be used, with at least 5-10 dark frames per observation night. These dark frames, after bias correction, can be added together to form a "master" dark which can in turn be subtracted from the flat and program frames (e.g. Calitz 2005; Massay 1997; Gilliland 1992).

Flat

The sensitivity of the CCD to the incident photon flux varies over the detector surface. The variation is both on a large scale, from side to side, and on a small scale, pixel per pixel. The variation is wavelength dependant, but can also be influenced by the optics of the telescope-CCD system. System influences include pixel non-uniformity, dust spots and vignetting. In astronomical telescope systems, the mounts of the optical elements cut into the oblique flux beams and prevent the flux beams from being perfectly circular, leading to a reduction in the oblique flux. Additional reduction in the oblique flux can also be due to mechanical vignetting in the optics, which will make the aperture noncircular. This reduction in flux in the outer parts of the field of view is known as vignetting. In an astronomical CCD-camera system this reduction in oblique flux results in darkened corners on the data frames (e.g. Calitz 2005; Gilliland 1992).

Flat frames are thus used to correct for these variations and defects. A flat frame is a data frame taken, in each filter, using a photometrically flat or uniform light source with the same optical setup as for the program frames. There are two types of flat fields that could be used, namely Dome-flats and Sky-flats (e.g. Calitz 2005; Gilliland 1992). Dome-flats are taken with the use of a stable light source that are used to illuminate a screen in the interior of the telescope dome. Sky-flats are taken with the use of the evening or morning twilight sky. Both have certain advantages, but it is generally believed that sky-flats are better representative of a true flat field, with the same global illumination as the program frames, as well as having a good signal/noise level. Flat frames are taken with exposure times that result in a high net signal value, with at least 5 flat frames per filter per observation night. The flat frames can be corrected for bias and dark-count, after which the filter specific flat frames are combined to form "master" flat fields for each specific filter. These flat fields can be used to correct the program frames, by dividing the program frame by the corresponding filter specific "master" flat (e.g. Calitz 2005; Massay 1997; Gilliland 1992).

4.3.2 Measuring Instrumental Magnitudes

After the data frames have been corrected for instrumental effects, they can be used to measure instrumental magnitudes. The instrumental magnitudes of the different objects of interest are usually measured relative to the sky background on the data frame. The instrumental magnitudes of the program and standard or check stars can be measured using one of two classes of measuring techniques, namely aperture photometry or point-spread-function fitting.

Aperture Photometry

The principle behind aperture photometry is the measuring of the starlight that falls within a defined circular region or aperture (e.g. Palmer and Davenhall 1999; DaCosta 1992 for general discussions). The aperture has to be large enough to enclose the entire stellar image, therefore measuring all the light from the stellar image. The total flux is the added flux from the separate pixels inside the defined aperture. The flux from the background sky is measured using a similar aperture technique with the aperture defined over a region free of stars. The difference between the two flux values gives the true apparent flux from the star. The instrumental magnitude thus measured is

$$m_{inst} = A - 2.5 \log \left(\frac{\left(\sum_{i=1}^{n} C_i \right) - nC_{sky}}{t} \right). \tag{4.36}$$

Here A is an arbitrary constant, C_i is the ith pixel count inside the aperture, C_{sky} is the average pixel count for the sky background, n is the number of pixels in the aperture, and t is the exposure time for the data frame. The exposure time component is used to normalize data frames with different exposure times. The sky background can be measured using a variety of different techniques. One is to use a defined aperture to measure a neighbouring region of blank sky, while the more preferred method is to use an annulus that surrounds the original aperture. Aperture photometry is preferred for sparse stellar fields, but can become difficult to perform on crowded stellar fields, as the apertures (images) of different stars may overlap.

Point-Spread-Function Photometry

Point-spread-function (psf) photometry is based on the principle that the image of a point source formed by a telescope and CCD system can be described by a mathematical function (e.g. Ridpath 1997; Palmer and Davenhall 1999; DaCosta 1992 for general discussions). This principle relies on the assumption that all star images have the same shape, with the only difference being the scaling factor. The shape of a conventional psf can be described as a "gaussian", with the height and width of the gaussian dependant on the brightness of the point source traced on the CCD data frame. Because stars cannot be resolved beyond a simple point source by a conventional telescope, the stellar images recorded with the CCD simply trace out the psf of the telescope on the data frame. For properly designed telescopes the psf will be independent of the position of the star in the focal plane.

There are two distinct methods used to contruct psf fitting models. The first uses the data itself to define an "empirical" psf. This could be accomplished by measuring well-defined and isolated stars on the data frame, which is used along with assumed positions and brightnesses of the observed stars to construct a psf of the light distribution in the data frame. The other method uses the data to fix the parameters that define a "model" psf through the use of an appropriate function, like a Gaussian function. This model is refined through different techniques, like varying the positions and brightness iteratively, or fitting the model to selected star profiles, until the model describes the observed light distribution. The defined psf can be fitted on the stars of interest: Therefore measuring the instrumental magnitudes by measuring the difference in the scaling factor between the fitted model and the chosen star. The psf magnitude is

$$m_{psf} = A - 2.5 \log{(SF)}. \tag{4.37}$$

Here m_{psf} is the relative measured magnitude, A an arbitrary zero point magnitude assigned to the psf, and SF the scaling factor. This technique is very effective for use on crowded stellar fields, but can also be used on sparse stellar fields. This technique, however, relies on the important factor that all the images have the same profile. Therefore this technique could be invalidated by the presence of extended objects, which have their own unique profiles.

4.3.3 Calibrating Instrumental Magnitudes

After the instrumental magnitudes have been measured for all the stars of interest in all the different data frames and for all the different filters, the instrumental magnitudes need to be calibrated (e.g. DaCosta 1992; Palmer and Davenhall 1999 for general discussions). The calibration needs to be applied to convert the measured instrumental magnitudes to a standard photometric system. There are two effects that have to be corrected for, namely the discrepancies between the instrumental and target standard system, and the effect of atmospheric extinction. The effect of atmospheric extinction is the scattering and absorption of radiation as discussed in Section 4.2.3. Atmospheric extinction will then scatter shorter wavelengths (blue) more then longer wavelengths (red). Short wavelength scattering effects can visually be seen by the "appearance" of a blue sky during the daytime, because of the scattering of sunlight. The extent of the calibration will depend upon the photometric research requirements. Thus, for differential photometry only corrections for atmospheric extinction have to be considered, whereas for absolute photometry both effects have to be considered.

The corrections for atmospheric extinction on the instrumental magnitudes can be applied by first determining the airmass and then determining the instrumental magnitudes for an airmass of $X = 0$. The airmass is a measure of the amount of atmosphere between the observer and the object. The airmass is normalized such that for an object at the zenith $X = 1$, and $X = 0$ for objects outside the atmosphere of the earth. The airmass can be calculated from the zenith distance, which is dependant on the position of the star, and the location of the observer. Taking all parameters, for instance refraction effects, curvature of the atmosphere and variations of air density with height, the relationship between airmass and zenith distance (Hardie 1962) is

$$X = \sec z - 0.0018167(\sec z - 1) - 0.002875(\sec -1)^2 - 0.0008083(\sec z - 1)^3. \quad (4.38)$$

This can be approximated for small zenith angles to

$$X = \sec z. \quad (4.39)$$

Fortunately most computerized telescope systems determine the airmass automatically. The DFM system at Boyden Observatory, for example, uses the Hardie equation in the control system software. It can therefore be used directly to determine the corrected in-

strumental magnitudes.

The instrumental magnitude for an airmass of X = 0 denoted by $m_0(\lambda)$, can therefore be calculated from the observed instrumental magnitude $m(\lambda)$ by

$$m_0(\lambda) = m(\lambda) - k'(\lambda)X - k"(\lambda)X(m(\lambda) - m(\lambda')). \tag{4.40}$$

Here $m(\lambda')$ is the instrumental magnitude in the second filter and the coefficients $k'(\lambda)$ and $k"(\lambda)$ are the first and second order extinction coefficients respectively. The extinction coefficients differ for each location. Thus each observatory has its own predetermined coefficient values.

The atmospheric extinction corrected instrumental magnitudes need to be calibrated in terms of a target standard photometric system. To do this the measured and catalogued standard star data for the different passbands are used. The instrumental magnitude data for the standard stars and the program objects are used to transform the data into the standard system using equations of the form

$$m_x = m_0(\lambda) + Z_x + C_x(m_x - m_y). \tag{4.41}$$

Here $m_0(\lambda)$ is the corrected instrumental magnitude, and m_x and m_y are the standard magnitudes for passbands x and y respectively. The coefficient C_x is the colour-correction term, and Z_x is the photometric zero-point between the standard and instrumental system. Equation 4.40 and Equation 4.41 can be combined to form a general equation that can be used to transform instrumental magnitudes into a standard photometric system

$$m_x = m(\lambda) - A_x + Z_x + C_x(m_x - m_y) - k'(\lambda)X - k"(\lambda)X(m(\lambda) - m(\lambda')). \tag{4.42}$$

This equation can be rewritten into a general form and extended to include other terms also needed for calibration purposes

$$(m_x)_{std} = (m_x)_{inst} - a_0 + a_1(m_x - m_y)_{std} - a_2X - a_3X(m_x - m_y)_{inst} + ... \tag{4.43}$$

Here $(m_x)_{std}$ and $(m_x - m_y)_{std}$ are the catalogued standard system magnitude and colour terms, $(m_x)_{inst}$ the exposure time corrected instrumental magnitude, X the airmass for the observation. Other terms like time and colour-squared dependencies can also be added.

Fortunately, extended terms like time and colour-squared dependences are not usually required. The coefficient terms are defined as follows:

1. a_0 is the zeropoint constant for the CCD-Telescope system - and is a measure of how sensitive the system is for the specific passband.

2. a_1 is the colour term - and is a measure of how well the instrumental system approximates the standard system.

3. a_2 is the first order extinction coefficient - and depends on the atmospheric transmission.

4. a_3 is the second order extinction coefficient - this terms is important because extinction varies rapidly across the passband.

These coefficients can be analyzed by defining a set of equations for different passbands, and solving the equations using least squares fitting. Thus for the UBVRI system a set of transformation equations can therefore be defined

$$
\begin{aligned}
U &= m_u - A_u + Z_u + C_u(U-B)_{std} - k'_u X - k"_u X(m_u - m_b)_{inst} \\
B &= m_b - A_b + Z_b + C_b(B-V)_{std} - k'_b X - k"_b X(m_b - m_v)_{inst} \\
V &= m_v - A_v + Z_v + C_v(B-V)_{std} - k'_v X - k"_v X(m_b - m_v)_{inst} \\
R &= m_r - A_r + Z_r + C_r(V-R)_{std} - k'_r X - k"_r X(m_v - m_r)_{inst} \\
I &= m_i - A_i + Z_i + C_i(V-I)_{std} - k'_i X - k"_i X(m_v - m_i)_{inst}.
\end{aligned}
$$

4.3.4 Solving the Transformation Equations

Although the transformation equations can be solved using least squares fitting, it is sometimes better to treat the two different components separately, that is solving the atmospheric extinction part seperatly from the photometric standard calibration part. The first and second order extinction coefficients can be solved as follows.

The first order extinction coefficients can be calculated by plotting the airmass against the instrumental magnitudes for a set of standard stars for a specific passband. The slope of the fitted line through the data points will yield the first order extinction coefficient value for the passband. This is under the assumption that the second order coefficients are approximately zero. If the second order coefficients are significant, the fitted line will

be curved. To solve the extinction coefficients for significant second order terms requires data values for two standard stars of different colours. A set of equations can be set up to first solve the second order terms for the two stars, and then to solve the first order terms. The zeropoint and colour term constants for the photometric standard calibrations can be determined using the calculated extinction coefficients and the catalogued and instrumental standard star data for two or more different passband equations.

The above mentioned techniques can best be explained and discussed through a practical example, and are therefore discussed in Chapter 6 through the determining of the extinction coefficients for the Boyden Observatory using a set of observed standard star-data that was acquired using the 1.5-m Rockefeller Telescope.

4.4   Data Analysis and Quality

After the calibrated magnitudes have been determined, the values can be used to analyse the data of the program star under investigation. Analysis techniques include the plotting of light curves, fitting of data on theoretical models, and refining and extending known data. The quality of the photometric data needs to be evaluated carefully. This is done by determining the signal-to-noise ratio for the photometric data (e.g. Gilliland 1992; Howell 1992 for general discussions).

The aim of performing CCD observations is not only because of the efficiency of CCDs in detecting photons, but to extract the most information possible from the observational data. Unfortunately, even near perfect detectors like CCDs, still contain intrinsic noise due to photon statistics, therefore high precision observations is limited by the amount of noise present versus the data signal, or the signal-to-noise (S/N) ratio. This could be quantified because photon detection behave according to Poisson statistics. The Poisson distribution or "law of small probabilities" is a special limit of the Binomial distribution where the probability of an event is very small i.e. $p \rightarrow 0$, for a very large number of events $n = \infty$. Thus in terms of photon detections in a CCD, the Poisson distribution can be defined as follows. With n the number of photons falling in on the CCD each having a probability p being detected, the probability of detecting k photons is represented by the

Poisson distribution, i.e.

$$P(k; \sigma) = \frac{\sigma^k}{k!} e^{-\sigma}. \tag{4.44}$$

With σ the variance defined as

$$\begin{aligned} \sigma &= pn \\ &= \langle k^2 \rangle - \langle k \rangle^2 \end{aligned} \tag{4.45}$$

A ideal photon detector will then have a S/N (equal to $1/\sigma$) of

$$\frac{S}{N} = \frac{N_*}{\sqrt{N_*}} = \sqrt{N_*}. \tag{4.46}$$

Here N_* represents the total counts in the source. CCDs however are not ideal photon detectors, with the standard equation for the S/N of a point source measurement using a CCD thus defined by

$$\frac{S}{N} = \frac{N_*}{\sqrt{N_* + n_{pix} \left(N_S + N_D + N_R^2 \right)}}. \tag{4.47}$$

Here N_* is the total counts in the source (electrons/integration), n_{pix} is the total number of pixels used in the measuring aperture, N_S is the sky level (electrons/pixel/integration), N_D is the dark level (electron/pixel/intergration), and N_R is the readout-noise (rms electrons/pixel/read). This equation is the typical equation used to determine the S/N of point source observations, or to estimate the required intergration times needed. For bright sources this equation can be approximated to

$$\frac{S}{N} \approx \sqrt{N_*}. \tag{4.48}$$

In general Equation 4.46 can be used for reduced data values. Since the total counts is dependant on the intergration time it can be seen that to increase the S/N the integration time has to be squared. The S/N value will also indicate the quality of the data, with a higher S/N value representing a higher data quality. The minimum S/N ratio required for a signal to be detected is 1:1, but photon statistics will limit the S/N to a value equal to or greater than the Poisson limit, with the error value for the Poisson limit being

$$\sigma(Poisson) = \frac{1}{\sqrt{N_*}}. \tag{4.49}$$

The Poisson limit therefore defines the final precision in the S/N of the calibrated data

achievable, with no further improvement being possible by image reduction techniques (bias-, dark- and flat-frame reductions). This means that a Poisson limited S/N value of 100:1 will give an error of 1% which will result in a precision of 0.01 magnitudes.

Chapter 5

Boyden IRAF Package

5.1 Introduction

In this chapter IRAF will be discussed in general, with specific emphasis on photometric procedures. The Boyden-IRAF package will also be examined, specifically why and how it was developed, how it works, and preliminary results will be presented. This discussion will be based to a large extent on web based technical discussions and guides from (IRAF.Net `http://iraf.net/`).

5.2 An overview of IRAF

There are a large number of astronomical and astrophysical data analysis software available, of which IRAF is but one. The choice between which of the many to use for data analysis depends on:

1. The type of data available.

2. The type of data analysis to be done.

3. The support, knowledge and experience available for specific software.

4. And personal choice.

Thus, when a choice was made on which data analysis software to use for the development of a photometric pipeline for the Boyden Observatory, the Image Reduction and

Analysis Facility (IRAF) was chosen, as it satisfied most of these criteria.

IRAF is a general purpose software system for the reduction and analysis of scientific data, and is developed and maintained by the National Optical Astronomy Observatories (NOAO) in the United States of America since 1980. It was designed to be system independent, but because its origins are Unix-based, it is mostly run inside a Linux environment, but it can also be run on Microsoft Windows based systems using Cygwin. Its Operating System (OS) independence is achieved through the use of its own applications programming language - SPP - Subset PreProcessor. The SPP language can be thought of a C/Fortran hybrid, with the SPP converted into Fortran 77 and compiled by the host OS. The base level routines in IRAF are written in C. IRAF also has a complete graphics system that supports vector graphics on a wide variety of devices. Full networking support is also built into the IRAF system, allowing users to access remote data for analysis and display purposes (Hanisch 1992).

Its architecture is as a "host" for a number of different software packages, which can be loaded and initialized into the system, dependant on the requirements. The packages and tasks, what commonly would be referred to as applications and functions, are made up of base packages and external packages. The base packages consists of general tasks that are used for general data analysis and functionality. The external packages add to the overall functionality of the IRAF software. The external packages include specific packages developed for the Gemini Telescopes, the Hubble Space Telescope and many more. Other external packages are for better data handling and analysis. Not nearly all of the available packages will be used during general day to day data analysis, but in terms of astronomical and astrophysical data analysis, packages that are available include photometric as well as spectroscopic data analysis tools.

The IRAF user interface is command line (i.e. text based and not a graphical user interface (GUI)). Thus IRAF consists of:

1. Command Language (CL), providing the user interface to IRAF

2. Application programs that are run under the control of the CL

3. System utilities

4. Scientific application programs

5. A Virtual Operating System (VOS), that provides IRAF with a host independent environment

6. A Kernel (Host System Interface, HSI), that provides the communication with the host machine

Because IRAF is a multiprocess system the CL handles all communication with the user terminal, with all application packages running as concurrent subprocesses with a single application process containing many executable programs. The advantages to this are that it offers significant flexibility over single process architectures and also offers significant efficiency over less modular systems. The disadvantages, however, are the difficult error recovery and it can also cause unnecessary hiding of processes.

The basic concepts of the CL are that it organizes the system and applications tasks into a logical hierarchy of packages with a package being a collection of logically related tasks, presented to the user by a menu. Each task has its own set of parameters with each task having a query and a hidden mode for optional parameters. Packages must be loaded into the CL before it can invoke their tasks, with the CL having the option of loading more than one package at a time. The CL is designed to serve as both a command language and as an interpreted programming language. It has the ability to:

1. Function as a programmable desk calculator

2. Evaluate expressions

3. Execute CL scripts

4. Execute tasks or external programs

5. Has command syntax much like UNIX

6. Has input/output (I/O) redirection and pipes

7. Hosts a parameter set editor

8. Contain menus and extensive on-line help.

5.3 IRAF Package descriptions

5.3.1 Base Packages

The IRAF system is usually initialized from within a XTERM terminal window, with the welcome banner and basic commands displayed along with the top level menu for the installed IRAF system. The top level menu contains all the defined base and external packages available to the user. The top level menu for IRAF on a standard system, without any external packages, contains:

Table 5.1: Data Analysis Packages:

dataio:	Data format conversion package
images:	General image processing package
noao:	The NOAO optical astronomy package
plot:	Standard plot facilities
softools:	Software tools for IRAF
system:	IRAF system utilities
utilities:	Miscellaneous utilities

The two most important packages available in the standard system are probably the **images** package and the **noao** package. This is because the data that are to be analyzed consists mainly of CCD images that are of a digital nature, stored either in IRAF .imh or in the standard .fits format. The **images** package contains many standard image manipulation routines, with the **noao** package containing software for the reduction and analysis of data. See Table 5.2 and Table 5.3 for details.

Table 5.2: Functions defined for the **images** Package:

Filters and convolutions, boxcar, Gauss, ...
Coordinates and transformations
Image file manipulations, copy, move, delete
Pixel manipulations
Image arithmetic (pixel based)
TV display interfacing
Image Display

Table 5.3: The **noao** Package:

artdata: Artificial data generation package
astutil: Astronomy utility programs (precess, coordinate conversions)
digiphot: Digital stellar photometry package
focas: Faint object classification and analysis package
imred: Image reduction package (CCD, echelle, spectra)
onedspec: 1D spectra reduction and analysis
twodspec: 2D spectra reduction and analysis
surfphot: Galaxy isophotal analysis package

5.3.2 External Packages

The two most widely used and popular external packages that are normally layered onto the standard IRAF system are the **stsdas** and **tables** packages. The Space Telescope Science Data Analysis System (**stsdas**) contains a set of tools and support software that are used in the calibration and analysis of Hubble Space Telescope (HST) data. The **tables** package serves as an additional package and contains a set of tools for creating and manipulating tabular data, reading and writing FITS images and tables, as well as the creation of customized graphics. **stsdas** and **tables** are portable and, because they are layered on IRAF, should run on any system for which an IRAF port exists. Together, **stsdas** and **tables** provide a wide range of data analysis tools and capabilities. See Table 5.4 for details (Hanisch 1992).

Table 5.4: The **stsdas** and **tables** capabilities:

Calibration of HST science instrument data
Synthetic photometry and HST throughput modelling
Interactive curve fitting and surface photometry
Image restoration
Fourier analysis
Non-parametric statistical analysis
Table creation and manipulation
FITS image and table I/O
Graphics tasks tailored to HST data

In addition to IRAF's support for SPP (Subset Preprocessor) programming and CL (IRAF command language) script writing, **stsdas** also supports user-developed applications through a Fortran programming interface, called F77VOS, within the IRAF environment. This interface provides access to data in both image and table formats, and

provides a full set of graphics I/O functions. The **tables** package also contains a full SPP programming interface for table creation and manipulation (Hanisch 1992).

5.3.3   Ccdred: The CCD Reductions Package

The most important package in terms of CCD reductions is **ccdred** in the **noao.imred** package. There are a number of manuals available within IRAF and on the Internet on the usage of IRAF and **ccdred** for CCD reductions, with (Massay 1997) one such example. The reduction package **ccdred** is designed to be used for batch-oriented processing of large amounts of data. It contains tasks for handling of bad pixels, setting instrument parameters, combining and processing CCD images and creating correction images. See Table 5.5 for the most commonly used tasks for optical photometry data:

Table 5.5: The **ccdred** Package:

setinstrument:	Set instrument parameters
combine:	Combine CCD images
ccdproc:	Process CCD images
darkcombine:	Combine and process dark count images
flatcombine:	Combine and process flat field images
zerocombine:	Combine and process zero level images

The basic procedure followed when using **ccdred** for CCD reductions can be outlined as follows:

1. Determining all the required parameter values, for instance CCD gain, read-noise, overscan, data section and etc.

2. Run **setinstrument** to set up the translation table for the image headers.

3. Use **zerocombine** to combine the individual bias frames into a master bias frame.

4. Use **ccdproc** to process all the necessary frames for bias level.

5. Use **darkcombine** to combine the individual dark frames into a master dark frame.

6. Use **ccdproc** to process all the necessary frames for dark-count (if required).

7. Use **flatcombine** to combine the individual flat fields into a filter specific flat frame.

8. Use **ccdproc** to process all the necessary frames for flat field corrections.

This is just a basic procedure, but it can become complicated and difficult if there are extra factors, like bad pixels, dome flat-fields and sky flat-fields, whether it is spectroscopic or photometric data that has to be reduced, and many more. Some reduction procedures will be observing site specific, while other will be data specific and would have to be customized accordingly.

5.3.4   Digiphot: The Digital Photometry Package

The most important package in terms of optical digital photometry is **digiphot** in the **noao** package. There are a number of manuals available within IRAF and on the Internet on the usage of IRAF and **digiphot** for determining of optical photometric data, with (Massay and Davis 1992) one such example. The package **digiphot** contains subpackages for processing and analysis of aperture photometry, psf photometry, photometric calibrations and etc. See Table 5.6 for details.

Table 5.6: The **digiphot** Package:

apphot:	Aperture Photometry Package
daophot:	Dao Crowded-Field Photometry Package
photcal:	Photometric Calibration Package
ptools:	Photometry Tools Package

One of the most important subpackages in **digiphot** is the **daophot** package. It is used for crowded-field photometry, and contains tasks for finding stars on an image, calculating sky values and initial magnitudes for stars, computing the psf model, fitting the psf to stars and setting up of parameters used within the different tasks. **daophot** was developed by Peter Stetson of the Dominion Astrophysical Observatory. (See Davis 1994 for a complete discussion on the package and its history and use.) It uses the empirical PSF method to construct the psf model that is used to measure the stellar magnitudes (DaCosta 1992).

The basic procedure followed when using **daophot** for optical digital photometry can be outlined as follows:

1. Use **imexamine** and **imhead** to determine the necessary parameters needed, and enter them into **datapars** and **daopars**. (The **daophot** parameter files).

2. Create a list of x and y positions for stars on the data frame by using **daofind** and **tvmark**.

3. Perform aperture photometry on the stars by using **phot**. This sets the zero-point and sky value.

4. Define the psf for the data frame by using **psf**.

5. Do simultaneous psf-fitting for the stars on the data frame using **allstar**, and produce a subtracted frame.

6. Use additional tasks like **txdump** to get the measured data for calibration and analysis.

This is just a basic procedure, but it can become complicated and difficult if there are extra factors, for instance densly crowded stellar fields, faint objects that has to be measured and many more. The procedure can be customized according to the observing and research requirements.

5.3.5 Display Servers and Visualization Applications

The IRAF package communicates with a separate X-Window to display its images. The SOAImage package allows the display of images within IRAF. (See (SAOImage DS9) for detailed information and discussions.) SAOImage DS9 is an astronomical imaging and data visualization application, and supports FITS images and binary tables, multiple frame buffers, region manipulation, and many scale algorithms and colourmaps. It also provides communication with external analysis tasks and is highly configurable and extensible. DS9 is a stand-alone application and requires no special installation or support files. Versions of DS9 currently exist for Sun Solaris, Sun Solaris64, Linux, Linux64, LinuxPPC, MacOSX, Darwin, and Windows NT/2000/XP.

DS9 supports advanced features such as multiple frame buffers, mosaic images, tiling, blinking, geometric markers, colourmap manipulation, scaling, arbitrary zoom, rotation, pan, and a variety of coordinate systems. DS9 also supports FTP and HTTP access. DS9 is a Tk/Tcl application which utilizes the SAOTk widget set with additional incorporation of the X Public Access (XPA) mechanism to allow external processes to access and control DS9 data, GUI functions, and algorithms. DS9 does not support IRAF .imh image files directly, but if it is needed to display them, DS9 in standalone mode requires the file ".ds9.fil" in the login directory. This file should contain the following:

File access descriptions:
help explanation
file template
file type
access command
IRAF IMH files
*.imh
IMH
i2f -s $filename

For this to work, the programme: "i2f" is utilized. This comes from a package called WCStools, which is a world coordinate manipulation package that can be downloaded from http://tdc-www.harvard.edu/software/wcstools. In effect, i2f transparently converts ".imh" files to ".fits" files before display.

5.4   The Boyden IRAF Package

The need for a scientific accurate in-house photometric pipeline prompted the development of the **boyden** IRAF package. This was because of the nature of the current and future research projects conducted at the Boyden Observatory using the 1.5-m Rockefeller Telescope by the University of the Free State Astrophysics Group. The research emphasis is on the photometric study and modelling of accretion driven systems, like Dwarf-novae, CV's, AGN's and X-ray binaries, as well as multi-wavelength studies of relevant and specifically identified systems, with the emphasis on systems that are potential high energy gamma-ray emitters.

The photometric pipeline needs to be reliable, upgradable and user friendly. It must also be able to handle not only small once-off data sets from a single observation, but also has to be able to handle very large and extensive data sets of a couple a hundred or more data frames. It has to be able to do dataframe reductions as well as photometric measurements in multiple filters of multiple objects from more than one observation run. It also requires to be independent to a degree, so that it could be used, with slight modifications, for photometric data analysis of external data, or change in the observational system setup (like a CCD camera change). Because of these requirements, the pipeline was developed

in a modular fashion, i.e. each process has its own tasks that can run independently of the rest, or together. This allows for modification, upgrading and changing of the different components of the photometric pipeline, depending on the specific requirements.

The structure and design of the pipeline is based on standard photometric recipes, with the core layout developed to a large extend using the methods and procedures used in (Massay 1997) and (Massay and Davis 1992). The following flowchart shows the basic layout of the **boyden** IRAF package.
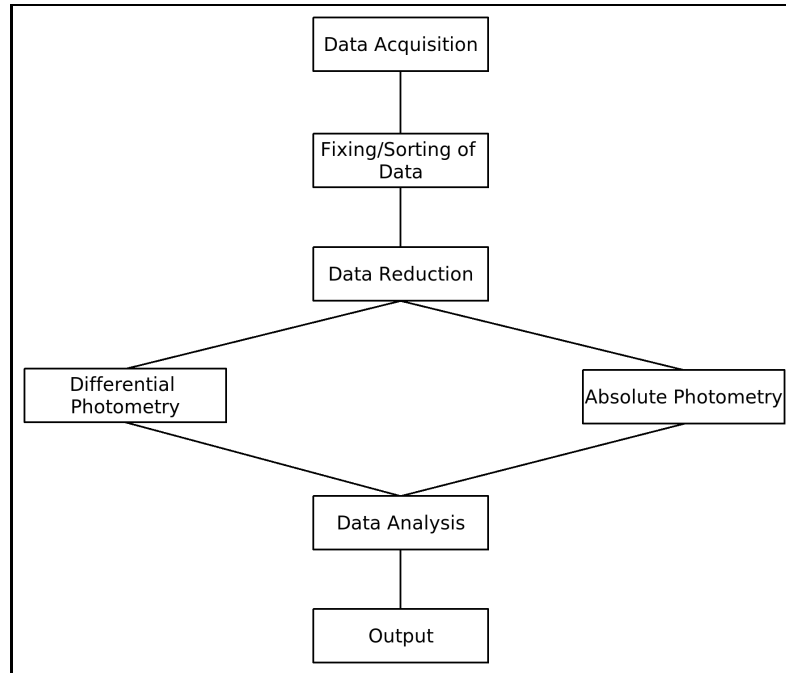
Figure 5.1: Flowchart layout of Boyden IRAF Package.

This **boyden** package was then developed through the use of .cl scripts. The full details on developing .cl scripts and combining them into an IRAF package, and then including that package into the IRAF system can be found in (Anderson and Seaman 1989). The IRAF environment allows for the development of .cl scripts, which essentially are just scripts that allow the developer to combine different IRAF tasks into a singular script. This capability allows for custom pipelines for observational programs, and research requirements. The **boyden** package, for instance, uses and combines a total of over 20 different IRAF tasks into its different scripts. The developed .cl scripts were combined into a package, and along with the relevant documentation, for instance help files and README files, were included into the locally maintained in-house IRAF system. The

IRAF system, along with all external systems, used in-house are the IRAF version 1.13 that was obtained from the IRAF.net repositories. The current **boyden** package contains the following scripts/tasks:

Table 5.7: The **boyden** Package:

biasred:	Do the biasframe reductions
darkred:	Do the darkframe reductions
dirsetup:	Sets up the directory by creating worklists
fixheader:	Include into the header of the fits the necessary information
flatred:	Do the flatframe reductions
imagepreview:	Preview images to keep good dataframes and delete bad dataframes
lightcurve:	Plots a lightcurve of the specified star data
magcor:	Apply atmospheric corrections on the measured star magnitudes
psfphot:	Do batch psf photometry on a set of images
psfsetup:	Sets up the photometry parameters for daophot
redsetup:	Sets up the reduction parameters for ccdred
reduction:	Apply reduction procedures to the desired images
stardump:	Dump the measured magnitudes of the stars into text files

These tasks can run independently, but for best results it is recommended that the tasks are called according to the flowchart layout. Thus, the basic photometric procedure will be as follows:

1. Acquire data and reduction frames using the Boyden 1.5-m Rockefeller CCD-System, in all the required filters.

2. A copy of the saved image frames will then be used to do the photometric data analysis.

3. Use **imagepreview** to check the image frames for corrupted image frames, and remove them from the workspace.

4. **fixheader** is used to check the fits headers for required values, and includes necessary header values as required by the pipeline.

5. **dirsetup** is used to sort the reduction and data frames into worklists that are both image type specific, and filter specific.

6. The worklists are inspected to remove unwanted images, or to edit them according to special requirements.

7. Data frames can be reduced for system influences using the different reduction tasks or the combined **reduction** task.

8. Use **redsetup** to setup the necessary parameter files.

9. Use **biasred** to create a master bias frame, and apply it on the specified image frames.

10. Use **darkred** to create a master dark frame, and apply it on the specified image frames.

11. Use **flatred** to create a master flat frame, and apply it on the specified image frames, for each filter.

12. Use **psfsetup** to set up the photometric analysis parameters, and use IRAF tasks to create a master stellar coordinate file, as well as a master psf model file.

13. Use **psfphot** to acquire instrumental psf magnitudes for the specified stars.

14. Use **stardump** to dump the relevant star's measurements to text files and **stsdas** table files.

15. Use **magcor** to correct the instrumental magnitudes for atmospheric extinction.

16. Use **lightcurve** to plot and save a lightcurve of the relevant star.

17. Use the saved text files and lightcurves for further data analysis on the relevant star.

The output or results of the package are data files containing measured psf magnitudes for the specified stars as well as their lightcurves. These data-files also contain the error in the measured magnitudes, the exposure times (UT), the filters used etc. The measured values can be used to either perform differential photometry or absolute photometry. The calibration of the measured data into a standard system could be done using the tasks available within IRAF, or it can be done manually using user preferred methods and/or techniques. The accuracies obtained can be determined from the error in the measured magnitudes, as well as the shape of the lightcurves.

5.4.1 Boyden Package Tasks: Detailed Descriptions

In the following section is a detailed description of the defined **boyden** tasks. The descriptions are partially representative of the help files that are available for the **boyden** package.

biasred:

biasred uses **zerocombine** to combine the biasframes entered into a master biasframe. This frame is applied on the project images using **ccdproc**. The project images include all the .fits files, i.e. the dark, flat, and object.fits files.

The input consists of all the required data frames, entered as .lis files containing the names of the frames to be processed. **biasred** passes the entered biasframes to **zerocombine** which combines them using specific parameters, and gives as output a predefined biasmaster.fits file. This biasmaster.fits file is displayed using DS9. If the biasmaster.fits file is acceptable for use on the project images, **biasred** applies the reductions on the project images using **ccdproc**. **ccdproc** produces as output the debiased images.

darkred:

darkred uses **darkcombine** to combine the darkframes entered into a master darkframe. This frame is applied on the project images using **ccdproc**. The project images include all the remaining fits files, i.e. the flat, and object.fits files.

The input consists of all the required data frames, entered as .lis files containing the names of the frames to be processed. **darkred** passes the entered darkframes to **darkcombine** which combines them using specific parameters, and gives as output a predefined darkmaster.fits file. This darkmaster.fits file is displayed using DS9. If the darkmaster.fits file is acceptable for use on the project images, **darkred** applies the reductions on the project images using **ccdproc**. **ccdproc** produces as output the dark-subtracted images.

dirsetup:

dirsetup sorts through the fitsfiles and writes the filenames to specific data lists. It sorts the fitsfiles according to the fitsheader data field "CCDTYPE". It thus creates a darklist

containing the darkframes, an imagelist containing the program-frames, a biaslist containing the biasframes, and a filter specific flatframe-list containing the flatframes for each filter, respectively. The lists can be used during the photometry (reduction and measurement) procedures.

fixheader:

IRAF requires certain header keyword values for some of its analysis tasks. **fixheader** includes these necessary values into the image headers via user input prompt. It updates and verifies the changes to the image header. It also calculates the airmass and UT from other header values.

The input values can be entered directly along with the fits files, or via prompt when asked by **fixheader** for specific values. **fixheader** checks for specific header keywords or fields, and either updates the header with new values or notifies that the field does exist and does not need updating. If specific fields need updating, the **imutil.hedit** task can be used.

flatred:

flatred uses **flatcombine** to combine the flatframes entered into a master flatframe. This frame is applied on the project images using **ccdproc**. The project images include all the program files, i.e. the program.fits files.

The input consists of all the required data frames, entered as .lis files containing the names of the frames to be processed. **flatred** passes the entered flatframes to **flatcombine** which combines them using specific parameters, and gives as output a predefined filter specific flatmaster.fits file. This filter specific flatmaster.fits file is displayed using DS9. If the flatmaster.fits file is acceptable for use on the program images, **flatred** applies the reductions for the specified filter on the program images using **ccdproc**. **ccdproc** produces as output the flattened images.

imagepreview:

imagepreview displays the dataframe in DS9 and queries the user if the dataframe is to be kept or not. If the dataframe is corrupted, the user is queried whether he/she wants to delete it or not. **imagepreview** is used specifically for the purpose of scanning through a very large dataset with minimum amount of effort.

lightcurve:

lightcurve is a procedure that plots a lightcurve of a specified star data table. The procedure plots the corrected magnitudes (MAG0) against the time (UT). The error in magnitude (MERR) is also plotted as errorbars. The lightcurve is named as "star#lc". The user also has the options to save the plotted lightcurve as a post-script file, "star#lc.ps".

magcor:

magcor uses the data from the "star#.tab" table files, as well as the observatory's extinction coefficients where data was acquired to apply instrumental magnitude corrections for atmospheric effects. The magnitude corrections are filter specific, for the filter specific table values generated by **stardump**.

The data from the tables includes the filter, airmass, obs-time, x & y coordinates, instrumental magnitudes, error in magnitudes, and the sky value. The table data are used to set up equations to correct the measured magnitudes for atmospheric corrections. Magcor also prints a set of tables with Theoretical and Observatory (Boyden) specific coefficients for U,B,V,R,I filters.

psfphot:

psfphot uses the **daophot** packages **allstar**, **psf** and **phot**, to do photometry measurements on a set of images. The input is a set of image frames, entered as a .lis file containing the names of the image frames to be processed. A predetermined master coordinate file, containing a list of stars and their coordinates is also entered, for resolving of the stars to be measured by **phot**. A predetermined master pstfile containing a list of output psf star

photometry data, used to measure and calibrate the **psfphot** measured images is also used during the measurement process.

The predetermined master.coo and master.pst files are created in a separate folder inside the working dir, using a chosen imagefile, and the packages **phot** and **psf**. The created *.coo and *.pst files are renamed to master.coo and master.pst and copied to the working directory for further use.

psfsetup:

psfsetup sets-up the parameter files **datapars**, **daopars** and enc. for the **psfphot** task. Some of the parameters are user defined, while others are default.

redsetup:

The **noao** package contains a procedure **setinstrument**, that sets-up the parameters for the reduction task **ccdproc**. This procedure/task calls a translation file that contains all the necessary defined parameters, the translations for the header keywords, and any other required data.

reduction:

The **noao** package contains procedures to reduce data. Procedures include **combine**, **ccdproc** and **setinstrument**. These procedures handles the bias-, flat- and dark-frames, and applies these on the project frames using **ccdproc**.

Hence **reduction** is a procedure that combines the individual scripts **redsetup**, **biasred**, **darkred**, and **flatred**. These scripts handle the setup process, the bias correction, the dark subtraction, and the flat fielding of the project images. Any of the individual processes can be turned off by setting its parameter to "no". These processes can be done manually, or that specific script can be called to run independently.

stardump:

stardump is a procedure to dump the x-coordinates, y-coordinates and magnitudes of the psf measured stars into a text and table file. It therefore creates individual text/data and table files for each measured star. These text and table files can be used for further analysis. The text/data file has the extention ".dat" with the table file being ".tab". **stardump** is to be used mainly after **psfphot** has been used to do psf photometry on a large variable star data set. It is recommended that the *.als* files be used to get the values for stardump. The *.mag* files can also be used, specifically when aperture photometry has been done instead of psf.

It is very important that the numstars parameter must correspond to the least amount of stars measured in the *.als* file. Thus if a master.coordinate file was used during **psfphot**, with the coordinates for 5 stars, the *.als* file will at most contain measured values for 5 stars only, and numstars $\leq$ 5. A carefull note must also be made of the star-id's that is sometimes given automatically by IRAF. In such a case the star-ids' does not go from 1 to 5, but can be named 3,12,24,17,6, and must be dumped with the specific star-id defined. The stars have to be dumped into filter specific "star#.dat" and "star#.tab" files. Thus make sure when entering the ".als" files that it is for specific filters, e.g. filter = "V"!

5.4.2   Testing and Implementation

The completed **boyden** package has to be tested to check for effectiveness, accuracy and any coding "bugs" that may be present. This was achieved through a practical photometric exercise. Because the atmospheric extinction coefficients had to be determined and calibrated for the Boyden Observatory, the photometric exercise consisted of the observation and analysis of standard stars, to be used in the determining of the extinction coefficients. This "testing" of the **boyden** package through the determining of the Boyden extinction coefficients will be discussed in full in Chapter 6.

Once the package is tested and calibrated it is to be included into the IRAF system that is in use at the Boyden Observatory. After the package is implemented it is to be maintained through the continual testing and improvement of the base package (i.e. Version 1.0). Further development and upgrades or expansion can be applied to enhance

the package as required (i.e. Versions 1.1, 1.2 ....). See Appendix A for full details on the structure and layout of the **boyden** package, as well as the scripts for the procedures defined above.

Chapter 6

Determining extinction coefficients for Boyden

6.1 Introduction

For accurate photometric analysis the transformation coefficients need to be determined. These coefficients can be determined using least squares fitting of photometric equations. Initial coefficient values are therefore needed to facilitate the fitting process. Because the atmospheric extinction coefficients are site specific and can be averaged to a year-end mean, they can be used to set good initial values for the fitting process. These site specific extinction coefficients therefore need to be measured and refined using standard star observations. In this chapter the experimental procedure used to determine the atmospheric extinction coefficients for the Boyden Observatory, using the 1.5 m Rockefeller Telescope, will be discussed.

6.2 Instrumentation

The instrumentation used are the 1.5 m Rockefeller Telescope with the Photometric CCD-camera system. The observational equipment and configuration are the same as used during the CCD characterization exercise. See Chapter 3, Section 3.2 on page 48 for a complete discussion on the instrumental configuration.

6.3 Experimental Procedure

6.3.1 Standard Star Observations

A set of standard stars were chosen from the E-region catalogue available from the South African Astronomical Observatory (SAAO) electronic web-sources, see Table 6.1 for details. The standard stars were observed on 18 and 19 August 2007 with 25 exposures taken per star. The BVR filter data were obtained on the 18th and the UI filter data on the 19th. Additional reduction frames were also acquired on each observing night, i.e. bias, dark and flat frames. The filter specific flat frames were obtained as required for the data frames, i.e. the BVR flat frames on the 18th and the UI flat frames on the 19th. See Appendix A on page 136 for the relevant observation logs.

Table 6.1: The Catalog values for the observed Standard Stars

star	sp.type	r.a.(2000)	dec.(2000)	V	B-V	U-B	V-R	V-I
E803	A0V	20:00:53	-45:41:57	8.74	0.03	0.02	0	0.01
E804	A0V	20:03:51	-43:50:00	9.25	0.07	0.06	0.02	0.05
E809	A9IV	20:04:29	-44:56:48	7.82	0.3	0.07	0.17	0.34
E815	F5V	20:06:03	-44:58:48	8.06	0.47	0.02	0.27	0.53
E816	F5V	20:08:01	-44:11:31	8.48	0.45	-0.03	0.26	0.52
E817	F3/5V	20:00:20	-44:40:49	9.13	0.44	-0.01	0.27	0.54
E836	K0III	20:17:40	-45:13;43	8.57	1.1	0.99	0.55	1.05
E837	K0III	20:08:44	-45:25:43	9.04	1.01	0.76	0.53	1.01
E846	G8IV	20:08:50	-44:24:55	9.98	0.89	0.5	0.49	0.94
E853	G8V	20:01:41	-44:28:08	9.4	0.88	0.45	0.49	0.94

The data frames for the observed standard stars and the reduction frames i.e. the bias, dark and flat fields were used during reduction and analysis procedures to determine the transformation coefficients and specifically the atmospheric extinction coefficients.

6.3.2 Photometric Analysis

The acquired data and reduction frames were processed using IRAF packages and specifically the Boyden IRAF package. The data frames were reduced using **reduction** after they were sorted and their headers checked using **dirsetup** and **fixheader**. The reduced

data frames were then stacked or combined into a single data frame per object per filter using **imcombine** with an "average" stacking algorithm with the data frames normilized for exposure time and shifted for tracking errors. These combined data frames were used to measure instrumental magnitudes using aperture photometry with the **daophot.phot** package. The parameter files **datapars**, **fitskypars**, **daopars** and **centerpars** for the **phot** task were set up, as well as coordinate files created for the stars to be measured using **imagepreview**, to determine the coordinates for the program stars. The results from the **phot** task were saved and used for further analysis. A observation file was created, from the results files from **phot** and an image-set file containing the relevant images for the corresponding stars, using **mknobsfile**. See Table 6.2 for the observation file results.

Table 6.2: The measured observation values for the observed stars

ID	FILTER	TIME	AIRMASS	XCENTER	YCENTER	MAG	σ_M
E803	U	18:11:06	1.16	195.99	287.10	16.16	00.002
*	B	17:37:32	1.25	144.96	243.10	13.42	00.001
*	V	17:41:48	1.24	132.11	244.98	12.7	00.001
*	R	17:45:43	1.23	121.04	246.88	12.28	00.001
*	I	18:07:40	1.17	189.83	287.05	12.13	00.001
E804	U	19:00:37	1.08	186.91	278.09	16.63	00.003
*	B	18:14:39	1.16	256.07	247.76	13.66	00.001
*	V	18:19:21	1.16	268.96	248.80	12.87	00.001
*	R	18:23:17	1.15	282.25	249.79	12.62	00.001
*	I	18:57:21	1.09	183.03	275.98	12.56	00.001
E809	U	19:14:38	1.07	173.89	280.99	15.37	00.002
*	B	18:29:12	1.14	220.88	280.01	12.51	00.001
*	V	18:32:52	1.14	222.94	280.93	11.54	00.001
*	R	18:36:22	1.13	225.06	282.00	11.07	00.001
*	I	19:12:34	1.08	170.97	281.89	10.84	00.001
E815	U	19:28:31	1.06	200.08	289.05	15.9	00.002
*	B	18:40:43	1.13	209.93	276.91	12.93	00.001
*	V	18:44:45	1.12	211.06	277.84	11.78	00.001
*	R	18:47:19	1.11	214.03	278.87	11.21	00.001
*	I	19:26:09	1.07	197.09	291.18	10.86	00.001
E816	U	19:43:08	1.05	180.077	281.95	16.32	00.002
*	B	18:53:51	1.10	189.06	272.00	13.25	00.001
*	V	18:57:52	1.10	187.04	273.04	12.17	00.001
*	R	19:00:40	1.10	189.12	274.99	11.68	00.001
*	I	19:39:56	1.05	179.00	281.10	11.38	00.001

118

ID	FILTER	TIME	AIRMASS	XCENTER	YCENTER	MAG	σ_M
E817	U	17:38:52	1.24	176.05	295.14	17.12	00.002
*	B	17:10:54	1.34	168.99	248.89	14.07	00.001
*	V	17:16:09	1.32	154.05	251.68	12.98	00.001
*	R	17:19:51	1.31	144.05	253.93	12.47	00.001
*	I	17:34:21	1.25	186.94	291.01	12.06	00.001
E836	U	21:14:00	1.05	238.07	275.04	18.39	00.004
*	B	19:44:04	1.06	224.96	265.08	13.94	00.001
*	V	19:49:55	1.06	230.16	264.93	12.35	00.001
*	R	19:54:13	1.06	238.04	264.90	11.49	00.001
*	I	21:11:28	1.05	216.15	275.04	11.04	00.001
E837	U	20:02:23	1.05	168.96	277.02	18.24	00.003
*	B	19:05:34	1.10	176.95	264.88	14.27	00.001
*	V	19:10:38	1.09	179.07	266.02	12.78	00.001
*	R	19:14:58	1.08	181.94	266.06	12.04	00.001
*	I	19:58:45	1.05	167.89	278.11	11.43	00.001
E846	U	20:36:04	1.04	215.99	270.07	18.97	00.005
*	B	19:22:08	1.07	206.10	257.98	15.10	00.002
*	V	19:32:38	1.06	212.11	258.92	13.74	00.001
*	R	19:37:42	1.06	214.90	258.88	13.01	00.001
*	I	20:32:10	1.04	183.09	271.10	12.59	00.001
E853	U	18:28:26	1.13	187.09	284.08	18.18	00.003
*	B	17:55:07	1.21	164.15	264.80	14.63	00.002
*	V	18:00:54	1.19	149.03	264.82	13.22	00.001
*	R	18:05:10	1.18	137.00	267.00	12.35	00.001
*	I	18:24:07	1.14	176.97	282.08	11.83	00.001

A configuration file was set up using a catalogue for the standards used, a file containing the definitions for the transformation equations, and the new observation file to set up the photometric equations to be used during the transformation process. The observation file was modified to include only eight of the observed stars to be used during the fitting process, with two stars (E803 and E853) excluded. These two stars will then be used later to test the transformation equations. The transformation equations defined in the configuration file are of the same structure as defined in Section 4.3.3 on page 92 in Chapter 4. The configuration file for the fitting of the transformation equations also contains initial values for the coefficients, with the previously calculated Boyden first order extinction coefficients used as initial values for the fitting of the new first order atmospheric extinction coefficients, and all other initial coefficient values set to zero. The transformation section

of the configuration file contains the transformation equations and initial coefficient values in the following forms:

Table 6.3: The Transformation Equations and Initial Coefficient Values

fit	u1=0.0, u2=0.491, u3=0.000
const	u4=0.0
UFIT :	mU = (UB + BV + V) + u1 + u2 * XU + u3 * UB + u4 * UB * XU
fit	b1=0.0, b2=0.280, b3=0.000
const	b4=0.0
BFIT :	mB = (BV + V) + b1 + b2 * XB + b3 * BV + b4 * BV * XB
fit	v1=0.0, v2=0.181, v3=0.000
const	v4=0.0
VFIT :	mV = V + v1 + v2 * XV + v3 * BV + v4 * BV * XV
fit	r1=0.0, r2=0.125, r3=0.000
const	r4=0.0
RFIT :	mR = (V - VR) + r1 + r2 * XR + r3 * VR + r4 * VR * XR
fit	i1=0.0, i2=0.091, i3=0.000
const	i4=0.0
IFIT :	mI = (V - VI) + i1 + i2 * XI + i3 * VI + i4 * VI * XI

With the variables defined as follows:

Table 6.4: The variables defined in terms of the standard equations.

u1,b1,v1,r1,i1	=	The zeropoint constant Z_x.
u2,b2,v2,r2,i2	=	The first order extinction coefficient k'_x.
u3,b3,v3,r3,i3	=	The colour term C_x.
u4,b4,v4,r4,i4	=	The second order extinction coefficient $k"_x$.
XU,XB,XV,XR,XI	=	The airmass value for the specific filter.
mU,mB,mV,mR,mI	=	The instrumental magnitude for the specific filter.
UB	=	The (U - B) standard catalogue colour term.
BV	=	The (B - V) standard catalogue colour term.
V	=	The standard V-magnitude catalogue term.
VR	=	The (V - R) standard catalogue colour term.
VI	=	The (V - I) standard catalogue colour term.

The "fit" coefficients are varied during the fitting process until the best least squares fitting is achieved. The "const" coefficients are held constant during the initial fitting process, but can be varied to check for a better least squares fitting. The **fitparams** task was used to interactively solve the photometric transformation equations using the observation, catalogue and configuration files, with the fitted results saved to an output file.

6.4 Photometric Results and Discussion

6.4.1 Photometric transformation equations

The photometric transformation equations and the resulting transformation coefficients were solved interactively using interactive plots from **fitparams**. These plots of the determined function versus residuals could be used to refine the fitted values by changing fitting parameters or by rejecting bad data values. The function in this case is the fitted magnitudes, and the residuals, the error between the fitted magnitudes and the measured magnitudes. This fitting process was completed for each individual filter (UBVRI). See the following figures for representative graphics for the interactive plots used during the fitting process.
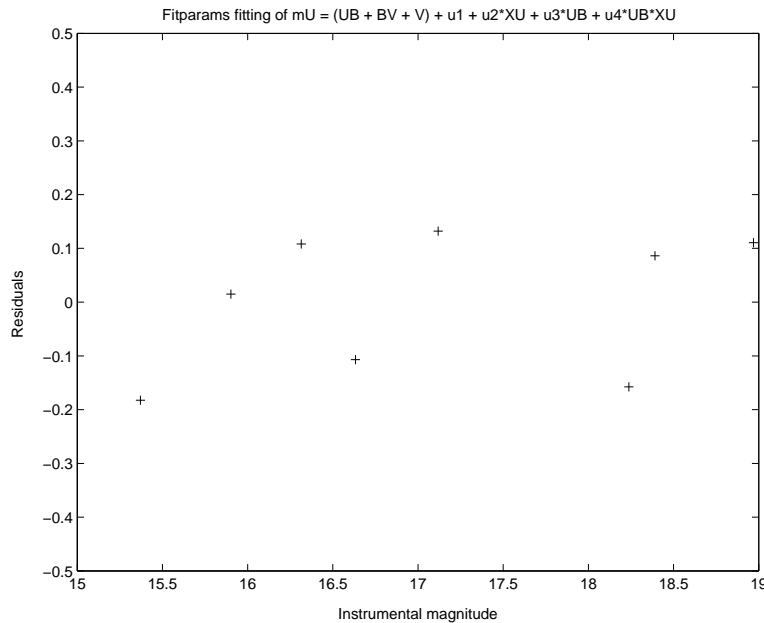
Figure 6.1: Interactive fitparams plot of fitted function vs residuals for U-filter data.
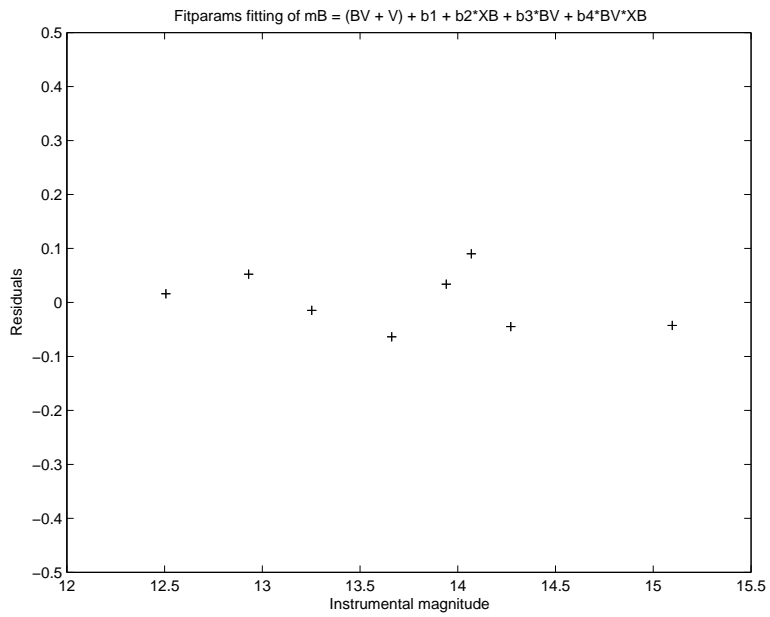
Figure 6.2: Interactive fitparams plot of fitted function vs residuals for B-filter data.
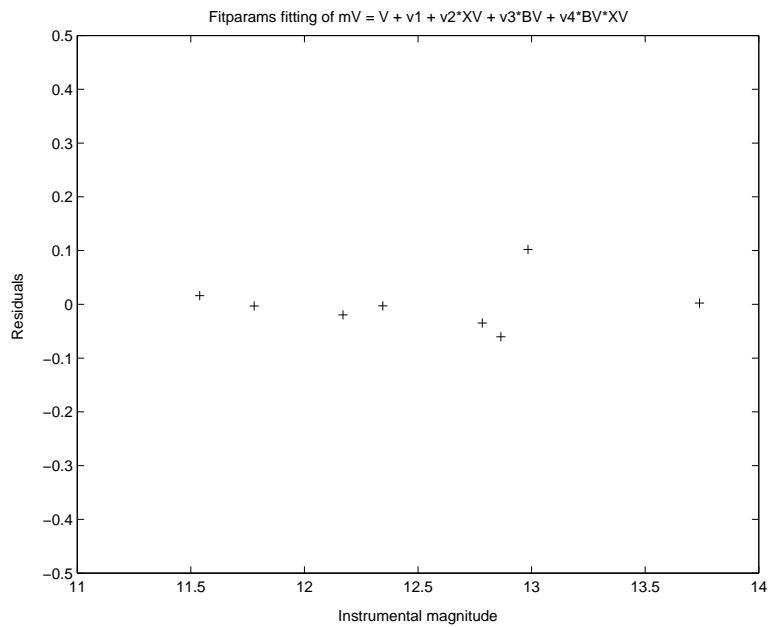
Figure 6.3: Interactive fitparams plot of fitted function vs residuals for V-filter data.

122
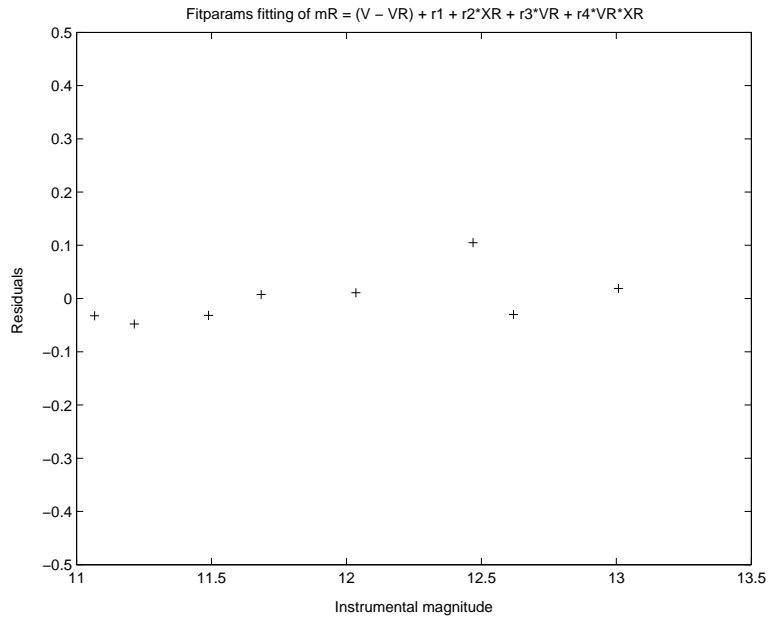
Figure 6.4: Interactive fitparams plot of fitted function vs residuals for R-filter data.
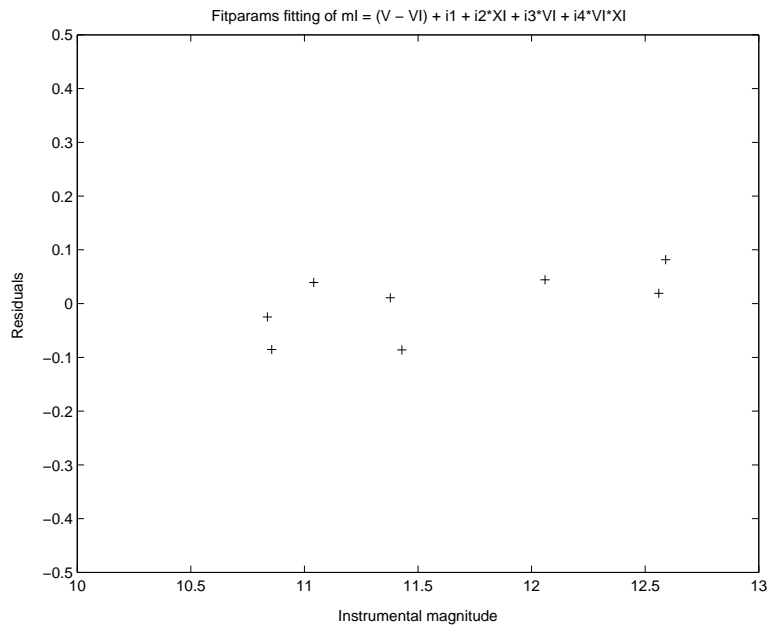
Figure 6.5: Interactive fitparams plot of fitted function vs residuals for I-filter data.

The calculated atmospheric extinction coefficients could be checked by plotting the airmass against the instrumental magnitude. This is done to see if there is a second order extinction coefficient present, which would be indicated in the data-point spread. See the following figures for representative graphs for the airmass versus instrumental magnitudes plotted.
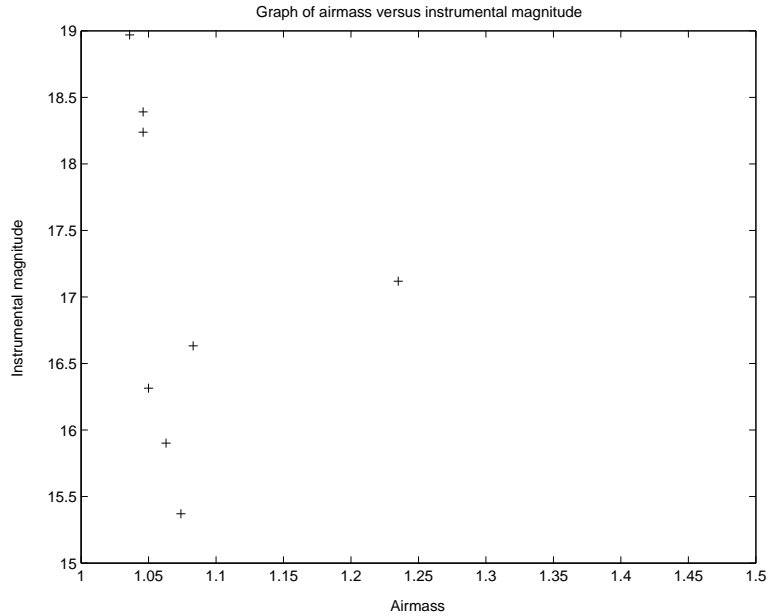
Figure 6.6: Graph of airmass versus intrumental magnitudes for U-filter data.

From the fitted results and graphs the second order extinction coefficients were determined to be "k2" ≈ 0. The calculated transformation coefficients from the saved output file were then tabulated to be used in further analytical processes, with "zero" the zero-point for the system, "k1" the first order extinction coefficients and "colour" the colour term for the system. See Table 6.5 for details.

Table 6.5: The calculated transformation coefficients.

Filter	zero	k1	colour
U	6.803	0.499	0.337
B	4.111	0.264	-0.134
V	3.484	0.161	0.116
R	3.222	0.172	0.189
I	3.311	0.021	0.145
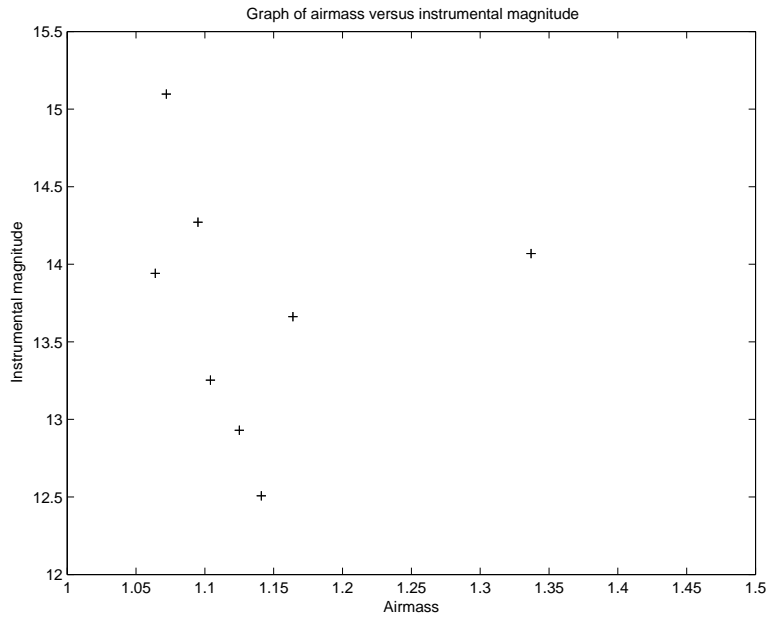
Figure 6.7: Graph of airmass versus intrumental magnitudes for B-filter data.
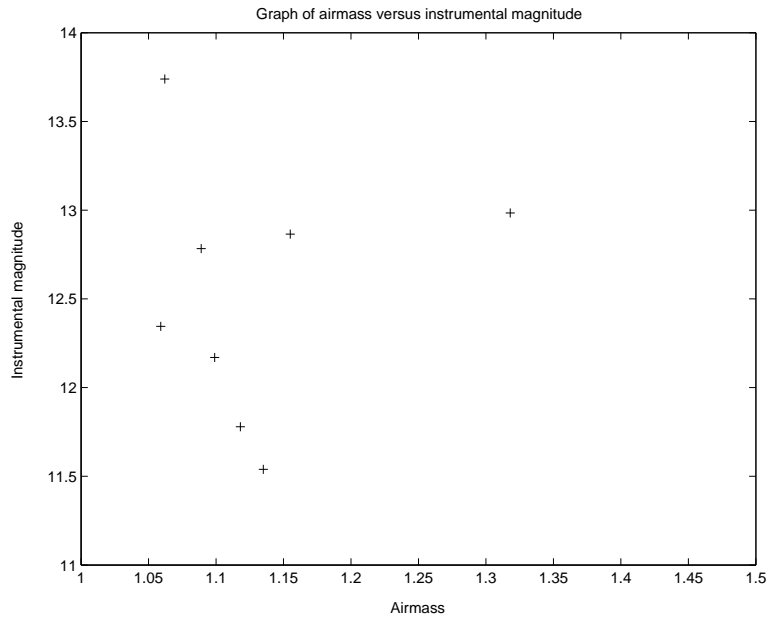
Figure 6.8: Graph of airmass versus intrumental magnitudes for V-filter data.

125
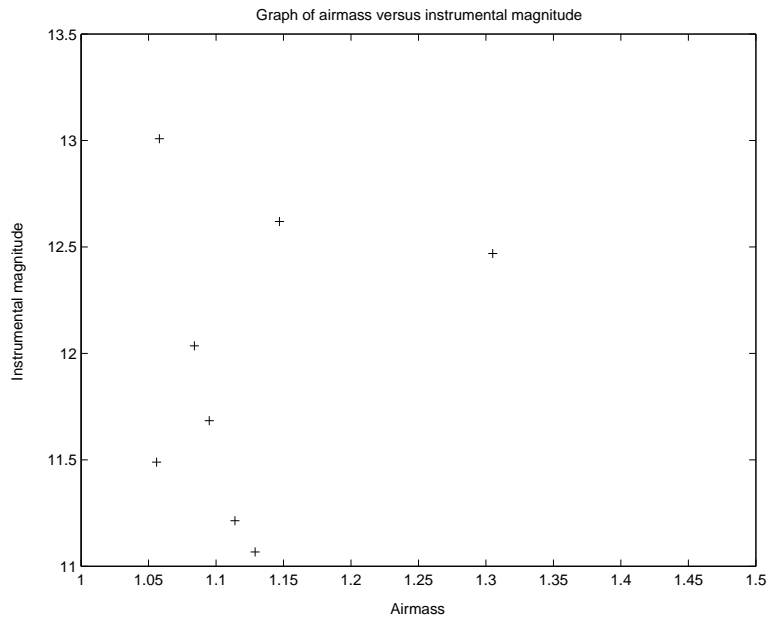
Figure 6.9: Graph of airmass versus intrumental magnitudes for R-filter data.
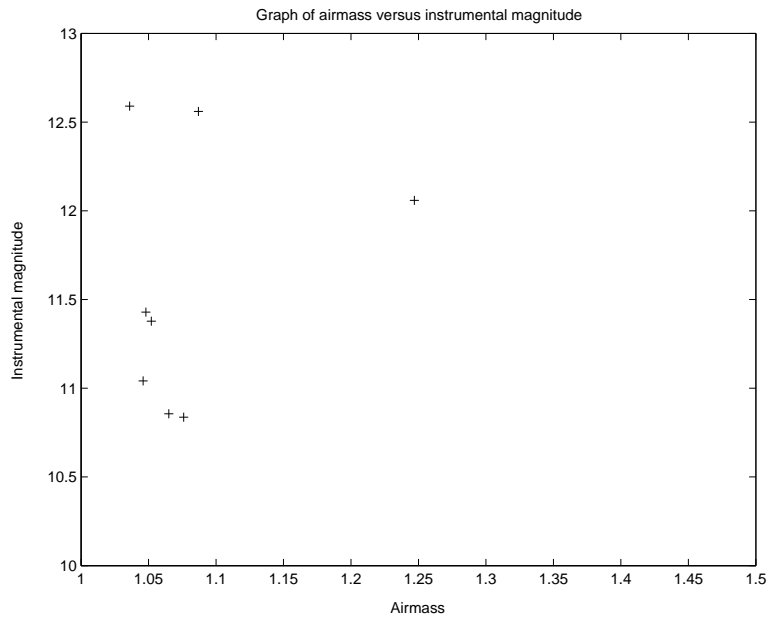
Figure 6.10: Graph of airmass versus intrumental magnitudes for I-filter data.

126

6.4.2 Testing of transformation coefficients

The calculated transformation coefficients were tested by using them to transform the measured instrumental magnitudes for stars E803 and E853 into the standard system, and checking the resulting values against the catalogued values through the calculation of the variance between values.

This was achieved by extracting the relevant data for the two stars from the observation file and the standard catalogue. These values along with the newly calculated transformation coefficients used to set up the transformation equations. These transformation equations were then used to determine the corrected magnitudes for the two stars, with the results tabulated. See Table 6.6.

Table 6.6: The transformed magnitudes.

star	V	B-V	U-B	V-R	V-I
E803	9.01	-0.03	-0.22	0.16	0.21
E853	9.44	0.87	0.35	0.61	1.09

The accuracy of the transformation process was tested by comparing the transformed magnitudes and the catalogued values for the two stars. This was achieved by determining the variance between the values. See Table 6.7.

Table 6.7: The variance between the transformed magnitudes and the catalogued values.

star	V	B-V	U-B	V-R	V-I
E803	0.036	0.002	0.028	0.013	0.021
E853	0.001	0.000	0.005	0.007	0.011

As can be seen the variance between the calculated magnitudes and the catalogued magnitudes are relatively small, showing the accuracy of the fitted transformation coefficients.

6.4.3 Discussion on atmospheric extinction coefficients and results

The determined atmospheric extinction coefficients and the previously calculated values were tabulated, discussed and compared against each other and known atmospheric extinction coefficients for the Landolt Catalogue and the SAAO. See Table 6.8 and Table 6.9 for details.

Table 6.8: The Calculated atmospheric extinction coefficients for Boyden Observatory.

Filter	k1	k2
Boyden Previous		
U	0.491	0
B	0.280	0
V	0.181	0
R	0.125	0
I	0.091	0
Boyden Calculated		
U	0.499	0
B	0.264	0
V	0.161	0
R	0.172	0
I	0.021	0

Table 6.9: Other Atmospheric extinction coefficients.

Filter	k1	k2
Landolt Catalogue		
U	0.650	0
B	0.350	0
V	0.170	0
R	0.080	0
I	0.030	0
SAAO Values		
U	0.560	0
B	0.270	0
V	0.150	0
R	0.100	0
I	0.070	0

These extinction coefficients compare relatively closely, and show the same trend with a decrease in value from the U-filter through to the I-filter. The study performed above was just a test to check the effectiveness of IRAF in general and the Boyden-IRAF package in particular. In terms of the extinction coefficients, to refine them and to increase their accuracies, they need to be recalculated for all standard star observations done, as atmospheric and environmental conditions have an influence on the coefficients. This means that a once-off calculation of the extinction coefficients may not be sufficient to facilitate accurate photometric studies. For accurate photometric studies at an observing site, with strongly varying extinction coefficients, it is advisable that an atmospheric extinction curve should instead be used, to compensate for seasonal variations. This curve can be determined and refined using extensive standard star observations.

Chapter 7

Conclusion

The aim of this project was the development of an IRAF-based scientific photometric package for the UFS-Boyden 1.5-m telescope. This required a detailed study of photometry, and photometric systems. The two main components necessary for photometric research studies are the instrumentation (CCD-telescope system) and the data analysis systems. Both of these components were therefore examined during the development of a photometric pipeline for research purposes.

The instrumentation component of the Boyden photometric pipeline consists of the 1.5-m telescope, the UBVRI photometric filters, and the CCD camera. From the research studies and characterization tests performed on the CCD-Telescope system the following conclusions were made. The telescope is completely computerized, with accurate tracking (including dome tracking) and focusing capabilities, which allow it to compete with modern-day telescope systems. The photometric filters are also a widely used and recognized system. The CCD camera used, when combined with the telescope allows for narrow field photometric research, because of the small FOV (2'29.82" by 3'44.29"). From the characterization tests performed the 16 bit camera was found to be highly linear (with a turnoff at 62 000 ADU) with a high dynamic range (86 dB) and a low read-noise (11.7 e$^-$). The dark count (1.31 e$^-$/p/s) for the CCD, although higher than the specified manufacturer value (0.7 e$^-$/p/s), is still relatively low, but is strongly temperature dependant, therefore the CCD has to be kept at operating temperatures ($\approx$-30 °C) as far as possible during observations. The CCD is a midband variant and is therefore red sensitive, which allows for a greater range of research programs. The CCD system also allows for fast photometry research of bright sources, due to the fast frame rate (0.35 fps) for the standard

2x2 binning 16 bit configuration for short (2 second) exposure times. These specifications for the instrumentation are of the required nature for a photometric CCD-telescope system to be recognized as being able to deliver research quality data. When looking at the data already obtained during the observational season, the system is able to deliver research quality data.

For the data obtained from the CCD-telescope system to be used and recognized, it has to be scientifically analyzed. The photometric analysis has to be accurate and scientifically correct. The Boyden-IRAF photometric package was therefore developed to fill this void that currently existed in the Boyden photometric system. The package development was based on the widely used and recognized scientific photometric analysis application IRAF. The photometric pipeline was structured on recognized recipes used for photometric analysis. The accuracy of the newly developed pipeline was tested through an observational and analysis exercise. Due to time constraints and weather conditions, not enough tests were performed, which will be rectified when the system is properly calibrated in 2008. This involved determining the atmospheric extinction coefficients for the Boyden Observatory, through the observation and analysis of standard stars. The calculated atmospheric extinction coefficients were comparable to other recognized values. The satisfactory correlation found between the calculated and "reference" atmospheric extinction coefficients can be seen as a measure of the efficiency of the new photometric package. The accuracy and efficiency of the new photometric package will, however, need to be tested thoroughly with extensive observational programs. Therefore the second component, required for a research capable photometric system, was now met.

To improve or maintain the photometric pipeline, the following recommendations can be made, including:

1. Maintenance of the CCD-telescope during the off-season: Rialuminization and alignment of the optics, maintenance of the telescope and dome drives, cleaning of the filters and CCD components and any other required maintenance actions.

2. To improve the system's capabilities, for long exposures, may require an additional autoguider system to be developed and installed.

3. The photometric data analysis pipeline requires a transformation script for the handling of absolute photometry studies, to transform measured instrumental magni-

tudes to the required standard system.

4. The photometric package then also requires the inclusion of the catalogues used at the observatory.

5. The pipeline can also be developed to include a fast realtime analysis procedure to check the quality of the observational data at the telescope, during observations.

6. The final photometric package also has to be maintained and improved depending on the changing research requirements.

7. The final photometric package will also require an user manual and data analysis cookbook.

8. For additional accuracy during analysis and transformation of photometric data, an atmospheric extinction curve can be determined, to compensate for seasonal changes that may be present. This can be achieved through the extensive observation and analysis of standard stars.

This new photometric pipeline fills a void in the research capabilities of the UFS Astrophysics group. The addition of photometric research capabilities broadens the research fields available. Photometry can then be used for independent studies, or supplementary to other research programs. Photometry research fields possible with the photometric pipeline involves fast photometry of bright sources and variable systems. Follow-up photometry of other fields of interest, such as GRB afterglow photometry is also possible. The main reason for the development of the new photometric pipeline is for the visual component of the new multi-wavelength studies that the UFS-Astrophysics group plans to conduct. These new multi-wavelength studies are to be collaborative studies performed on a wide variety of objects, with the more exotic and specifically high gamma-ray emitters the main objects of interest. This new addition to the capabilities of the UFS-Astrophysics group will not only strengthen, but will also lead to a possible growth of the group. These new developments will therefore usher in a new era for Boyden Observatory and the UFS-Astrophysics group.

Bibliography

Peter Abrahams. Historic Telescopes of Poland. `http://www.europa.com/~telscope/tspoland.doc`.

E. Anderson and R. Seaman. *An Introductory User's Guide to IRAF Scripts*. Central Computer Services, National Optical Astronomy Observatories, September 1989.

A. D. Andrews. The Boyden Observatory. *Irish Astronomical Journal*, 25:129–+, July 1998.

Apogee Instruments Inc. `http://www.ccd.com/`, a.

Apogee Instruments Inc. CCD University. `http://www.ccd.com/`, b.

J. Ashbrook. *The Astronomical Scrapbook*. Cambridge University Press, Cambridge, USA, 1984.

Astronomical Society of Southern Africa. Boyden Observatory (Harvard). Historical Section: `http://www.saao.ac.za/assa/html/his-pl-obs_-_boyden.html`.

A. Beiser. *Concepts of Modern Physics*. McGraw-Hill Higher Education, McGraw-Hill, sixth edition, 2003.

J.J. Calitz. The development of an UFS-Boyden photometric pipeline to facilitate the observational study of accretion driven systems. Master's thesis, University of the Free State, South Africa, 2005.

G.S. DaCosta. Basic Photometry Techniques. In S.B. Howell, editor, *Astronomical CCD Observing and Reduction Techniques*, volume 23 of *Astronomical Society of the Pacific Conference Series*, pages 90–105, 390 Ashton Ave, San Francisco, California, USA, 1992. Astronomical Society of the Pacific, BookCrafters Inc.

L.E. Davis. *A Reference Guide to the IRAF/DAOPHOT Package*, January 1994.

DFM Engineering Inc. The Boyden 1.52 m Rockefeller Telescope Upgrade. Newsworthy Articles. `http://www.dfmengineering.com/news_boyden_obsrv.html`.

R.L. Gilliland. Details of Noise Sources and Reduction Processes. In S.B. Howell, editor, *Astronomical CCD Observing and Reduction Techniques*, volume 23 of *Astronomical Society of the Pacific Conference Series*, pages 86–90, 390 Ashton Ave, San Francisco, California, USA, 1992. Astronomical Society of the Pacific, BookCrafters Inc.

R.J. Hanisch. Image Processing,Data Analysis Software, and Computer Systems for CCD Data Reduction and Analysis. In S.B. Howell, editor, *Astronomical CCD Observing and Reduction Techniques*, volume 23 of *Astronomical Society of the Pacific Conference Series*, pages 86–90, 390 Ashton Ave, San Francisco, California, USA, 1992. Astronomical Society of the Pacific, BookCrafters Inc.

L. Hanlon, J. French, and et al. Watcher: A Telescope for Rapid GRB Follow-up Observations and Extra-Solar Planet Searches. Published as an Information Poster, 2006a.

L. Hanlon, J. French, B. McBreen, and G. Melady. Watcher: An Irish Robotic Telescope in South Africa. Published as an Information Poster, 2006b.

R.H. Hardie. *Astronomical Techniques*, volume II of *Star and Stellar Systems*, chapter 8, pages 178–208. University of Chicago Press, Chicago, USA, 1962.

S.B. Howell. *Handbook of CCD Astronomy*. Cambridge University Press, Cambridge, USA, second edition, 2006.

S.B. Howell. Introduction to Differential Time-Series Astronomical Photometry Using Charge-Coupled Devices. In S.B. Howell, editor, *Astronomical CCD Observing and Reduction Techniques*, volume 23 of *Astronomical Society of the Pacific Conference Series*, pages 105–130, 390 Ashton Ave, San Francisco, California, USA, 1992. Astronomical Society of the Pacific, BookCrafters Inc.

K. Huang. *Introduction to Statistical Physics*. Taylor & Francis, London, UK, first edition, 2001.

IRAF.Net. IRAF software and user support. `http://iraf.net/`.

J Janesick and T Elliot. History and Advancements of Large Area Array Scientific CCD Imagers. In S.B. Howell, editor, *Astronomical CCD Observing and Reduction Techniques*, volume 23 of *Astronomical Society of the Pacific Conference Series*, pages 1–86, 390 Ashton Ave, San Francisco, California, USA, 1992. Astronomical Society of the Pacific, BookCrafters Inc.

A.H. Jarret. Boyden Observatory. Occasional Publication no. 2, Institute and Department of Astronomy, University of the Orange Free State, South Africa, April 1985.

A.H. Jarret. Boyden Observatory [A Concise History]. *Acta Academica*, (12), 1979.

P. Massay. *A User's Guide to CCD Reductions with IRAF*, February 1997.

P. Massay and L.E. Davis. *A User's Guide to Stellar CCD Photometry with IRAF*, April 1992.

P. Moore. Armagh Observatory, A History, 1790 - 1967. `http://star.arm.ac.uk/history/moore/`.

P. Moore and P. Collins. *Astronomy in Southern Africa*. Robert Hale & Co., London, UK, 1977.

J. Palmer and A.C. Davenhall. *The CCD Photometric Calibration Cookbook*. Starlink Project, Rutherford Appleton Laboratory, SC/6.3 edition, June 1999.

I. Ridpath. *Dictionary of Astronomy*. Oxford University Press, Oxford, 1997.

G.B. Rybicki and A.P. Lightman. *Radiatve Processes in Astrophysics*. John Wiley & Sons Inc., USA, 1979.

SAOImage DS9. `http://hea-harvard.edu/RD/ds9`.

M.A. Seeds. *Foundations of Astronomy*. Brooks/Cole Thomson Learning, USA, sixth edition, 2001.

R.N. Tubbs. *Lucky Exposures: Difraction Limited Astronomical Imaging Through The Atmosphere*. PhD thesis, St Johns College, Cambridge University, UK, 2003.

Appendix A

Observation logs

A.1 Introduction

In this appendix the observation logs will be presented. The observation logs consists of the relevant weather data and the tables containing the neccesary information. The table for each observation exercise will be summarized first, after which the weather data will be presented graphically. The observation log tables contains information such as the time and date of observation, the filters used, the airmass and the type of observations or object observed. Thereafter the relevant weather data will be presented graphically for each observation date, with the graphs containing the ambient temperature values, as well as relative humidity. In the weather data graphs the red curve represents the temperature with the light red area the temperature difference. The dew point is represented by the blue curve. The weather data is from the weather-station of the Boyden-Watcher robotic telescope.

Table A.1: Observation log for linearity test data

IMGTYPE	FILTER	DATE	TIME-BEGIN (UT)	TIME-END (UT)
FLAT	C	08/13/07	16:12:53	16:15:28
FLAT	C	08/14/07	16:04:59	16:10:31

Table A.2: Observation log for dark-count test data

IMGTYPE	FILTER	DATE	TIME-BEGIN (UT)	TIME-END (UT)
DARK	Close	06/26-27/2007	17:59:35	7:49:24
BIAS	Close	06/28/2007	8:19:27	8:22:00
BIAS	Close	08/14/2007	15:38:59	15:41:32
DARK	Close	08/14/2007	15:43:49	16:03:20
BIAS	Close	08/18/2007	16:05:53	16:08:26
DARK	Close	08/18/2007	16:08:56	16:33:35
BIAS	Close	08/19/2007	15:47:54	16:18:04
DARK	Close	08/19/2007	16:18:31	16:43:11

Table A.3: Observation log for readout-noise and system gain test data

IMGTYPE	FILTER	DATE	TIME-BEGIN (UT)	TIME-END (UT)
BIAS	Close	06/15/07	15:47:33	15:48:28
FLAT	C	06/15/07	15:44:41	15:46:32
BIAS	Close	08/13/07	16:11:16	16:12:01
FLAT	C	08/13/07	16:04:21	16:05:29

Table A.4: Observation log for standard star data

IMGTYPE	FILTER	AIRMASS-BEGIN	AIRMASS-END	DATE	TIME-BEGIN (UT)	TIME-END (UT)
Bias	Close			6/28/2007	8:19:27	8:22:00
Dark	Close			6/26/2007	17:59:35	7:49:24
Flat	U	1	1	8/19/2007	15:42:52	15:45:35
Flat	B	1	1	8/18/2007	15:57:53	16:00:10
Flat	V	1	1	8/18/2007	16:00:54	16:02:49
Flat	R	1	1	8/18/2007	16:03:27	16:05:22
Flat	I	1	1	8/19/2007	16:10:50	16:14:12

E817	U	1.24	1.17	8/19/2007	17:38:52	18:04:10
E817	B	1.34	1.32	8/18/2007	17:10:54	17:15:12
E817	V	1.32	1.31	8/18/2007	17:16:09	17:19:21
E817	R	1.3	1.29	8/18/2007	17:19:51	17:23:01
E817	I	1.25	1.24	8/19/2007	17:34:21	17:37:05
E803	U	1.16	1.15	8/19/2007	18:11:06	18:20:29
E803	B	1.25	1.24	8/18/2007	17:37:32	17:40:57
E803	V	1.24	1.23	8/18/2007	17:41:48	17:45:09
E803	R	1.23	1.22	8/18/2007	17:45:43	17:48:58
E803	I	1.17	1.17	8/19/2007	18:07:40	18:10:12
E853	U	1.13	1.09	8/19/2007	18:28:26	18:53:45
E853	B	1.21	1.19	8/18/2007	17:55:07	18:00:21
E853	V	1.19	1.18	8/18/2007	18:00:54	18:04:09
E853	R	1.18	1.17	8/18/2007	18:05:10	18:08:40
E853	I	1.14	1.13	8/19/2007	18:24:07	18:26:33
E804	U	1.08	1.07	8/19/2007	19:00:35	19:09:57
E804	B	1.16	1.16	8/18/2007	18:14:39	18:18:47
E804	V	1.15	1.15	8/18/2007	18:19:21	18:22:39
E804	R	1.15	1.14	8/18/2007	18:23:17	18:26:32
E804	I	1.09	1.08	8/19/2007	18:57:21	19:00:10
E809	U	1.07	1.06	8/19/2007	19:14:38	19:24:00
E809	B	1.14	1.14	8/18/2007	18:29:12	18:31:48
E809	V	1.13	1.13	8/18/2007	18:32:52	18:35:00
E809	R	1.13	1.13	8/18/2007	18:36:22	18:38:05
E809	I	1.08	1.07	8/19/2007	19:12:34	19:14:08
E815	U	1.06	1.06	8/19/2007	19:28:31	19:37:48
E815	B	1.12	1.12	8/18/2007	18:40:43	18:43:34
E815	V	1.12	1.12	8/18/2007	18:44:45	18:46:48
E815	R	1.11	1.11	8/18/2007	18:47:19	18:49:28
E815	I	1.06	1.06	8/19/2007	19:26:09	19:27:48
E816	U	1.05	1.04	8/19/2007	19:43:08	19:56:35
E816	B	1.1	1.1	8/18/2007	18:53:51	18:57:11
E816	V	1.1	1.1	8/18/2007	18:57:52	19:00:00
E816	R	1.09	1.09	8/18/2007	19:00:40	19:03:04
E816	I	1.05	1.05	8/19/2007	19:39:56	19:41:52

E837	U	1.05	1.04	8/19/2007	20:02:23	20:27:44
E837	B	1.09	1.09	8/18/2007	19:05:34	19:10:00
E837	V	1.09	1.09	8/18/2007	19:10:38	19:13:54
E837	R	1.08	1.08	8/18/2007	19:14:58	19:17:56
E837	I	1.05	1.05	8/19/2007	19:58:45	20:01:10
E846	U	1.04	1.04	8/19/2007	20:36:04	21:09:11
E846	B	1.07	1.07	8/18/2007	19:22:08	19:29:04
E846	V	1.06	1.06	8/18/2007	19:32:38	19:37:05
E846	R	1.06	1.06	8/18/2007	19:37:42	19:41:32
E846	I	1.04	1.04	8/19/2007	20:32:10	20:34:59
E836	U	1.05	1.06	8/19/2007	21:14:00	21:39:13
E836	B	1.06	1.06	8/18/2007	19:44:04	19:49:17
E836	V	1.06	1.06	8/18/2007	19:49:55	19:53:13
E836	R	1.06	1.05	8/18/2007	19:54:13	19:58:46
E836	I	1.05	1.05	8/19/2007	21:11:28	21:13:25
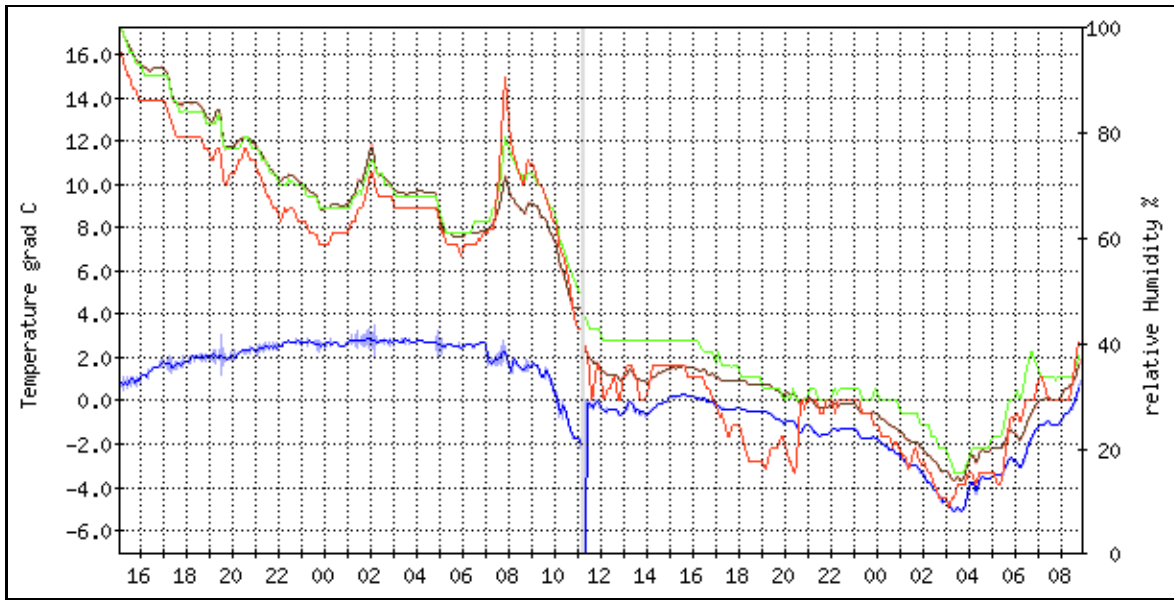
Figure A.1: Graph of temperature and humidity values.
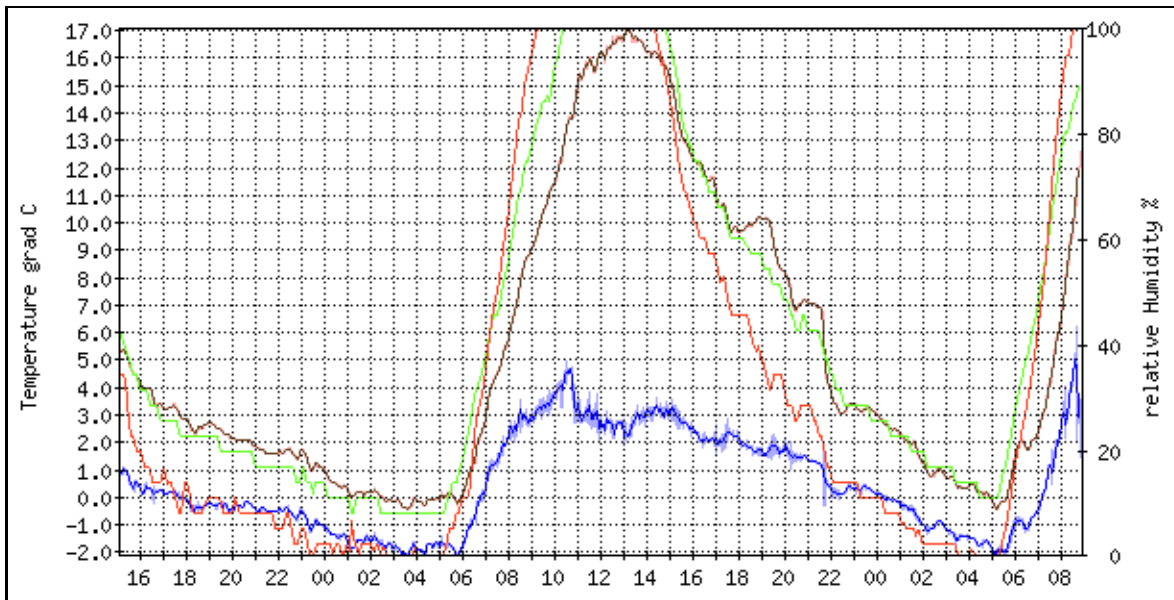
Figure A.2: Graph of temperature and humidity values.
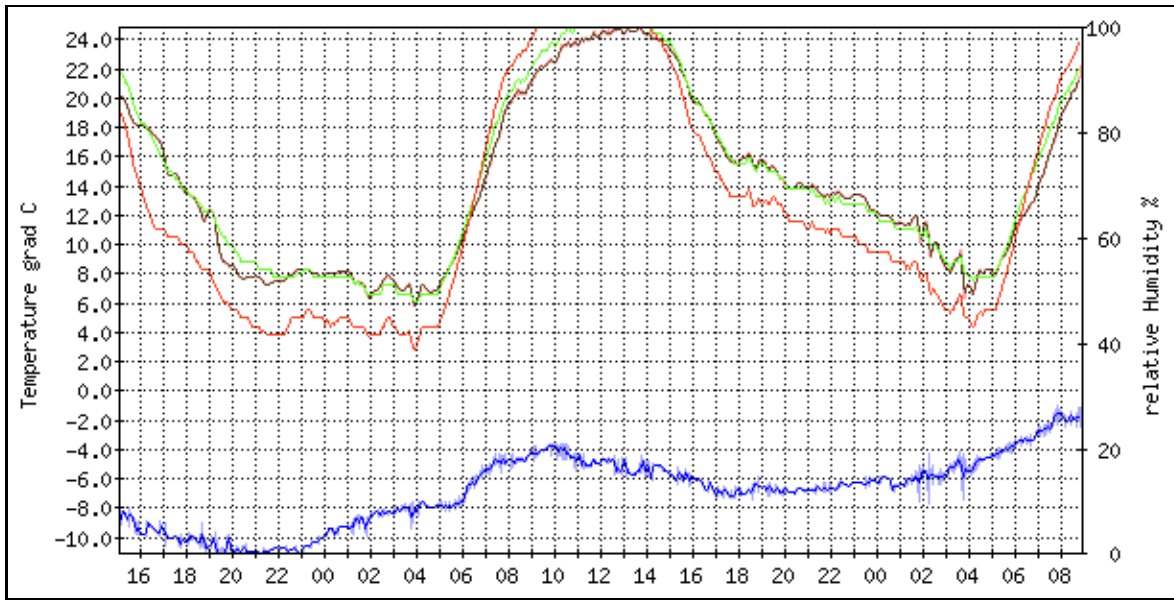
Figure A.3: Graph of temperature and humidity values.
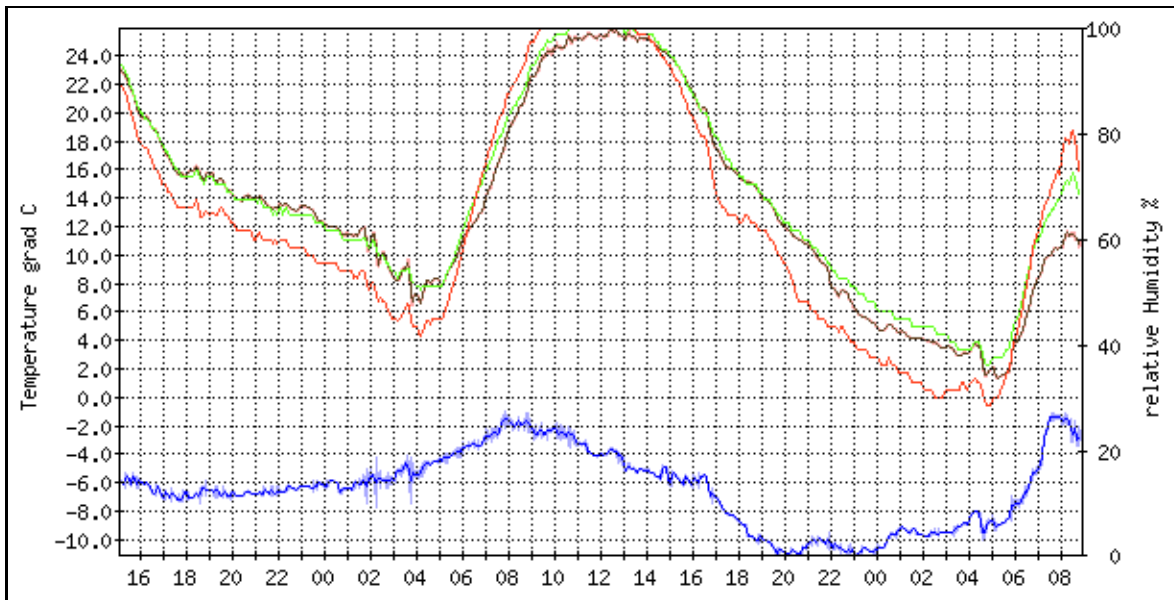
Figure A.4: Graph of temperature and humidity values.
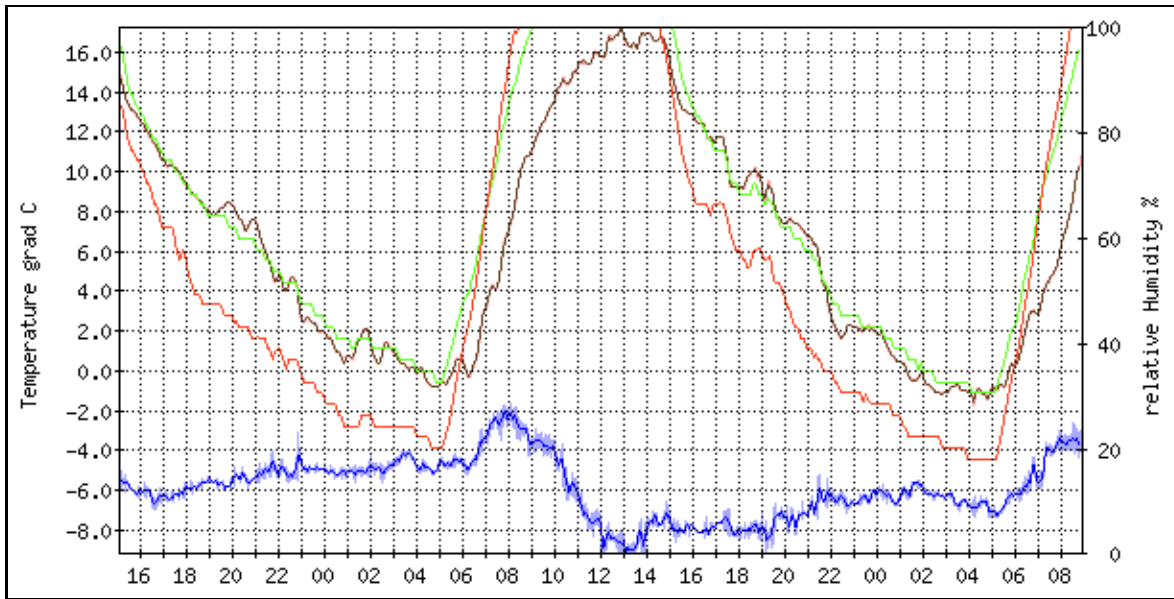
Figure A.5: Graph of temperature and humidity values.
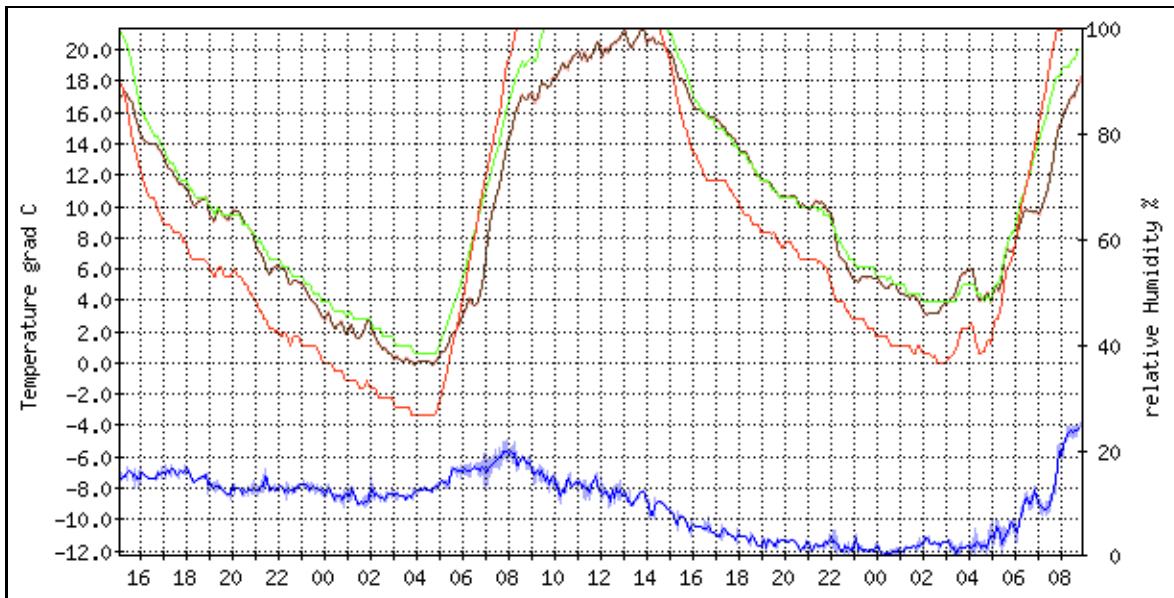
Figure A.6: Graph of temperature and humidity values.
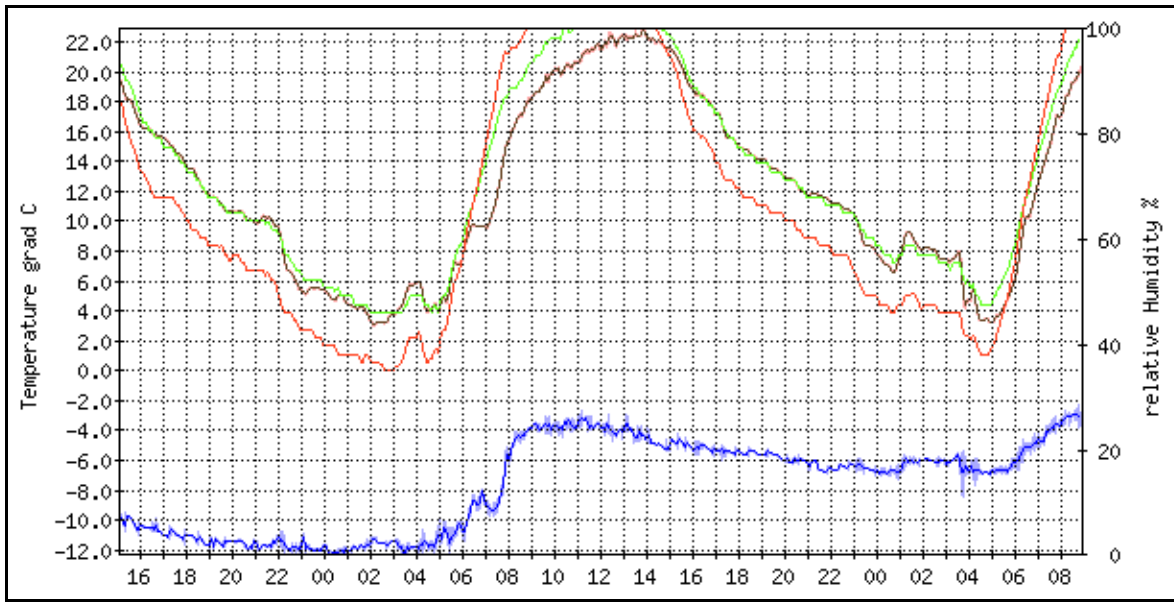
Figure A.7: Graph of temperature and humidity values.

Appendix B

Boyden IRAF Package layout and scripts

B.1   Introduction

In this appendix the Boyden IRAF package layout and main scripts will be discussed. The package layout in terms of the directory structure, control scripts and incorporation into IRAF will be examined. The main scripts used within the package will be presented.

B.2   Boyden IRAF Package layout

For the Boyden package to be incorporated into IRAF the package needs a control script and a help database. The control script and help database then needs to be defined into the IRAF extern.pkg script in the /iraf/iraf/unix/hlib directory. The Boyden IRAF package scripts and support documentation are then "installed" into a specified external packages directory inside the IRAF environment. The directory structure and layout for the Boyden IRAF package are then as follows:

/iraf/extern/boyden	The main directory containing the package control scripts and package README file.
/iraf/extern/boyden/doc	The directory containing help files for the Boyden package and tasks.
/iraf/extern/boyden/lib	The directory containing the help database and other support files.
/iraf/extern/boyden/pkg	The directory containing the scripts for the Boyden tasks.

The package control scripts are defined as follows:

boyden.cl	This script checks and sets the environment, defines the different tasks, calls the package load script and prints the welcome screen.
boyden.hd	This script sets up the help structures and environment and defines the help and source files for the Boyden package tasks.
boyden.men	The Boyden package menu for the different tasks.
boyden_motd	The Boyden package welcome screen/banner.
boyden.par	The Boyden package parameters, e.g. version number, release date, etc.
load.cl	Checks that the necessary IRAF packages are loaded, and loads the packages if absent.
README	The README file for the Boyden package, discusses the package, and explains its use.

The /lib directory contains the following files:

Boydencoeff.tab	A table containing the boyden extinction coefficients.
boydeninst.dat	The instrument translation file for the Rockefeller CCD-Telescope system.
columns.cd	The column definition file for the data tables for the photometry output results.
helpdb.mip	The Boyden IRAF package help database.
rootboyden.hd	The help definition file for the Boyden package.
root.hd	The directory definition file for the root help file.
Theoretcoeff.tab	A table containing a set of theoretical extinction coefficients.

The /doc directory contains the help files for the boyden package and the 13 defined tasks. The /pkg directory contains the .cl scripts for the 13 defined tasks.

B.3 Boyden IRAF Package scripts

Following are the scripts for the 13 defined tasks in the following order:

biasred.cl
darkred.cl
dirsetup.cl
fixheader.cl
flatred.cl
imagepreview.cl
lightcurve.cl
magcor.cl
psfphot.cl
psfsetup.cl
redsetup.cl
reduction.cl
stardump.cl

```
# BIASRED.CL - Biasred script for the BOYDEN package.
# Version 1.0 June 2007. Developed by H.J. van Heerden B.Sc.Hon
# Biasred script for creating a compiled bias frame and applying it on
# the project images.

procedure    biasred (biasframes, images, proccess) # Define procedure

# Define procedure variables

string biasframes          {"biaslist.lis",prompt="The biasframes to be combined"}
string images              {prompt="The images to be reduced"}
bool   proccess = yes      {prompt="Process images"}
bool   overscan = no       {prompt="Correct for overscan using BIASSEC"}
bool   trim = no           {prompt="Trim image using TRIMSEC"}

struct *bslist
struct *imglist

begin

        # Define script variables
        int    i
        string img, imgfile, bsfile, biasmaster, proc, bias, project

        # Make sure the necessary packages are loaded
        if (! defpac ("noao") || ! defpac ("imred")) {
               bye()
        }
        ;

        # Check for null value for biasframes
        bias = biasframes
        if (bias != "") {

               # Expand the bias template into a text file list
               bsfile = mktemp ("tmp$red")
               sections (bias, option = "fullname", > bsfile)
        }
        else {
               print ("No biasframes defined")
               bye()
        }
        ;


        # Check for null value for imageframes
        project = images
        if (project != "") {

               # Expand the image template into a text file list
               imgfile = mktemp ("tmp$red")
               sections (project, option = "fullname", > imgfile)
        }
        else {
               print ("No images defined")
               bye()
        }
        ;

        # Redirect
        bslist = bsfile
        imglist = imgfile

        # Declare biasmaster
        biasmaster = "biasmaster.fits"
```

```
        if (access (biasmaster)){
              imdelete (biasmaster)
        }
        ;

        # Implement zerocombine
        zerocombine ("@"//bslist, output = biasmaster, ccdtype = "", reject='minmax',
        process-)

        # Check the acceptability of the master-frame
        if (access (biasmaster)) {
              display (biasmaster, 1)

              # Process the images with ccdproc
              if (proccess) {

                     # Scan through the imagelist
                     while (fscan (imglist, img) != EOF) {

                            # Get rid of the ".fits" extention
                            i = strlen (img)
                            if (substr (img, i-4, i) == ".fits") {
                                  img = substr (img, 1, i-5)
                            }
                            ;

                            # Call ccdproc
                            if (access (img // ".fits")) {
                                  ccdproc (img, ccdtype = "", fixpix-, overscan=overscan,
                                  trim=trim, biassec="image", trimsec="image", zerocor+,
                                  darkcor-, flatcor-, illum-, fringe-, zero=biasmaster)
                            }
                            ;
                     }
                     ;
              }
              ;
        }
        ;

        # Clean up
        bslist = ""
        imglist = ""
        delete (bsfile, ver-, >& "dev$null")
        delete (imgfile, ver-, >& "dev$null")

end
```

```
# DARKRED.CL - Darkred script for the BOYDEN package.
# Version 1.0 June 2007. Developed by H.J. van Heerden B.Sc.Hon
# Darkred script for creating a compiled dark-frame and applying it on the
# project images

procedure    darkred (darkframes, images, proccess)        # Define procedure

# Define procedure variables

string darkframes            {"darklist.lis",prompt="The darkframes to be combined"}
string images                {prompt="The images to be reduced"}
bool   proccess = yes        {prompt="Process images?"}
bool   overscan = no         {prompt="Correct for overscan using BIASSEC"}
bool   trim = no             {prompt="Trim image using TRIMSEC"}

struct *dklist
struct *imglist

begin

        # Define script variables
        int    i, s
        string img, imgfile, dkfile, darkmaster, proc, dark, project

        # Make sure the necessary packages are loaded
        if (! defpac ("noao") || ! defpac ("imred")) {
                bye()
        }
        ;

        # Check for null value for darkframes
        dark = darkframes
        if (dark != "") {

                # Expand the dark-template into a text-file list
                dkfile = mktemp ("tmp$red")
                sections (dark, option = "fullname", > dkfile)
        }
        else {
                print ("No darkframes defined")
                bye()
        }
        ;

        # Check for null value for imageframes
        project = images
        if (project != "") {

                # Expand the image-template into a text-file list
                imgfile = mktemp ("tmp$red")
                sections (project, option = "fullname", > imgfile)
        }
        else {
                print ("No images defined")
                bye()
        }
        ;

        # Redirect
        dklist = dkfile
        imglist = imgfile

        # Decalre darkmaster
        darkmaster = "darkmaster.fits"

        if (access (darkmaster)){
```

```
            imdelete (darkmaster)
     }
     ;

     # Implement darkcombine
     darkcombine ("@"//dklist, output = darkmaster, scale = 'exposure', reject = 'minmax',
     ccdtype = "", process-)

     # Check the acceptability of the master-frame
     if (access (darkmaster)) {
            display      (darkmaster, 1)

            # Process the images with ccdproc
            if (proccess) {

                    # Scan through the imagelist
                    while (fscan (imglist, img) != EOF) {

                            # Get rid of the ".fits" extention
                            i = strlen (img)
                            if (substr (img, i-4, i) == ".fits") {
                                    img = substr (img, 1, i-5)
                            }
                            ;

                            # Call ccdproc
                            if (access (img // ".fits")) {
                                    ccdproc (img, ccdtype = "", overscan=overscan, fixpix-,
                                    trim=trim, biassec="image", trimsec="image", zerocor-,
                                    darkcor+, flatcor-, illum-, fringe-, dark=darkmaster)
                            }
                            ;
                    }
                    ;
            }
            ;
     }
     ;

     # Clean up
     dklist = ""
     imglist = ""
     delete (dkfile, ver-, >& "dev$null")
     delete (imgfile, ver-, >& "dev$null")

end
```

```
# DIRSETUP.CL - Dirsetup script for the BOYDEN package.
# Version 1.0 June 2007. Developed by H.J. van Heerden B.Sc.Hon
# Dirsetup script for creating datalists of the appropriate files from the
# header field values. This creates lists containing the dark-, bias-, object-
# and filter specific flatframes.

procedure    dirsetup (fitfiles) # Define procedure

# Define procedure variables

string fitfiles     {"*.fit*",prompt="The fitfiles to be used"}
bool   filernm = yes{prompt="Rename fitfiles"}
bool   sortfls = yes{prompt="Sort fitfiles"}

struct *fitlist

begin

        # Define script variables
        int    i
        bool   renm, sortfiles
        string ffiles, ftfls, data, fits, fitf, filter, biaslist, darklist, Uflatlist,
               Bflatlist, Vflatlist, Rflatlist, Iflatlist, Cflatlist, Uimagelist, Bimagelist,
               Vimagelist, Rimagelist, Iimagelist, Cimagelist

        data = ""
        filter = ""

        # Make sure the necessary packages are loaded
        if (!defpac ("imutil")){
                bye()
        }
        ;

        # Set the environment
        unlearn psfphot, biasred, darkred, flatred, fixheader, reduction, stardump

        # Expand the fitfiles into a text file list
        print("Task does not check filetypes. Make sure to pass only *.fit files")
        fitf = fitfiles
        renm = filernm
        if (filernm) {
                rename (fitf, "fits", field="extn")
        }
        ffiles = mktemp ("tmp$stp")
        sections (fitf, option="fullname", > ffiles)

        # Check if have to sort files
        sortfiles = sortfls
        if (sortfiles) {

                # Redirect
                fitlist = ffiles
                biaslist = "biaslist.lis"
                darklist = "darklist.lis"
                Uflatlist = "Uflatlist.lis"
                Bflatlist = "Bflatlist.lis"
                Vflatlist = "Vflatlist.lis"
                Rflatlist = "Rflatlist.lis"
                Iflatlist = "Iflatlist.lis"
                Cflatlist = "Cflatlist.lis"
                Uimagelist = "Uimagelist.lis"
                Bimagelist = "Bimagelist.lis"
                Vimagelist = "Vimagelist.lis"
                Rimagelist = "Rimagelist.lis"
                Iimagelist = "Iimagelist.lis"
```

```
Cimagelist = "Cimagelist.lis"

if (access (biaslist)){
      delete (biaslist)
}
;
if (access (darklist)){
      delete (darklist)
}
;
if (access (Uflatlist)){
      delete (Uflatlist)
}
;
if (access (Bflatlist)){
      delete (Bflatlist)
}
;
if (access (Vflatlist)){
      delete (Vflatlist)
}
;
if (access (Rflatlist)){
      delete (Rflatlist)
}
;
if (access (Iflatlist)){
      delete (Iflatlist)
}
;
if (access (Cflatlist)){
      delete (Cflatlist)
}
;
if (access (Uimagelist)){
      delete (Uimagelist)
}
;
if (access (Bimagelist)){
      delete (Bimagelist)
}
;
if (access (Vimagelist)){
      delete (Vimagelist)
}
;
if (access (Rimagelist)){
      delete (Rimagelist)
}
;
if (access (Iimagelist)){
      delete (Iimagelist)
}
;
if (access (Cimagelist)){
      delete (Cimagelist)
}
;

# Scan through the fitlist
while (fscan (fitlist, fits) != EOF) {

      # Check for master.fits files
      if (fits == "biasmaster.fits"){
            print("Warning: Fits reduction-master file - Skipping file")
      }
```

```
        else if (fits == "darkmaster.fits"){
                print("Warning: Fits reduction-master file - Skipping file")
        }
        else if (fits == "flatmasterU.fits"){
                print("Warning: Fits reduction-master file - Skipping file")
        }
        else if (fits == "flatmasterB.fits"){
                print("Warning: Fits reduction-master file - Skipping file")
        }
        else if (fits == "flatmasterV.fits"){
                print("Warning: Fits reduction-master file - Skipping file")
        }
        else if (fits == "flatmasterR.fits"){
                print("Warning: Fits reduction-master file - Skipping file")
        }
        else if (fits == "flatmasterI.fits"){
                print("Warning: Fits reduction-master file - Skipping file")
        }
        else if (fits == "flatmasterC.fits"){
                print("Warning: Fits reduction-master file - Skipping file")
        }
        else {

                # Sort files into lists
                # Get the exptype from the fits files
                hselect (fits, "EXPTYPE", yes) | scan(data)

                if (nscan() != 0) {

                        # Write the fit-files to specific predefined lists
                        if (data == "BIAS") {
                                sections (fits, option="fullname", >> biaslist)
                        }
                        else if (data == "DARK") {
                                sections (fits, option="fullname", >> darklist)
                        }
                        else if (data == "FLAT") {

                                # Check the filter type
                                hselect (fits, "FILTER", yes) | scan(filter)
                                if (nscan() != 0) {

                                        # Sort the files into filter specific lists
                                        if (filter == "U") {
                                                sections (fits, option="fullname", >>
                                                Uflatlist)
                                        }
                                        else if (filter == "B") {
                                                sections (fits, option="fullname", >>
                                                Bflatlist)
                                        }
                                        else if (filter == "V") {
                                                sections (fits, option="fullname", >>
                                                Vflatlist)
                                        }
                                        else if (filter == "R") {
                                                sections (fits, option="fullname", >>
                                                Rflatlist)
                                        }
                                        else if (filter == "I") {
                                                sections (fits, option="fullname", >>
                                                Iflatlist)
                                        }
                                        else if (filter == "C") {
                                                sections (fits, option="fullname", >>
                                                Cflatlist)
```

```
                                                }
                                                ;
                                        }
                                        ;
                                }
                                else if (data == "DATA") {

                                        # Check the filter type
                                        hselect (fits, "FILTER", yes) | scan(filter)
                                        if (nscan() != 0) {

                                                # Sort the files into filter specific lists
                                                if (filter == "U") {
                                                        sections (fits, option="fullname", >>
                                                        Uimagelist)
                                                }
                                                else if (filter == "B") {
                                                        sections (fits, option="fullname", >>
                                                        Bimagelist)
                                                }
                                                else if (filter == "V") {
                                                        sections (fits, option="fullname", >>
                                                        Vimagelist)
                                                }
                                                else if (filter == "R") {
                                                        sections (fits, option="fullname", >>
                                                        Rimagelist)
                                                }
                                                else if (filter == "I") {
                                                        sections (fits, option="fullname", >>
                                                        Iimagelist)
                                                }
                                                else if (filter == "C") {
                                                        sections (fits, option="fullname", >>
                                                        Cimagelist)
                                                }
                                                ;
                                        }
                                        ;
                                }
                                else {
                                        print ("Warning: Unknown image type")
                                }
                                ;
                        }
                        ;
                }
                ;
        }
        ;

        # Clean up
#       fitlist = ""
#       delete (ffiles, ver-, >& "dev$null")

end
```

```
# FIXHEADER.CL - Fixheader script for the BOYDEN package.
# Version 1.0 June 2007. Developed by H.J. van Heerden B.Sc.Hon
# Fixheader script that includes necessary information into the fits
# header, via user prompt. Key info include, Observat, Airmass, RA, dec, filter,
# ... enc.

procedure    fixheader (images, filter, observatory, rdnoise, gain, trimsec, biassec, ra,
dec, equinox)# Define procedure

# Define procedure variables

string images             {prompt = "Images which headers are to be fixed"}
string filter             {prompt = "The filter at which the frames was taken"}
string observatory        {"boyden",prompt = "Observatory where frames were taken"}
string rdnoise            {"11.7",prompt = "The CCD read-noise in electrons"}
string gain               {"3.54",prompt = "The system gain in epadu"}
string trimsec            {"[1:385,1:576]",prompt = "The section of raw image to save"}
string biassec            {"[1:17,1:576]",prompt = "The overscan region for bias"}
string ra                 {prompt = "The RA of the image center or star"}
string dec                {prompt = "The dec of the image center or star"}
string equinox            {prompt = "The equinox of the stars coordinates"}
bool   add = yes          {prompt = "Overwrite existing field values"}
bool   addonly = no       {prompt = "Add new field only if it doesn't exist"}
bool   verify = no        {prompt = "Verify header editing?"}
bool   show = no          {prompt = "Print record of edits?"}

struct *imglist

begin

        # Define script variables
        string img, imgfile, data, obj, cmdfile, filt, obs, rdn, epadu, trim, bias, RA, DEC,
              epoch, UT, ST, fitfiles

        # Make sure the necessary packages are loaded
        if (! defpac ("astutil") || ! defpac ("imutil")) {
              bye()
        }
        ;

        # Check for null value for images
        fitfiles = images
        if (fitfiles != "") {

              # Expand the image template into a text file list
              imgfile = mktemp ("tmp$fhd")
              sections (fitfiles, option="fullname", > imgfile)
        }
        else {
              print ("No images defined")
              bye()
        }
        ;

        # Create a file with commands to process
        cmdfile = mktemp ("tmp$fhd")
        print ("st = mst(@'date-obs', ut, obsdb( observat, 'longitude'))", > cmdfile)

        # Redirect
        imglist = imgfile

        # Open the list of images and scan through it
        while ( fscan (imglist, img) != EOF) {

              # Print the imagename that is being processed
              print (img)
```

```
# Check for darkframe
hselect (img, "OBJECT", yes) | scan (obj)      # Pipe the object value to
                                                 variable

if ((obj != "Dark") && (obj != "Bias")) {

        # Check for filter value and update if nessecary
        hselect (img, "FILTER", yes) | scan (data)     # Pipe the filter value to
                                                         variable

        if (nscan() == 0) {         # Check for filter value
                filt = filter        # Get the new filter value
                # Update the header file with the new field and value.
                hedit (img, "FILTER", filt, add=add, addonly=addonly,
                verify=verify, show=show)
        }
        else {
                print ("Header field FILTER already has a value")
        }
        ;
}
else {

        # Check for filter value and update if nessecary
        hselect (img, "FILTER", yes) | scan (data)     # Pipe the filter value to
                                                         variable

        if (nscan() == 0) {
                filt = "CLOSE"              # Get the filter value
                # Update the header file with the new field and value.
                hedit (img, "FILTER", filt, add=add, addonly=addonly,
                verify=verify, show=show)
        }
        else {
                print ("Header field FILTER already has a value")
        }
        ;
}
;

# Check for observatory value and update if nessecary
hselect (img, "OBSERVAT", yes) | scan (data)  # Pipe the observatory value to
                                                variable

if (nscan() == 0) {                  # Check for observatory value
        obs = observatory          # Get the new observatory value
        # Update the header file with the new field and value.
        hedit (img, "OBSERVAT", obs, add=add, addonly=addonly, verify=verify,
        show=show)
}
else {
        print ("Header field OBSERVAT already has a value")
}
;

# Check for ccd readnoise value and update if nessecary
hselect (img, "RDNOISE", yes) | scan (data)    # Pipe the rdnoise value to
                                                 variable

if (nscan() == 0) {                  # Check for rdnoise value
        rdn = rdnoise                # Get the new rdnoise value
        # Update the header file with the new field and value.
        hedit (img, "RDNOISE", rdn, add=add, addonly=addonly, verify=verify,
        show=show)
}
```

```
          else {
                print ("Header field RDNOISE already has a value")
          }
          ;

          # Check for gain value and update if nessecary
          hselect (img, "GAIN", yes) | scan (data)      # Pipe the gain value to variable

          if (nscan() == 0) {               # Check for gain value
                epadu = gain              # Get the new gain value
                # Update the header file with the new field and value.
                hedit (img, "GAIN", epadu, add=add, addonly=addonly, verify=verify,
                show=show)
          }
          else {
                print ("Header field GAIN already has a value")
          }
          ;

          # Check for trimsec value and update if nessecary
          hselect (img, "TRIMSEC", yes) | scan (data)   # Pipe the trimsec value to
                                                        variable

          if (nscan() == 0) {               # Check for trimsec value
                trim = trimsec            # Get the new trimsec value
                # Update the header file with the new field and value.
                hedit (img, "TRIMSEC", trim, add=add, addonly=addonly, verify=verify,
                show=show)
          }
          else {
                print ("Header field TRIMSEC already has a value")
          }
          ;

          # Check for biassec value and update if nessecary
          hselect (img, "BIASSEC", yes) | scan (data)   # Pipe the biassec value to
                                                        variable

          if (nscan() == 0) {               # Check for biassec value
                bias = biassec            # Get the new biassec value
                # Update the header file with the new field and value.
                hedit (img, "BIASSEC", bias, add=add, addonly=addonly, verify=verify,
                show=show)
          }
          else {
                print ("Header field BIASSEC already has a value")
          }
          ;

          # Check for ut value and update if nessecary
          hselect (img, "UT", yes) | scan (data) # Pipe the ut value to variable

          if (nscan() == 0) {       # Check for ut value

                # Check for time-obs field
                hselect (img, "TIME-OBS", yes) | scan (data)  # Pipe the time-obs value
                                                              to variable

                if (nscan() == 0) {       # Check for time-obs value

                       # Check for dat-obs field
                       hselect (img, "DATE-OBS", yes) | scan (data)  # Pipe the date-obs
                                                                     value to variable

                       if (nscan() == 1) {       # Check for date-obs value
                             UT = data            # Get the new ut value
```

```
                        # Update the header file with the new field and value.
                        hedit (img, "UT", UT, add=add, addonly=addonly,
                        verify=verify, show=show)
                }
                ;
        }
        else {
                UT = data             # Get the new ut value
                # Update the header file with the new field and value.
                hedit (img, "UT", UT, add=add, addonly=addonly, verify=verify,
                show=show)
        }
        ;
}
else {
        print ("Header field UT already has a value")
}
;

# Check for airmass value and update if nessecary
# Skip if darkframe
hselect (img, "OBJECT", yes) | scan (obj)      # Pipe the object value to
                                                 variable
if ((obj != "Dark") && (obj != "Bias")) {

        hselect (img, "AIRMASS", yes) | scan (data)   # Pipe the airmass value
                                                        to variable

        if (nscan() == 0) {        # Check for airmass value

                # Check for ra value and update if nessecary
                hselect (img, "RA", yes) | scan (data) # Pipe the ra value to
                                                         variable

                if (nscan() == 0) {        # Check for ra value
                        RA = ra            # Get the new ra value
                        # Update the header file with the new field and value.
                        hedit (img, "RA", RA, add=add, addonly=addonly,
                        verify=verify, show=show)
                }
                else {
                        print ("Header field RA already has a value")
                }
                ;

                # Check for dec value and update if nessecary
                hselect (img, "DEC", yes) | scan (data) # Pipe the dec value to
                                                          variable

                if (nscan() == 0) {        # Check for dec value
                        DEC = dec          # Get the new dec value
                        # Update the header file with the new field and value.
                        hedit (img, "DEC", DEC, add=add, addonly=addonly,
                        verify=verify, show=show)
                }
                else {
                        print ("Header field DEC already has a value")
                }
                ;

                # Check for equinox value and update if nessecary
                hselect (img, "EPOCH", yes) | scan (data)      # Pipe the equinox
                                                                 value to variable

                if (nscan() == 0) {        # Check for equinox value
                        epoch = equinox    # Get the new equinox value
```

```
                            # Update the header file with the new field and value.
                            hedit (img, "EPOCH", epoch, add=add, addonly=addonly,
                            verify=verify, show=show)
                    }
                    else {
                            print ("Header field EPOCH already has a value")
                    }
                    ;

                    # Check for st value and update if nessecary
                    data = ""
                    hselect (img, "ST", yes) | scan (data)  # Pipe the st value to
                                                            variable

                    if (nscan() == 0) {           # Check for st value
                            hedit (img, "ST", "", add=yes, verify=no, show=no)
                            asthedit (img, cmdfile)
                    }
                    else {
                            print ("Header field ST already has a value")
                    }
                    ;

                    setairmass (img, show=show, update+)
            }
            else {
                    print ("Header field AIRMASS already has a value")
            }
            ;

        }
        ;

    }
    ;

    # Clean up
    imglist = ""
    delete (imgfile, ver-, >& "dev$null")
    delete (cmdfile, ver-, >& "dev$null")

end
```

```
# FLATRED.CL - Flatred script for the BOYDEN package.
# Version 1.0 June 2007. Developed by H.J. van Heerden B.Sc.Hon
# The flatred script for creating a compiled flat-frame and applying it on
# the project images

procedure    flatred (flatframes, images, proccess, filter)          # Define procedure

# Define procedure variables

string flatframes            {prompt="The flatframes to be combined"}
string images                {prompt="The images to be reduced"}
bool   proccess = yes        {prompt="Process images?"}
string filter                {prompt="Specific filter for flats"}
bool   overscan = no         {prompt="Correct for overscan using BIASSEC"}
bool   trim = no             {prompt="Trim image using TRIMSEC"}

struct *ftlist
struct *imglist

begin

        # Define script variables
        int    i
        string img, imgfile, ftfile, flatmaster, proc, filt, flat, project

        # Make sure the necessary packages are loaded
        if (! defpac ("noao") || ! defpac ("imred")) {
                bye()
        }
        ;

        # Check for null value for flatframes
        flat = flatframes
        if (flat != "") {

                # Expand the flat-template into a text-file list
                ftfile = mktemp ("tmp$red")
                sections (flat, option = "fullname", > ftfile)
        }
        else {
                print ("No flatframes defined")
                bye()
        }
        ;

        # Check for null value for images
        project = images
        if (project != "") {

                # Expand the image-template into a text-file list
                imgfile = mktemp ("tmp$red")
                sections (project, option = "fullname", > imgfile)
        }
        else {
                print ("No images defined")
                bye()
        }
        ;

        # Redirect
        ftlist = ftfile
        imglist = imgfile
        filt = filter

        # Declare flatmaster
        flatmaster = "flatmaster"
```

```
        if (access (flatmaster // filt // ".fits")){
              imdelete (flatmaster // filt // ".fits")
        }
        ;

        # Implement flatcombine
        flatcombine ("@"//ftlist, output = flatmaster, scale = 'mode', reject = 'crreject',
                     gain = 'gain', rdnoise = 'rdnoise', ccdtype = "", process-)

        # Check the acceptability of the master-frame
        if (access (flatmaster // filt // ".fits")) {
              display (flatmaster // filt // ".fits", 1)

              # Process the images with ccdproc
              if (proccess) {

                      # Scan through the imagalist
                      while (fscan (imglist, img) != EOF ) {

                            # Get rid of the ".fits" extention
                            i = strlen (img)
                            if (substr (img, i-4, i) == ".fits") {
                                   img = substr (img, 1, i-5)
                            }
                            ;

                            # Call ccdproc
                            if (access (img // ".fits")) {
                                   ccdproc (img, ccdtype="", overscan=overscan, fixpix-,
                                   trim=trim, biassec="image", trimsec="image", zerocor-,
                                   darkcor-, flatcor+, illum-, fringe-,
                                   flat=flatmaster//filt//".fits")
                            }
                            ;
                      }
                      ;
              }
              ;
        }
        ;

        # Clean up
        ftlist = ""
        imglist = ""
        delete (ftfile, ver-, >& "dev$null")
        delete (imgfile, ver-, >& "dev$null")

end
```

```
# IMAGEPREVIEW.CL - Imagepreview script for the BOYDEN package
# Version 1.0 June 2007. Developed by H.J. van Heerden B.Sc.Hon
# Imagepreview script for checking the data quality and deleting bad frames.

procedure    imagepreview (dataframes, keep, delete)       # Define procedure

# Define procedure variables

string dataframes    {prompt="The dataframes to preview"}
bool   keep = yes    {prompt="Keep dataframe?"}
bool   delete = yes {prompt="Delete dataframe?"}

struct *datalist

begin

        # Define script variables
        string datafile, images, data

        # Check for null value for dataframes
        images = dataframes
        if (images != "") {

                # Expand the images template into a text file list
                datafile = mktemp ("tmp$imp")
                sections (images, option = "fullname", > datafile)
        }
        else {
                print ("No dataframes defined")
                bye()
        }
        ;

        # Redirect
        datalist = datafile

        # Scan through the datafile
        while (fscan (datalist, data) != EOF) {

                # Check the acceptability of the dataframe
                if (access (data)) {
                        display (data, 1)
                }
                ;

                # Quary to keep the dataframe or not
                if (keep) {
                        print ("Keeping data frame")
                }
                else {

                        # Quary if want to delete dataframe
                        if (delete) {
                                print ("Deleting dataframe!")
                                delete (data)
                        }
                        else {
                                print ("Keeping data frame!")
                        }
                        ;
                }
                ;
        }
        ;

        # Clean up
```

```
        datalist = ""
        delete (datafile, ver-, >& "dev$null")

end
```

```
# LIGHTCURVE.CL - Lightcurve script for the BOYDEN package.
# Version 1.0 June 2007. Developed by H.J. van Heerden B.Sc.Hon
# Lightcurve is a procedure to plot the lightcurve of the specified
# star data and display it, as well as the options to save it.

procedure    lightcurve (stardata)      # Define procedure

# Define procedure variables

string stardata      {prompt="The table containing the star data"}
bool   save=yes      {prompt="Save the lightcurve to file"}
bool   psfile=yes    {prompt="Save the lightcurve to post-script"}
bool   epsfile=no    {prompt="Save the lightcurve to eps-file"}

struct *datalist

begin

        # Define script variables
        int    i
        string stard, datafile, dataf, lcfile

        # Make sure the nessecary packages are loaded
        if ( ! defpac ("tbplot")) {
                bye()
        }
        ;

        # Check for null value for stardata
        stard = stardata
        if (stard != "") {

                #Expand the table template into a text file list
                datafile = mktemp("tpm$plc")
                sections (stard, option="fullname", > datafile)
        }
        else {
                print ("No star table file defined")
                bye()
        }
        ;

        # Redirect
        datalist = datafile

        # Scan through datalist and get starfile to plot
        while (fscan (datalist, dataf) != EOF) {

                # Get rid of the ".tab" extention
                i = strlen (dataf)
                if ( substr(dataf, i-3, i) == ".tab") {
                        dataf = substr(dataf, 1, i-4)
                }
                ;

                # Define lcfile
                lcfile = dataf // "lc"

                # Plot lightcurve and display using default graphix
                # lightcurve
                sgraph (dataf // ".tab UT MAG", point+, marker='cross', xlabel="UT (hh:mm:ss)",
                ylabel="MAG", title="Lightcurve of " // dataf // " with errorbars",margin=0.25,
                sysid-, device='stdgraph')

                # errorbars
                sgraph (dataf // ".tab UT MAG", point-, erraxis=2, errcol="MERR", append+)
```

```
            # Flush graphix buffer
            gflush

            # Save lightcurve using psdump and save as star#lc.ps
            if (save) {

                    if (psfile) {

                            # lightcurve
                            sgraph (dataf // ".tab UT MAG", point+, marker='cross', xlabel="UT
                            (hh:mm:ss)", ylabel="MAG",title="Lightcurve of " // dataf // "
                            with errorbars",margin=0.25, sysid-, device='psdump')

                            # errorbars
                            sgraph (dataf // ".tab UT MAG", point-, erraxis=2, errcol="MERR",
                            append+)

                            # Flush graphix buffer
                            gflush

                            # Capture dumped file and rename
                            copy ("/tmp/irafdmp*.ps", "/iraf/work/")
                            delete ("/tmp/irafdmp*.ps", ver-, >& "dev$null")
                            rename ("irafdmp*.ps", lcfile, field='root')

                    }
                    ;

                    if (epsfile) {
                            # lightcurve
                            sgraph (dataf // ".tab UT MAG", point+, marker='cross', xlabel="UT
                            (hh:mm:ss)", ylabel="MAG", title="Lightcurve of " // dataf // "
                            with errorbars",margin=0.25, sysid-, device='epsfl')

                            # errorbars
                            sgraph (dataf // ".tab UT MAG", point-, erraxis=2, errcol="MERR",
                            append+)

                            # Flush graphix buffer
                            gflush

                            # Capture dumped file and rename
                            rename ("sgi*.eps", lcfile, field='root')

                    }
                    ;
            }
            ;
        }
        ;

        # Clean up
        datalist = ""
        delete (datafile, ver-, >& "dev$null")

end
```

```
# MAGCOR.CL - Magcor script for the BOYDEN package.
# Version 1.0 June 2007. Developed by H.J. van Heerden B.Sc.Hon
# Magnitude correction script to correct the measured magnitudes for atmospheric
# invluence

procedure    magcor (starfiles, coeff) # Define procedure

# Define procedure variables

string starfiles      {prompt="The files containing the measured star data"}
real   coeff          {prompt="The k1 coefficient for the specific filter"}

struct*      starlist

begin

        # Define script variables
        real   k1
        string starf, startab, star

        # Make sure the nessecary packages are loaded
        if ( !defpac ("ttools")) {
                bye()
        }
        ;

        # Check for null value for starfiles
        startab = starfiles
        if (startab != "") {

                #Expand the image template into a text file
                starf = mktemp ("tmp$cor")
                sections (startab, option="fullname", > starf)
        }
        else {
                print ("No star#.tab file defined")
                bye()
        }
        ;

        # Print the known coeff tables for observatory
        tprint ("boyden$lib/Theoretcoeff.tab,boyden$lib/Boydencoeff.tab")

        # Redirect
        starlist = starf
        k1 = coeff

        # Scan through starlist
        while (fscan (starlist, star) != EOF) {

                # Do the magnitude corrections
                tcalc (star, "MAG0", "MAG - (" // k1 // "*AIRMASS)")
        }
        ;

        # Clean up
        starlist = ""
        delete (starf, ver-, >& "dev$null")

end
```

```
# PSFPHOT.CL - Psfphot script for the BOYDEN package.
# Version 1.0 June 2007. Developed by H.J. van Heerden B.Sc.Hon
# The script uses daophot to do batch psf photometry on a defined set of images.

procedure    psfphot (images, master_coo, master_pst)       # Define procedure

# Define procedure variables

string images         {prompt="Images to be used"}
string master_coo     {prompt="The master.coo file containing the stars' coordinates"}
string master_pst     {prompt="The master.pst file containing the PSF template stars"}
struct *imglist

begin

        # Define script variables
        int    i
        string img, imgfile, coord, pststar, project

        # Make sure the necessary packages are loaded
        if (! defpac ("digiphot") || ! defpac ("daophot")) {
                bye()
        }
        ;

        # Check for null value for images
        project = images
        if (project != "") {

                # Expand the image template into a text file list
                imgfile = mktemp ("tmp$apt")
                sections (project, option="fullname", > imgfile)
        }
        else {
                print ("No images defined")
                bye()
        }
        ;

        # Get the rest of the parameters
        coord = master_coo
        pststar = master_pst

        # Redirect
        imglist = imgfile

        # Scan through the imaglist
        while (fscan (imglist, img) != EOF) {

                # Get rid of the ".fits" extention
                i = strlen (img)
                if (substr (img, i-4, i) == ".fits") {
                        img = substr (img, 1, i-5)
                }
                ;

                # Perform aperture photometry
                if (access (img // ".fits")){
                        phot (img, coord, 'default', verify = no)
                }
                ;

                # Generate modal psf
                if (access (img // ".fits")) {
                        psf (img, 'default', pststar, 'default', 'default', 'default',
                        interactive = no, showplots = no, verify = no)
```

```
		}
		;

		# Perform psf-fitting photometry
		if (access (img // ".fits")) {
			allstar (img, 'default', 'default', 'default', 'default', 'default',
			verify = no)
		}
		;
	}
	;

	# Clean up
	imglist = ""
	delete (imgfile, ver-, >& "dev$null")

end
```

```
# PSFSETUP.CL - Psfsetup script for the BOYDEN package.
# Version 1.0 June 2007. Developed by H.J. van Heerden B.Sc.Hon
# Psf-photometry setup script. Sets the parameter files for psf-photometry

procedure     psfsetup ()  # Define procedure

# Define procedure variables
real   fwhm_psf      {prompt="The predetermined fwhmpsf for datapars"}
real   sig_ma        {prompt="The predetermined sigma for datapars"}
real   data_max      {prompt="The predetermined datamax for datapars"}
real   data_min      {prompt="The predetermined datamin for datapars"}
real   thres_hold    {prompt="The predetermined threshold for findpars"}
real   psf_rad       {prompt="The predetermined psfrad for daopars"}
real   fit_rad       {prompt="The predetermined fitrad for daopars"}

begin

       # Define script variables
       real  fwhmpsf, sigma, datamax, datamin, threshold, psfrad, fitrad

       # Set the environment
       unlearn phot, psf, allstar
       unlearn datapars, findpars, daopars

       # Redirect
       fwhmpsf       = fwhm_psf
       sigma         = sig_ma
       datamax       = data_max
       datamin       = data_min
       threshold     = thres_hold
       psfrad        = psf_rad
       fitrad        = fit_rad

       # Set up the datapars file
       datapars.filter    = "filter"
       datapars.obstime   = "time-obs"
       datapars.exposure  = "exptime"
       datapars.airmass   = "airmass"
       datapars.gain      = "gain"
       datapars.ccdread   = "rdnoise"
       datapars.fwhmpsf   = fwhmpsf
       datapars.sigma     = sigma
       datapars.datamax   = datamax
       datapars.datamin   = datamin
       update datapars

       # Set up the findpars file
       findpars.threshold = threshold
       update findpars

       # Set up the daopars file
       daopars.psfrad     = psfrad
       daopars.fitrad     = fitrad
       update daopars

end
```

```
# REDSETUP.CL - Redsetup script for the BOYDEN package.
# Version 1.0 June 2007. Developed by H.J. van Heerden B.Sc.Hon
# Reduction setup script. Calls setinstrument and sets the reduction process
# parameters using a translation.dat file, created specifically for the package.

procedure    redsetup (transfile)              # Define procedure

# Define procedure variables

string transfile    {prompt="The translation file for the reduction process"}
bool   review = no  {prompt="Review the paramfiles for ccdred and ccdproc"}

begin

        # Define script variables
        string translation

        # Get variable data
        translation  = "boydeninst"

        # Set parameters
        ccdred.pixeltype = "ushort real"
        update ccdred

        # Call setinstrument with the nessecary params
        setinstrument (translation, directory="boyden$lib/", site="", review=review)


end
```

```
# REDUCTION.CL - Reduction script for the BOYDEN package.
# Version 1.0 June 2007. Developed by H.J. van Heerden B.Sc.Hon
# Reduction script to apply reduction procedures to desired images in
# batch mode. Reductions are in the form of dark field and flat field
# substraction.

procedure reduction (nfilter)     # Define procedure

# Define procedure variables

string nfilter              {prompt="The number of filters used for flatred process"}
bool   setup = yes          {prompt="Setup the parameters for reduction"}
bool   bias = yes           {prompt="Apply bias frame reductions on images"}
bool   dark = yes           {prompt="Apply dark frame reductions on images"}
bool   flat = yes           {prompt="Apply flat frame reductions on images"}


begin

        # Define script variables
        int    k, n, s
        string nfilt
        bool   setp, bred, dred, fred

        # Redirect
        setp = setup
        bred = bias
        dred = dark
        fred = flat

        # Setup the translation parameters for ccdproc
        if (setp) {
                redsetup ()
        }
        ;

        # Combine the bias frames and apply new frame on images, using ccdproc
        if (bred) {
                biasred ()
        }
        ;

        # Combine the dark frames and apply new frame on images, using ccdproc
        if (dred) {
                darkred ()
        }
        ;

        # Combine the flat frames and apply new frame on images, using ccdproc
        if (fred) {

                # Redirect
                nfilt = nfilter

                #Scan through nfilt to get the number of filters
                print (nfilt) | scan (s)
                if (nscan() != 0) {

                        #Do flatred for the number of filters
                        n = int(nfilt)
                        for (k = 1; k <= n; k+=1) {
                                flatred ()
                        }
                        ;
                }
                ;
```

```
        }
    ;

end
```

```
# STARDUMP.CL - Stardump script for the BOYDEN package.
# Version 1.0 June 2007. Developed by H.J. van Heerden B.Sc.Hon
# Stardump is a procedure to dump the calculated psf.data to a text file
# for each star calculated. The amount of text files created depends on the
# amount of stars measured.

procedure stardump (als_temp, als_files, num_stars, filter)# Define procedure

# Define procedure variables

string als_temp     {prompt="The alsfile template for the star id's"}
string als_files    {prompt="The alsfiles containing the calculated magnitudes"}
string num_stars    {prompt="The number of stars, or the starnumber to be dumped"}
string filter       {prompt="The specific filter for the als files"}
bool   star_id = yes{prompt="Check alsfile template for star id's"}

struct *alslist

begin

        # Define script variables
        int    i, n, k, s
        string alsstar, als, nstars, starfile, startable, expr, starid, alsid,
               afiles, cdfile, filt

        starid = ""

        # Make sure the nessecary packages are installed
        if ( ! defpac ("daophot") || ! defpac ("ttools")) {
               bye()
        }
        ;

        # Check for null value for als template file
        if (star_id) {
               alsid = als_temp
               if (alsid != "") {

                       # Get the star id's from the als file, and display them for the user to
                       choose.
                       starid = mktemp ("tmp$als")
                       txdump (alsid, "id", yes, > starid)
                       print ("Measured stars' id's!")
                       type (starid)
               }
               else {
                       print ("No als template file defined")
                       bye()
               }
               ;
        }
        ;

        # Check for null value for als_files
        afiles = als_files
        if (afiles != "") {

               # Expand the image template into a text file list
               alsstar = mktemp ("tmp$als")
               sections (afiles, option="fullname" , > alsstar)
        }
        else {
               print ("No alsfiles defined")
               bye()
        }
        ;
```

```
# Get the rest of the parameters/redirect
cdfile = "boyden$lib/columns.cd"
nstars = num_stars
alslist = alsstar
filt = filter

# Scan through nstars to get the starnumber
print (nstars) | scan (s)
if (nscan () != 0) {

        # If there is a starnumber do the textdump
        i = strlen (nstars)

        if (substr (nstars, i, i) == "'" ) {          # Check for specific stars
              n = int(substr (nstars, 1, i-1))

              # Do the txdump. The textfiles containing the data will
              # appear in the same directory as the source files!

              starfile = "star" // n // filt // ".dat"
              expr = "id ==" // n
              while (fscan (alslist, als) != EOF ) {
                      txdump (als, "image,ifilter,otime,xairmass,xcenter,
                      ycenter,mag,merr,msky", expr, >> starfile)
              }
              ;

              # Create a table file from the data/text file
              startable = "star" // n // filt // ".tab"
              tcreate (startable, cdfile, starfile)

        }
        else {
              n = int(nstars)              # Dump all the stars in order, if numbered
                                           from 1 to n

              # Do the txdump. The textfiles containing the data will
              # appear in the same directory as the source files!

              while (fscan (alslist, als) != EOF ) {
                      for (k = 1;  k <= n; k+=1) {

                              starfile = "star" // k // filt // ".dat"
                              expr = "id ==" // k
                              txdump (als, "image,ifilter,otime,xairmass,
                              xcenter,ycenter,mag,merr,msky", expr, >> starfile)
                      }
                      ;
              }
              ;

              # Create a table file from the data/text file
              for (k = 1;  k <= n; k+=1) {

                      starfile = "star" // k // filt // ".dat"
                      startable = "star" // k // filt // ".tab"
                      tcreate (startable, cdfile, starfile)
              }
              ;
        }
        ;
}
;

# Clean up
```

```
        alslist = ""
        delete (alsstar, ver-, >& "dev$null")
        delete (starid, ver-, >& "dev$null")

end
```